2014

Influence of geochemical processes on the geomechanical response of the overburden due to CO2 storage in saline aquifers

Sai Bharath Kumar Varre

INFLUENCE OF GEOCHEMICAL PROCESSES ON THE GEOMECHANICAL RESPONSE OF THE OVERBURDEN DUE TO CO_2 STORAGE IN SALINE AQUIFERS

Sai Bharath Kumar Varre

Dissertation submitted to the
Benjamin M.Statler College of Engineering and Mineral Resources
at West Virginia University
in partial fulfillment of the requirements
for the degree of

Doctor of Philosophy
in
Civil & Environmental Engineering

Hema J.Siriwardane, Ph.D., Chair
John D. Quaranta, Ph.D.
Thomas H.Wilson, Ph.D.
Samuel Ameri, M.S.
Raj K. Gondle, Ph.D.

Department of Civil and Environmental Engineering

Morgantown, West Virginia
2014

Keywords: CO_2 storage, Geochemistry, Geomechanics, Multiphase flow, Numerical modeling

ProQuest LLC.
789 East Eisenhower Parkway
P.O. Box 1346
Ann Arbor, MI 48106 - 1346

ABSTRACT

INFLUENCE OF GEOCHEMICAL PROCESSES ON THE GEOMECHANICAL RESPONSE OF THE OVERBURDEN DUE TO CO_2 STORAGE IN SALINE AQUIFERS

Sai Bharath Kumar Varre

Saline aquifers have been identified as desirable geologic formations, suitable for the storage of carbon dioxide (CO_2) in large amounts. While the impermeable caprock layer(s) in the overburden provide(s) the primary trap for injected carbon dioxide, other trapping mechanisms, such as solubility, residual, ionic or mineral trapping, help contribute to CO_2 storage. Geochemical reactions alter the petrophysical properties such as porosity in the target reservoir, and may have an influence on the reservoir storage capacity. When CO_2 is injected for long periods of time, it changes the fluid pressures and the overburden geomechanical response. The geomechanical response associated with time-dependent geochemical reactions may also influence the integrity of the caprock layer and the long-term fate of injected CO_2.

In the current study, coupled multiphase fluid flow and geomechanical modeling with geochemical reactions was performed to simulate the long-term (1,000 years), large-scale injection of CO_2 (up to10 million metric tons per year) into a deep saline aquifer. The primary objective of the study is to investigate the influence of geochemical reactions on the geomechanical response of the overburden during long-term CO_2 injection. The geochemical modeling results show that geochemical reactions, such as mineral dissolution and precipitation, do not have a significant influence on reservoir rock porosity (about 2% reduction). However, an increase in the mineral reaction rate constants resulted in a reduction of about 35% in rock porosity. Modeling results show that the inclusion of geochemical reactions in the geomechanical models does not have a significant influence on the computed ground displacements during the injection and post-injection periods. However, brine salinity and CO_2 solubility have an influence on the computed pressure buildup and ground displacements during CO_2 injection. In this study, the influence of a vertical permeable zone (damage zone) around the wellbore on CO_2 leakage during long-term CO_2 injection was investigated. Modeling results show that the damage zone permeability and the vertical extent of the damage zone have a significant influence on the amount of CO_2 leakage. Modeling results also show that the vertical extent of the damage zone does not have a significant influence on the computed ground displacements. Therefore, the computed ground displacements may not be a good indicator of the extent of damage zone around the wellbore.

ACKNOWLEDGEMENT

I would like to take this opportunity to thank all the committee members for serving on my dissertation committee. Even though my name appears first on the cover of this dissertation, there have been many people who have contributed to its production. I owe my utmost gratitude to all those people who have made this dissertation possible and because of whom I had great research experiences that I will cherish forever. I would like to thank my advisor and committee chairman, Dr. Hema Siriwardane, for providing his valuable guidance and continuous support throughout this project. I thank Dr. Raj Gondle, Dr. John Quaranta, Dr. Thomas Wilson, and Professor Samuel Ameri for their words of encouragement which kept me going.

My deepest gratitude is to my advisor, Dr. Hema Siriwardane. I have been amazingly fortunate to have an advisor who has been a backbone to my success. Dr.Siri as I call him, taught me how to question thoughts and express ideas. His patience and support helped me overcome many crisis situations and finish this dissertation

I would like to thank Dr.Raj Gondle who is a dear friend of mine first and then my dissertation committee member. He has always been there to listen and give me advice during the course of my graduate study. I am also thankful to him for his guidance from time to time

I would like to thank Dr.John Quaranta for his insightful comments and constructive criticisms at different states of my research which were thought-provoking. I am also thankful to him for encouraging the use of correct grammar and consistent notation in my dissertation.

Dr. Thomas Wilson and Professor Samuel Ameri are among the best teachers that I have had in my life. They have always set high standards for their students and have always encouraged me to meet those standards.

I gratefully acknowledge the financial support provided by United States Department of Energy through a research project funded through West Virginia University.

I gratefully acknowledge the use of reservoir simulation software provided by Computer

Modeling Group (CMG). I offer my special thanks to Jim Erdle, Vikram Chandrasekhar, and Thanh Nguyen for providing assistance and training to CMG software.

Many friends have helped me stay sane through these difficult years. Their support and care helped me overcome setbacks and stay focused on my graduate study. I greatly value their friendship and I deeply appreciate their belief in me. I would like to take this opportunity to all my friends and colleagues - Karthik Dandu, Sodith Reddy, Benjamin Bowes, Andrew Dietz, Sumanth Gundagatti, Hari Nambu, and Zainab Jawad for giving me a helping hand whenever it was required.

Most importantly, none of this would have been possible without the love and patience of my family and the divine blessings of God. My immediate family, to whom this dissertation is dedicated to, has been a constant source of love, concern, support and strength all these years. I would like to express my heart-felt gratitude to my family. Last but not the least, I would like to thank my fiancée Sravya Chepuru, who has been always supportive of my endeavors and I greatly appreciate her love and patience, without which I would not have made it to the end. My extended family have always been encouraged me throughout this endeavor and I greatly appreciate their generosity and understanding.

.

TABLE OF CONTENTS

LIST OF FIGURES

LIST OF TABLES

NOMENCLATURE

A_β	reactive surface area of mineral β
$A_{i,\beta}$	initial surface area
a_k	activity of component k
$A_{t,\beta}$	surface area at time "t" of mineral β
$A_{s,\beta}$	total surface area of mineral β
b	body force per unit mass of fluid
c_r	rock compressibility
$E_{\alpha\beta}$	activation energy for reaction mineral β
G	shear modulus
K	bulk modulus
k	permeability
$K_{eq,\beta}$	chemical equilibrium constant for mineral reaction.
k_β	rate constant of reaction of mineral β
$k_{\beta,\ reference}$	reaction rate constant for mineral reaction β at the reference temperature
$k_{\beta,Tres}$	reaction rate constant at reservoir temperature
k_i	initial permeability
k_t	permeability at time "t"
N^0_β	total moles of mineral β per bulk volume initially
N_β	total moles of mineral β per bulk volume at current time
p_{ref}	reference pressure
p	pressure at time "t"
Q_f	fluid flow rate
Q_β	activity product for mineral chemical equilibrium reaction
R	universal gas constant
$r_{k\beta}$	mineral reaction rate per unit bulk volume of rock when pore space is filled with water.
r_β	rate of mineral reaction
Ti	reference temperature (usually 298.15 K or 25°C)
T_{res}	reservoir temperature0

$VF_{\beta,i}$	initial volume fraction of mineral β
$VF_{\beta,t}$	volume fraction at time "t" of mineral β
$v_{k,\beta}$	stoichiometry coefficients
α	Biot's constant ($\varphi \leq \alpha \leq 1$)
ε_v	volumetric strain
ε	strain tensor
ϕ_t	porosity at time "t"
ϕ_i	initial porosity
ϕ^*	reference porosity without mineral dissolution/precipitation
ϕ_{min}	reference porosity including mineral dissolution/precipitation
ϕ_t	reservoir porosity
ϕ	true porosity
σ'_{ij}	effective stress tensor
δ_{ij}	Kronecker delta
μ	fluid viscosity
ρ_f	density of fluid

Chapter 1: INTRODUCTION

1.1 Background

Over the past three decades, global warming has become more apparent, with the earth's mean surface temperature increasing by about 0.8°C (1.4° F) (Olivier et al., 2012). The primary source for such a major change in the temperature is the increase in the atmospheric concentration levels of greenhouse gases. Greenhouse gases (GHG) are the by-products of human activities which includes burning of fossils fuels and deforestation, among others. Greenhouse gases absorb and emit infrared radiations, which leads to an increase in atmospheric temperature (Ming et al., 2014). Based on the global emission records for the past three decades, it has been reported that carbon dioxide (CO_2) is the major contributor (9%-26%) to global warming besides other greenhouse gases such as methane (CH_4), nitrous oxide (N_2O), and fluorinated gases (FC's) (Lee et al., 2013).

In the United States of America, CO_2 alone contributes to almost 80 % of the total greenhouse gas emissions (NRC, 2011). In 2011, CO_2 global emissions have increased by 3%, reaching a record high of 34 billion tonnes (Olivier et al., 2012). As of December 2013, it has been reported that the CO_2 concentration levels in the atmosphere has increased to 396 parts per million (ppm), which translates to an increase of 2.07 ppm per year in the last decade (www.CO_2NOW.org). Since fossil fuels provide for almost 75% of the world's energy and are likely to meet energy demands for atleast a few more decades, it is believed that CO_2 emissions from human activities are likely to increase continuously (Dhakal, 2010; Gu, 2009). Scientific studies have indicated that if the cumulative emissions in the next three decades are kept below 1,500 billion tonnes, then the average global rise in temperature can be limited to 2° C (1.11° F) (Olivier et al., 2012). It is important to reduce CO_2 emissions in the atmosphere as it not only controls the greenhouse gas effects, but also stabilizes the ecosystem (Gu, 2009). There are several ways to reduce CO_2 emissions into the atmosphere, which include energy conversion and geological sequestration, among others (Audigane et al., 2007; Bachu et

al., 2007; U.S.D.O.E, 2012). Energy conversions involve the efficient usage of energy by using low-carbon or carbon-free fuels, and technologies such as renewable energy sources which include solar, wind, and biomass fuels (Audigane et al., 2007; Bachu et al.,2007;U.S.D.O.E, 2012). Geological sequestration of CO_2 involves the storage of CO_2 in deep geological formations such as saline aquifers, depleted oil or gas reservoirs, and unmineable coal seams (Audigane et al., 2007; Bachu et al., 2007; Cantucci et al., 2009; CO2CRC, 2008; Hosa et al., 2011).

1.2 Geologic Sequestration of Carbon Dioxide

Geologic sequestration involves the process of capturing CO_2 released into the atmosphere from various sources such as high CO_2 natural gas fields, liquefied natural gas (LNG), or coal-fired power stations. CO_2 is then transported through pipelines and injected into geological formations, such as depleted oil or gas reservoirs, coal seams, deep oceans, basalt formations, shale formations, and saline formations for long-term storage (Audigane et al.,2007; Bachu et al., 2007; Cantucci et al., 2009; CO2CRC, 2008; Hosa et al., 2011). These subsurface geological units are believed to have both, large storage capacities and the ability to securely store CO_2. A brief description of the CO_2 storage in three main geological sequestration sites is given below.

1.2.1 Oil and Gas Fields

CO_2 can be stored in oil and gas reservoirs when they have been depleted, or can be used for enhance oil or gas recovery operations in fields that are still producing (Cantucci et al., 2009; CO2CRC, 2008; Hill et al., 2013). Such reservoirs are usually porous rock formations overlain by layers of low permeability rock(s) acting as a seal. It has been reported by the National Petroleum Council (NPC) that approximately 3,000 million cubic feet per day of CO_2 are presently being injected for enhanced oil recovery (EOR), producing about an additional 3 million barrels of oil per day (Hill et al., 2013; NPC, 2011). The advantage of selecting depleted oil or gas reservoirs for CO_2 storage is that they have both, a proven record of hydrocarbon containment for millions of years, as

well as the availability of well established geologic and engineering data required for detailed site characterization (IPCC, 2005). A few projects related to CO_2 storage in oil and gas reservoirs, reported in the literature include the Weyburn Project, Canada (Cantucci, et al., 2009; Uddin et al., 2013), West Pearl Queen site, USA (Cooper et al.,2008; Pawar et al., 2004; Westrich et al.,2001), K12-B gas field, North Sea (van der Meer et al., 2004; Vandeweijer et al., 2011), and the CO_2CRC Otway Basin Project, Australia (Sharma and Cook, 2007).

1.2.2 **Unmineable Coal Seams**

Coal seams are also considered to be another option for CO_2 storage due to their long-term storage potential and enhanced coalbed methane production (Day et al., 2011; Garnier et al., 2011; White et al., 2005). CO_2 storage in coal seams is controlled by adsorption onto the coal micropore surface as opposed to storage in the rock pore space, with more than 95% of CO_2 stored as an adsorbed phase (Dutta et al., 2011; Perera et al., 2012). Since coal has more affinity towards CO_2, it releases methane (CH_4) and adsorbs CO_2 during the storage process (Busch and Gensterblum, 2011; Harpalani et al., 2006; Ottiger et al., 2008). Several pilot studies, which include both site characterization and field monitoring activities using titlmeters and tracers, have been conducted to demonstrate the potential of CO_2 sequestration in unmineable or depleted coal seams (Siriwardane et al., 2011; Wageningen et al., 2009; Winschel et al., 2010).

1.2.3 **Saline Aquifers**

Saline aquifers are reported to have large storage capacities, exceeding 100 Mega tonnes (Eke et al., 2011; Hosa et al., 2011; Liu et al., 2011). Saline aquifers suitable for CO_2 storage are deep sedimentary formations, saturated by water whose salinity is above the permissible limits of water that is useful for human consumption, agricultural or industrial use. Some of the industrial-scale projects which involve CO_2 injection in deep saline aquifers include the Sleipner project in North Sea (Chadwick et al., 2004; Torp and

Gale, 2004), the In Salah project in Algeria (Idling and Ringrose, 2009; Rutqvist et al., 2009; Shi et al., 2012), the Gorgon project in Australia (Hosa et al., 2011; Michael et al., 2011), and the Snøhvit project in Norway (Eiken et al., 2011). Figure 1-1 shows some of the major saline aquifers in the United States of America (Szulczewski et al., 2012).The injection of CO_2 into saline aquifers occurs at supercritical conditions, which generally exist in deep aquifers where CO_2 has high density and solubility in the aqueous phase (Eke et al., 2011; Nghiem et al., 2004). Under such pressure and temperature conditions, CO_2 occupies less volume enabling more storage (Eke et al., 2011). Saline aquifers are usually overlain by a low permeability overburden layer(s) that can trap CO_2 for long geological periods. The current research work presented in this report mainly deals with the storage of CO_2 in deep saline aquifers at a hypothetical sequestration site. More details of the study are presented in later sections.

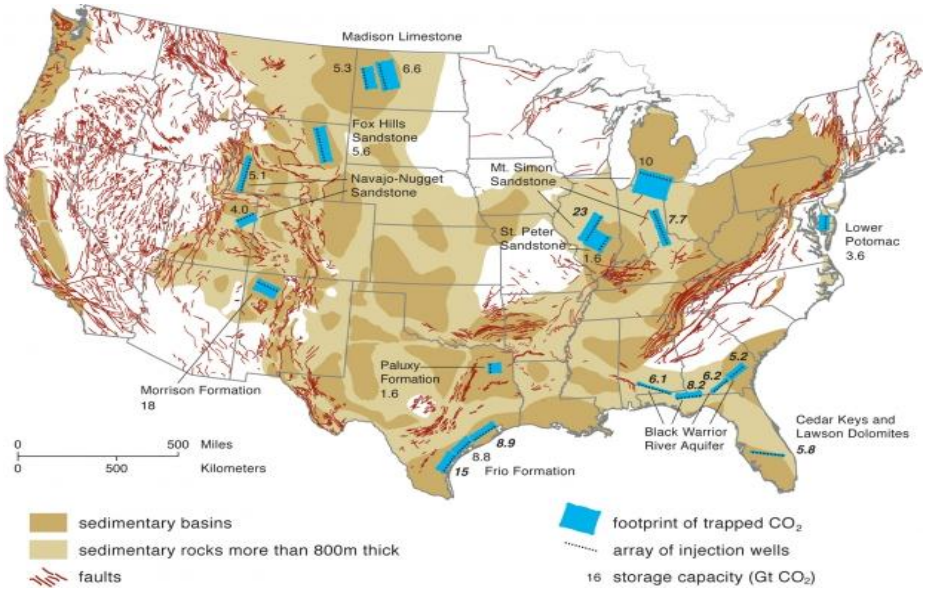

Figure 1-1: Major saline aquifers in the USA (Adapted from Szulczewski et al., 2012).

1.3 Problem statement

While the impermeable caprock layer(s) in the overburden provide(s) the primary trap for injected CO_2, other trapping mechanisms such as solubility, residual, ionic or

mineral trapping, help contribute to safe storage of CO_2 in saline aquifers (Bachu et al., 1994; Bachu, 2000; Basbug and Bennion, 2005; Dilmore et al., 2008; Doughty, 2010; Fang et al., 2010; Goodman et al., 2011; Liu and Maroto-Valer, 2011). The flow behavior of CO_2 in deep saline aquifers was demonstrated by a few long-term, large-scale field projects. The understanding gained from these field studies are reported in published literature (Arts et al., 2008; Hosa et al., 2011; Michael et al., 2010; Morris et al., 2011). Several numerical modeling studies were also performed to understand the flow behavior of CO_2 in saline aquifers due to different trapping mechanisms at different time scales (Bachu et al., 1994; Bachu, 2000; Basbug and Bennion, 2005; Dilmore et al., 2008; Doughty, 2010; Fang et al., 2010). More details of CO_2 trapping mechanisms are given in Chapter 3 of this report

Geochemical reactions that occur over longer period of time have a significant influence on trapping mechanisms in saline aquifers. Geochemical reactions at reservoir conditions depend upon several factors such as temperature, pressure, water salinity, rock mineralogy, fluid injection rates, and time-scale of geological storage (CO2CRC, 2008; Fang et al., 2010; van der Meer, 2005). Depending upon the nature and scale of geochemical reactions, CO_2 may interact with the formation water, the reservoir rock, and the overburden caprock layer(s). These interactions may alter the rock properties such as porosity and permeability (Luquot and Gouze, 2009; Gaus et al., 2008; Yoo et al., 2013). Leakage pathways may be created in the form of fractures in the wellbore cement, and along wellbore-cement-rock interfaces influencing CO_2 injectivity, storage capacity, and seal integrity (Carroll et al., 2012; Jun et al.,2013; Mason et al., 2013; Walsh et al., 2012). Several experimental and numerical studies have shown that geochemical reactions may have an influence on fracture geometry and hydrodynamic properties of reservoir rock (Andreani et al., 2008; Deng et al., 2013; Ellis et al., 2011; Gherardi et al., 2007).

During CO_2 injection, fluid pressure increases in the reservoir and the surrounding layers. This leads to a reduction in effective stresses and an increase in vertical displacements in the overburden. Excessive surface deformation can lead to failure of

well casings, pipelines, and other underground utilities (Khakim et al., 2012). Moreover, excessive deformations may also cause significant damage to surface structures. The presence of geologic features such as a caprock fracture or fault may cause CO_2 leakage into the overburden layers, which may lead to geomechanical instability (Keating et al., 2013). Some geomechanical issues related to large-scale CO_2 injection in saline reservoirs have been reported recently (Goodarzi et al., 2012; Morris et al., 2011;Rutqvist et al., 2008; Rutqvist, 2011;Siriwardane et al., 2013; Tran et al., 2009; Vilarrasa et al.,2011). In addition to coupled fluid flow and geomechanical modeling of CO_2 storage, field monitoring studies using tiltmeters and interferometric synthetic aperture radar (InSAR), are being carried out to measure ground deformations with a precision in the sub-millimeter range over large areas (Khakim et al., 2012; Rutqvist et al., 2010; Siriwardane and Gondle, 2011). Such ground monitoring technologies have been used in the past at the Belridge and Lost Hills oil field (California, USA), and the InSalah site located in Krechba, Algeria (Mathieson et al., 2011; Morris et al., 2011; Patzek et al., 2001). Although ground monitoring technologies provide great insight into the magnitudes and patterns of ground displacements (Siriwardane et al., 2013), and the fluid flow behavior, it is important to develop advanced modeling methods as the time-scale for evaluation of storage safety is usually in terms of hundreds and thousands of years. Such modeling studies require coupling between multiphase fluid flow, geomechanics, and the consideration of geochemical processes (Kvamme and Liu, 2009). Limited studies have been reported in the published literature with reference to the geomechanical response associated with the time-dependent geochemical reactions (Kvamme and Liu, 2009; Walsh et al., 2012; Xiong et al., 2013; Zhang, 2013). In the research study presented in this report, the influence of geochemical processes on the geomechanical response is investigated.

1.4 Research objectives

The objective of this study is to investigate the influence of geochemical processes on the geomechanical response of overburden during CO_2 injection into saline

aquifers. As a part of this study, multiphase fluid flow models coupled with geomechanics and geochemical processes were used to investigate the following:

- Influence of geochemical processes on petrophysical properties, such as porosity and permeability of the target formation.
- Transient pressure buildup during and after CO_2 injection
- Ground response during long-term (up to 1,000 years), large-scale (up to10 million metric tons per year) injection of CO_2.
- Influence of a damage zone around the wellbore on CO_2 leakage and ground displacements.

Subsequent chapters present the research work performed to achieve the above objectives. Chapter 2 provides a review of ~~s~~ recent research work on the potential of CO_2 storage and various issues related to CO_2 sequestration in saline aquifers as reported in the literature. Chapter 3 presents different CO_2 trapping mechanisms in saline aquifers. Mathematical details and numerical methodology of coupled fluid flow, geomechanical, and geochemical modeling of CO_2 sequestration in saline aquifers is presented in Chapter 4 and Chapter 5. A validation of the coupled fluid flow, geomechanics and geochemical modeling presented in Chapter 4 and Chapter 5 is presented in Chapter 6. The numerical methodology used to investigate the geomechanical response during large-scale CO_2 injection is presented in Chapter 7. This chapter also contains the details of the numerical modeling work performed to determine the influence of a damage zone around the wellbore on CO_2 leakage into the overburden. A summary and conclusions of this research work are presented in Chapter 8.

Chapter 2: CO_2 SEQUESTRATION IN DEEP SALINE AQUIFERS

2.1 Introduction

Saline aquifers are deep geological formations which are spread over large geographic areas making them an excellent candidate for CO_2 sequestration in terms of storage capacity (Bergman and Winter, 1995; Birkholzer et al., 2009). North America is a very active region for carbon capture and storage (CCS) development with more than 10 demonstration and small-scale projects (Hosa et al., 2011). Some of the major onshore and offshore sequestration projects all around the world include the In Salah project, Algeria (17 million tons) (Chadwick et al., 2008;Hosa et al., 2011; IEA GHG, 2008; Michael et al., 2010; Riddiford et al., 2003; Ringrose et al., 2009), the Sleipner project, North Sea (25 Mt) (Chadwick et al., 2004; Chadwick et al., 2008;Hosa et al., 2011; IEA - GHG, 2008; Michael et al., 2010), Snohvit, Norway (23 Mt) (Eiken et al., 2011), and the Gorgon project, Australia (129 Mt) (Hosa et al., 2011; Michael et al., 2010). Table 2.1 provides a list of projects all around the world with the estimated total CO_2 storage capacity. A brief description of some of the major CO_2 sequestration projects, as listed in Table 2.1, is provided in the following sections.

Table 2-1:World wide CO_2 sequestration projects (Modified from Hosa et al.,2010)

Project Name	Location	Total Estimated CO_2 Storage Capacity (Mt)	Purpose
MRCSP R.E. Burger	USA	0	Small Scale Technical Development Projects
MRCSP East Bend	USA	0.0010	
Frio	USA	0.0016	
WESTCARB Cholla	USA	0.0018	
WESTCARB Rosetta	USA	0.0020	
SECARB Escatawpa	USA	0.0028	
Nagaoka	Japan	0.0104	
MRCSP Gaylord	USA	0.0600	
Ketzin	Germany	0.0600	Small Scale Technical Development Projects
Total Lacq	France	0.1500	
PCOR Zama	Canada	0.2500	
MGSC Decatur	USA	1.00	Large-Scale Industrial Feasibility Projects
SECARB Cranfield	USA	2.10	
K12-B	Netherlands	8.00	
In Salah	Algeria	17.00	
Weyburn	Canada	20.00	
Snohvit	Norway	23.00	
Sleipner	Norwegian North Sea	25.00	
Rangely	USA	26.00	
Gorgon	Australia	129.00	

2.2 Review of a major CO_2 storage sites

2.2.1 The Sleipner Project

The Sleipner project (Central North Sea) run by Statoil was one of the first, large-scale, and long-term CO_2 injection programs initiated to investigate the effectiveness of CO_2 storage over long periods of time in an aquifer (Arts et al., 2008) . In the vicinity of the Sleipner field is the Utsira sandstone reservoir which has a very high porosity (30-40%), permeability (1-8 Darcy), and a weakly consolidated sandstone (Arts et al., 2008; Hosa et al., 2011). CO_2 was injected into the saline aquifer (Utsira sand), at a depth of 1,012 m below the sea level. An injection rate of 1 Mt/year was achieved since 1996. Overlying the thick sandstone reservoir (250 m) is the Nordland Formation (250-330 m) which consists of layers of shale, clayey silt or silty sand. The monitoring of the CO_2 plume in the Utsira formation has been achieved using 3D seismic data, electromagnetic surveys, and time-lapse seafloor gravity surveys (Arts et al., 2008). The time lapse 3D seismic data were acquired prior to injection at 1994 and then published 7 times since 1999 with around 11.4 million tonnes of CO_2 in the reservoir at the last time of the last survey (Singh et al., 2010). The 3-D seismic surveys and time-lapse gravity surveys show that the CO_2 has reached the top of the reservoir due to buoyancy within 3 years from start of injection (Arts et al., 2008). From the above monitoring studies it was evident that the caprock acts as an effective seal and prevents CO_2 migration into the overburden layers (Torp and Gale, 2004). A few numerical and field studies have been reported in the literature related to the geochemical and geomechanical response due to CO_2 injection at the Sleipner field. A brief discussion of such studies is given below.

Gaus et al., (2005) performed numerical modeling studies to investigate the long term effects of geochemical reactions on the porosity of the cap rock during CO_2 injection into the Utsira saline formation (Gaus et al., 2005). Reactive transport modeling including reaction kinetics was performed using PHREEQC (V2.6). Details of the mineralogy, mineral kinetic reaction data, and brine compositions used in the models for the Utsira formation and the Nordland formation can be found elsewhere (Gaus et al.,

2005). Results from this modeling study have shown that diffusion of CO_2 in the caprock is a slow process. It was reported that after 3,000 years there was an increase in the levels of dissolved CO_2 in the lower 10 m of the 250 m thick caprock. It was also reported that there was a small change in the caprock porosity due to geochemical reactions, but this was limited to the lower portion of the caprock.

Audigane et al., (2007) used 2D radially symmetric reactive transport models to simulate a 25 years of CO_2 injection into the Utsira saline formation followed by a 10,000 year storage period. Reactive transport modeling was performed using TOUGHREACT. The evolution of structural, dissolution, and mineral trapping of injected CO_2 was considered in the model. Results from the numerical study have shown that the geochemical reactivity of the Utsira formation was low and had little significance on the porosity of the reservoir and cap rock.

Chadwick et al., (2012) used 4D seismic datasets to measure the changes in pressure in the Utsira sand. The small time-lapse travel time changes were consistent with the pressure increase of less than 100 kPa at a distance between 500 m and 4,000 m from the injection point.

Rutqvist et al., 2007 performed coupled reservoir-geomechanical simulations to assess the potential for tensile and shear failure caused by CO_2 injection. In this study, the numerical model geometry was based on the Sleipner's Utsira Formation (Chadwick et al., 2004). In this study, the potential for mechanical failure associated with the upward migration of the CO_2, including associated buoyancy effects on the pressure column in relation to the depth dependent insitu stress field were analyzed.

No direct (geodetic or microseismic) or indirect measurements (numerical models) of the geomechanical deformations by CO_2 injection have been reported in the literature for the Sleipner site. However, it is believed that with the estimated small pore pressure change of 100 kPa, it is unlikely that significant geomechanical deformations will have occurred (Verdon et al., 2013).

2.2.2 **The In Salah Project**

The In Salah Gas Project (Algeria) run jointly by BP, Sonatrach and StatOil is one of the large-scale CO_2 storage projects in a gas reservoir (Hosa et al., 2011). The project involves re-injecting the CO_2 obtained from the natural gas produced from several field into the water leg of the Krechba reservoir. The target reservoir is a 20-m thick, fractured sandstone at depths of 1,850 m to 1,950 m with an average porosity of 15% and permeability of 5 mD (Hosa et al., 2011; Mathieson et al., 2010; Verdon et al., 2013). CO_2 injection was initiated in 2004, while gas production was still active (Verdon et al., 2013). CO_2 was injected at 1.2 Mt/year, and to date 3.85 Mt has been stored (Verdon et al., 2013). The top seal is a thick caprock layer (950 m) which consists of a sequence of mudstones (Verdon et al., 2013). A brief discussion of the geochemical and geomechanical responses associated with the CO_2 injection at the In Salah site is presented below.

McNab and Carroll (2011) performed reactive transport modeling using PHREEQC to investigate the influence of geochemical reactions that take place between wellbore cement, formation rock, and injected supercritical CO_2 on the formation rock porosity and permeability. The influence of geochemical interactions on the sealing of fractures in the formation or wellbore cement was also investigated. More details of the study can be found elsewhere (McNab and Carroll, 2011). Results from the numerical models have shown that the porosity of cement changes due to shallow carbonation of cement along the interface. However, the change in formation rock porosity was insignificant.

Bissell et al., (2011) performed coupled fluid flow and geomechanics modeling to match field history data of gas production, CO_2 injection, and geomechanical displacements. Modeling results have shown an increase of 18,000 kPa to 30,000 kPa in the pore pressure at the injection points. The pore pressure at the producing crest of the reservoir was reduced to 10,000 kPa. Deflandre et al., (2013) used available field data to compute surface displacements by coupling 3D fluid flow and geomechanical modeling.

Computed surface displacements matched well with the measurements obtained through InSAR imaging measurements. Similar studies were performed by Rutqvist et al., (2010). More details on the CO_2 sequestration monitoring and verification technologies applied at In Salah site can be found elsewhere (Mathieson et al., 2011; Oye et al., 2013).

2.2.3 **The Weyburn Project**

The Weyburn oilfield is a commercial-scale, CO_2-enhanced oil recovery (CO_2-EOR) project located in the Saskatchewan Province, Canada. The Weyburn oilfield covers an area of 80,000 km^2. Most of the hydrocarbon in the area is produced from the Middle Beds of Mississipian Madison Group (Hosa et al., 2011). The reservoir consists of a densely fracture limestone with porosity ranging from 8-20% and a permeability of about 10-300 md. This oilfield has been under production since 1955 and since production has decline steadily over the years, alternate solutions to enhance oil recovery such as CO_2 injection driven production has been initiated in the year 2000. The estimated CO_2 storage capacity of the reservoir is about 20 Mt. About 3 billion m^3 of supercritical CO_2 has been injected into the Weyburn reservoir since 2000 with an injection rate of 5,000 ton/day (Cantucci et al., 2009)

Durst et al., (2003) performed geochemical modeling studies to investigate the CO_2 storage capacity and potential for long-term mineral trapping in the Weyburn reservoir. Numerical modeling was performed using PHREEQC code. Modeling results have shown that the quick dissolution of carbonates occurs in the initial stages which cause an increase in the amount of dissolved carbon and decreases the amount of carbon in mineral form (Czernichowksi-Lauriol et al., 2006). With time, CO_2 was trapped in the mineral form due to formation of dawsonite and siderite, thus reducing carbon concentration in the solution. It was predicted that about 50% of the dissolved brine was trapped in mineral form after 1,000 years. Modeling results also showed that there was no significant change in porosity due to geochemical reactions (Czernichowksi-Lauriol et al., 2006).

Cantucci et al., (2009) performed geochemical modeling using PHREEQC (V2.14) code to investigate the dissolution/ precipitation processes of the Weyburn brine over 100 years of CO_2 injection. Baseline mineralogy and brine properties used in the modeling study can be found elsewhere (Cantucci et al., 2009). Modeling results have shown that primary reactions such as CO_2 and carbonate dissolution occur in the first year of CO_2 injection. Results also suggested that CO_2 can be safely stored by solubility of CO_2 into brine and mineral trapping via precipitation of dawsonite.

Verdon et al., (2011) performed geomechanical modeling accounting for the initial reservoir depletion during oil production, followed by injection of CO_2 and oil production during EOR process. From the numerical analyses, Verdon et al., 2011 reported that the deformations caused during production and injection, cause stress changes which are transferred into the overburden. This stress transfer into the overburden lead to an increase in shear stress above production wells and is believed to be a primary cause for the microseismic events located in the overburden. Based on the microseismic activity data available at the site, it is believed that the induced deformations during oil production and CO_2 injection did not create fluid flow pathways into the overburden. Thus, it was concluded that these geomechanical deformations do not pose a risk to storage capacity.

2.2.4 **The Decatur Project**

The Mt.Simon Sandstone is located in the Central Illinois basin which covers a major portion of Illinois, and extends into south-western Indiana and western Kentucky (Medina et al., 2011). The injection zone at the Decatur site, Illinois is the Cambrian-age Mt.Simon sandstone is at a depth of 1690 m to 2,184 m below the ground surface with a gross thickness of 464 m (ADM, 2012; Hosa et al., 2011; U.S.EPA, 2012). The sandstone formation primarily consists of quartz, although some intervals contain more than 15% feldspar (ADM, 2012; U.S.EPA, 2012**).** A widespread low-permeability sealing unit, Cambrian Eau Claire formation overlies the Mt.Simon sandstone. The Mt.Simon

sandstone rests unconformably on the Precambrian granitic basement which occurs at a depth of 2184 m. As part of the Midwest Geological Sequestration Consortium (MGSC) initiative, ~ 1 million U.S tons of CO_2 was injected over a period of 3 years at the Decatur site (Liu et al., 2011; Zhou et al., 2010).A brief summary of experimental and numerical studies associated with the CO_2 storage in Mt.Simon sandstone is discussed below.

Numerical simulations were performed by Balashov et al., (2012) to investigate the influence of diffusive-reactive partitioning of CO_2 across the interface of sandstone rock in a saline aquifer (Mt.Simon sandstone) between supercritical CO_2 and brine. A simple baseline mineralogy based on sandstones derived from continental block lithologies were used in the geochemical simulation. It was reported that in the first 30 years of the process, CO_2 was trapped in the aqueous form ($CO_{2\ (aq)}$) with very little mineral trapping. It was also reported that the process for mineral equilibration continues for several thousands of years and changing the reactions rate constants had little effect on the geochemical reactions. Based on this study, it was concluded that the most important mineral-brine reactions are those that consume the maximum H^+ ions, which lead to a reduction in pH. A reduction in pH would lead to more dissolution of CO_2 into brine.

Carroll et al., (2012) performed both experimental and numerical studies to measure the geochemical reactivity of the Mt.Simon sandstone and Eau Claire shale caprock at CO_2 storage conditions present at the Archer Daniel's Midland (ADM) demonstration site, Illinois Basin. An important finding of this study was the identification of reactive iron clay minerals under CO_2 storage conditions in the Mt.Simon sandstone and the Eau Claire shale formation. It was reported that the change in iron clay concentration may be a source of long-term mineral trapping of CO_2, which could have significant influence on the reservoir and seal permeability.

Chapter 3: CO_2 TRAPPING IN SALINE AQUIFERS

3.1 Introduction

Geological sequestration of CO_2 in saline aquifers depends on multiple trapping mechanisms. When CO_2 is injected, it migrates through the porous media away from the injection well and moves upward due to buoyant forces. Tight, impermeable caprock layer(s), which overlie the target aquifer, provides the primary trap for injected CO_2 into a deep saline aquifer. In addition to tight, impermeable caprock layer(s) in the overburden, several other trapping mechanisms in saline/brine aquifers that occur over a period of time contribute to the storage of CO_2. Some of these trapping mechanisms in saline aquifers include structural/stratigraphic, residual, hydrodynamic, solubility, ionic, and mineral trapping (Bachu et al., 1994; Ennis-King and Patterson, 2002; Gunter et al., 1993; Holtz, 2002; Flett et al., 2005; Perkins and Gunter, 1995).

3.2 Structural/stratigraphic trapping

When CO_2 is injected into a deep saline aquifer, CO_2 gets physically trapped as free gas (immiscible CO_2) or supercritical fluid into geologic media (Bachu, 2007; Nghiem et al., 2004). The free-phase CO_2 rises to the top until it reaches a tight, impermeable caprock layer, and some part of the injected CO_2 dissolves into formation water becoming CO_2-rich brine (Bachu et al., 1994). The free-phase, immiscible CO_2 which rises upwards due to buoyancy (due to differences in the density of CO_2 and formation water), and gets physically trapped in structural or stratigraphic traps (Bachu, 2007; CO2CRC, 2008).Typical traps include anticlinal structures, folds, faults, salt domes, and stratigraphic traps such as depositional pinch outs (CO2CRC, 2008).

3.3 Residual trapping

The free-phase, immiscible CO_2 also gets physically trapped and becomes immobile in the porous geologic media by capillary forces, which is known as residual-gas trapping (Basbug et al., 2005; Bachu, 2007). At the tail of the migrating CO_2 plume, imbibition processes are reported to be dominant as the formation water (wetting-phase) displaces the immiscible CO_2 (non-wetting phase) (CO2CRC, 2008). Capillary pressure forces become dominant when the concentration of the CO_2 falls below a certain level. The dominant capillary pressure forces trap the CO_2, thus leaving a trace of residual, immobile CO_2 behind the plume as it migrates upward (Ennis-King & Paterson, 2000; Flett et al., 2005; Holtz, 2002; Juanes et al., 2006).

3.4 Hydrodynamic trapping

Generally, fluid flow velocities are low in saline aquifers (CO2CRC, 2008). For this reason, the injected CO_2 in the subsurface may take long periods of time before it reaches the bottom surface of the overlying caprock (Bachu et al., 2007; CO2CRC, 2008; Fang et al., 2010). This geological time-scale trapping process of injected CO_2 in the subsurface is known as hydrodynamic trapping (Bachu et al., 1994; CO2CRC, 2008; Fang et al., 2010).

3.5 Solubility trapping

In addition to the physical trapping of injected CO_2, chemical trapping occurs when CO_2 gets dissolved in the formation water. CO_2 dissolution into the formation water is referred to as solubility trapping (Bachu et al., 2007). A weak carbonic acid is produced when CO_2 dissolves in the formation water (solubility trapping), which rapidly dissociates into bicarbonate ions (ionic trapping) (Eke et al., 2011; Xu et al., 2001). The reaction steps for CO_2 dissolution and subsequent dissociation of weak carbonic acid into carbonate species are shown in eq's (3.1) and (3.2) as given below:

$$CO_2\ (g) + H_2O = H_2CO_3\ (solubility\ trapping) \quad \text{.....} (3.1)$$

$$H_2CO_3 = H^+ + HCO_3^- \quad (ionic\ trapping) \quad \text{.....} (3.2)$$

Formation temperature, pressure, water salinity, and time-scale of geological storage are important factors that contribute to the solubility or dissolution of CO_2 (CO2CRC, 2008; Fang et al., 2010). CO_2 solubility increases with an increase in fluid pressure and decreases with an increase in formation temperature and water salinity (Fang et al., 2010; Jun et al., 2013; Ji and Zhu, 2012). When CO_2 dissolves in the formation water, the density of CO_2-enriched brine increases and the dissolved CO_2 sinks to the bottom of the reservoir. The time-scale for complete dissolution is predicted to occur on a scale of hundreds to thousands of years (Ennis-King & Paterson, 2002).

3.6 Mineral trapping

The dissolution of CO_2 in the formation water decreases the pH of the brine (i.e., increases acidity), which lead to geochemical reactions between CO_2-enriched brine and the rock matrix resulting in the formation of stable carbonate materials such as Calcite ($CaCO_3$) (CO2CRC, 2008; Eke et al., 2011; Gaus et al., 2008). This process is known as mineral trapping. The geochemical reactions associated with dissolution of primary rock minerals, and dissolved bicarbonate ions reacting with divalent cations (such as calcium (Ca^{2+}), magnesium (Mg^{2+}), and iron (Fe^{2+})) to precipitate new carbonate minerals are shown in eq's (3.3) through (3.6) as given below (Xu, 2001):

$$Ca^{2+} + HCO^{3-} = CaHCO_3^+ \quad \text{.....} (3.3)$$

$$HCO^-_3 + Ca^{2+\ -} = CaCO_3\ (solid) + H^+ \quad \text{.....} (3.4)$$

$$HCO^-_3 + Mg^{2+\ -} = MgCO_3\ (solid) + H^+ \quad \text{.....} (3.5)$$

$$HCO^-_3 + Fe^{2+\ -} = FeCO_3\ (solid) + H^+ \quad \text{.....} (3.6)$$

It is believed that many of these newly precipitated carbonate minerals, such as calcite ($CaCO_3$), dolomite [$CaMg(CO_3)_2$], and siderite ($FeCO_3$) remain stable for significant time periods, enhancing CO_2 permanence (Gunter et al., 1993; Bachu et al., 1994; Perkins & Gunter, 1995; CO2CRC, 2008). It is also reported that silicastic reservoirs, especially the calcium, magnesium, or iron-rich reservoirs are more favorable for mineral trapping compared to other carbonate reservoirs (CO2CRC, 2008). Mineral trapping is formation specific and mainly depends on factors such as mineralogical composition of geologic formation, chemical composition of formation brine, formation temperature and pressure, and fluid flow rate (CO2CRC, 2008; Gunter et al., 2004). Geochemical reactions may occur soon after injection or over time scales of hundreds or thousands of years (Hu et al., 2013; Jun et al., 2013). Figure 3-1 shows a simple representation of the change of dominant trapping mechanisms and increasing CO_2 storage security with time.

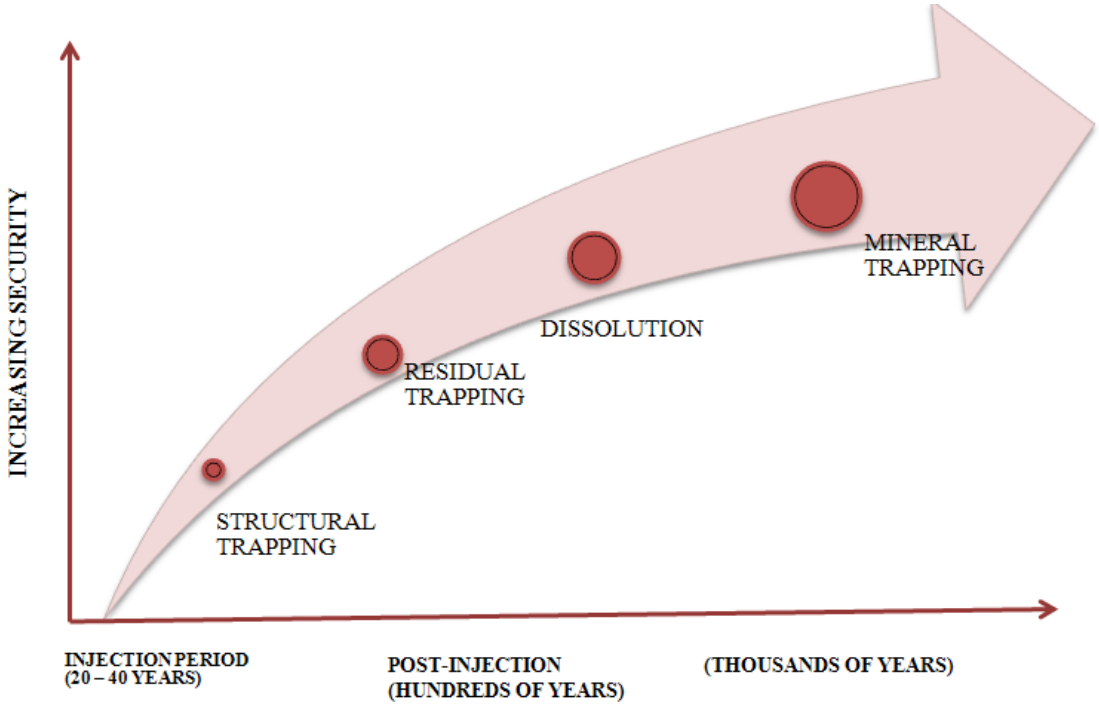

Figure 3-1:CO_2 storage security.

3.6.1 **Influence of mineral trapping on porosity and permeability**

When a fluid is injected into the reservoir, the injected fluid displaces the formation water depending on rock properties, and the fluid properties of connate water and injected fluid (van der Meer, 2005). When supercritical CO_2 is injected into an aquifer, it rises to top of the aquifer and moves through the pore structures of the formation rock due to low density and viscosity (van der Meer, 2005). Interaction between CO_2, brine, and formation rock may have an influence on porosity and permeability of the formation rock (Luquot and Gouze, 2009). These geochemical reactions depend on several factors such as reservoir temperature, pressure, water salinity, rock mineralogy and texture, fluid injection rates, and time-scale of geological storage (CO2CRC, 2008; Fang et al., 2010; van der Meer, 2005).

The porosity and the permeability near the injection region increases due to rapid dissolution of carbonates at high pressures, and decreases further from the well along the flow direction due to carbonate precipitation (van der Meer, 2005). Excess dissolution of rock and CO_2 interaction with overburden caprock materials may alter the caprock properties and create high permeable zones (e.g., in carbonates) and could elevate the risk of CO_2 leakage (van der Meer, 2005). While the excess rock dissolution increases porosity, permeability, and injectivity, it could also lead to wellbore instability and subsidence if the integrity of formation rock is compromised (Luquot and Gouze, 2009). Also, it is reported that the precipitation of dissolved CO_2 into new carbonate materials (due to geochemical reactions) may significantly reduce the porosity, permeability and cause serious injectivity issues (Luquot and Gouze, 2009).

Chapter 4: FLUID FLOW AND GEOCHEMICAL MODELING OF CO_2 SEQUESTRATION IN SALINE AQUIFERS

4.1 Introduction

In this study, numerical models were constructed to investigate the influence of geochemical processes on the fluid flow behavior and reservoir rock properties during CO2 sequestration in saline aquifers. These numerical models consider:

1. Vertical migration of CO_2 due to buoyancy towards the impermeable cap rock
2. Dissolution of CO_2 in formation brine
3. Mineral dissolution and precipitation due to the interaction between dissolved CO_2 and formation rock
4. Changes in rock porosity due to mineralization

In this study, 'CMG-GEM' was used to perform the modeling work. 'CMG-GEM' is a commercially available advanced compositional simulator developed by Computer Modeling Group (CMG, 2012).

4.2 Modeling of CO_2-Brine-Rock Interaction

When CO_2 is injected into a saline aquifer, some of it dissolves in the aqueous phase. It is assumed that the gaseous and aqueous phase exist in a thermodynamic equilibrium (Nghiem et al., 2004). Such equilibrium is attained when the dissolution rate of CO_2 in the aqueous phase is quick. In this study, the Peng-Robinson equation of state was used to calculate the PVT properties of CO_2 (Peng and Robinson, 1976). Henry's Law was used to calculate solubility of CO_2 in the aqueous phase. Henry's constants depend on pressure, temperature, and salinity (Li and Nghiem, 1986). Henry's constants

are computed internally within the computer code using Harvey (1996) correlations. The aqueous phase density is calculated using Rowe and Chou (1970) correlation, which is function of pressure, temperature and salinity. Geochemical reactions in a saline aquifer occur between components in the aqueous phase, and also between components in the aqueous phase and minerals. The intra-aqueous reactions taking place during mineral dissolution and precipitation are rapid when compared to geochemical reactions (Nghiem et al., 2004). Mineral dissolution and precipitation are rate-dependent reactions and can be computed using the rate law as shown below (Bethke, 1996):

$$r_\beta = A_\beta\, k_\beta \left(1 - \frac{\prod_{k=1}^{n_{aq}} a_k^{v_{k\beta}}}{K_{eq,\beta}} \right), \beta = 1,2,...R_{mn}$$

$$= A_\beta\, k_\beta \left(1 - \frac{Q_\beta}{K_{eq,\beta}} \right), \beta = 1,2,...R_{mn} \qquad \text{..... (4.1)}$$

Where

A_β = reactive surface area of mineral β

$A_{i,\beta}$ = initial surface area of mineral β

a_k = activity of component k

$K_{eq,\beta}$ = chemical equilibrium constant for mineral reaction.

k_β = rate constant of reaction of mineral β

$r_{k\beta}$ = mineral reaction rate per unit bulk volume of rock when pore space is filled with water.

r_β = rate of mineral reaction

$v_{k,\beta}$ = stoichiometry coefficients

The rate law used to model the formation and consumption of different aqueous components is obtained using the following equation (CMG, 2012):

$$r_{k\beta} = v_{k\beta} * r_{\beta} \quad \text{.....(4.2)}$$

Where

$r_{k\beta}$ = mineral reaction rate per unit bulk volume of rock when pore space is filled with water.

r_{β} = rate of mineral reaction

$v_{k,\beta}$ = stoichiometry coefficients

The reaction rates for mineral dissolution and precipitation is a function of reactive surface area of a mineral, rate constant, chemical equilibrium constants, and activity product of mineral reactions (CMG, 2012; Nghiem et al., 2004). Mineral dissolution and precipitation depends on the magnitude of the saturation index. The ratio of activity product of mineral reactions and chemical equilibrium constant for mineral reactions is called the saturation index of the mineral reaction (CMG, 2012). For mineral dissolution to occur, saturation index should be greater than 1 and for mineral precipitation to occur the saturation index is less than 1 (CMG, 2012). The rate constant at the reservoir temperature is calculated using the Arrhenius equation as shown below (Lasga, 1984, Nghiem et al., 2004):

$$k_{\beta,T_{res}} = k_{\beta,reference} \exp\left[-\frac{E_{\alpha\beta}}{R} \left(\frac{T_i - T_{res}}{T_i T_{res}} \right) \right] \quad \text{..... (4.3)}$$

Where

$k_{\beta,\ reference}$ = reaction rate constant for mineral reaction β at the reference temperature(mol/m^2s)

$k_{\beta,Tres}$ = reaction rate constant at reservoir temperature

Ti = reference temperature (usually 298.15 K or 25°C)

T_{res} = reservoir temperature

$E_{\alpha\beta}$ = activation energy for reaction mineral β

The initial surface area ($A_{i,\beta}$) of each mineral is calculated using the total surface area($A_{s,\beta}$) and volume fraction of the mineral (VF_β) equation as shown below (CMG, 2012):

$$A_{i,\beta} = A_{s,\beta} * VF_\beta \quad \text{..... (4.4)}$$

The changes in the surface area ($A_{t,\beta}$) of a mineral due to mineralization can be calculated using the following equation (CMG, 2012):

$$A_{t,\beta} = A_{i,\beta} * \frac{VF_{\beta,t}}{VF_{\beta,i}} \quad \text{..... (4.5)}$$

Due to mineral dissolution and precipitation, rock porosity changes with time. The porosity at the end of each time step due to mineral dissolution/precipitation can be expressed as below (CMG, 2012):

$$\phi_{\min} = \left[\phi^* - \sum_{\beta=1}^{n_m} \left(\frac{N_\beta}{\rho_\beta} - \frac{N_\beta^0}{\rho_\beta^0} \right) \right] \quad \text{..... (4.6)}$$

$$\phi_t = \phi_{\min} [1 + c_r (p - p_{ref}) \quad \text{..... (4.7)}$$

$$\phi_t = \left[\phi^* - \sum_{\beta=1}^{n_m} \left(\frac{N_\beta}{\rho_\beta} - \frac{N_\beta^0}{\rho_\beta^0} \right) \right] [1 + c_r (p - p_{ref}) \quad \text{..... (4.8)}$$

Where

c_r = rock compressibility

N^0_β = total moles of mineral β per bulk volume initially

N_β = total moles of mineral β per bulk volume at current time

p_{ref} = reference pressure

p = pressure at time "t"

ϕ_t = porosity at time "t"

ϕ_i = initial porosity

ϕ^* = reference porosity without mineral dissolution/precipitation

ϕ_{min} = reference porosity including mineral dissolution/precipitation

The changes in absolute permeability with respect to porosity due to mineralization can be computed using the Kozeny-Carman equation as shown below (CMG, 2012):

$$k_t = k_i \left(\frac{\phi_t}{\phi_i} \right)^3 \left(\frac{1-\phi_i}{1-\phi_t} \right)^2 \quad \text{..... (4.9)}$$

Where k_i and ϕ_i are the initial permeability and porosity, respectively.

4.3 Modeling details

In this study, axisymmetric and single porosity numerical models were constructed to study the influence of geochemical changes on fluid flow and reservoir properties such as porosity and permeability. Figure 4-1 shows the schematic diagram of the hypothetical CO_2 storage site and the boundary conditions used in this study. The model consists of an overburden layer, a tight caprock layer, a sandstone reservoir layer, and an underburden layer. The axisymmetric model consists of 230 grid-blocks in the radial direction and 13 layers in the z-direction. A radial length of 150,000 m was used in this model. Reservoir thickness was assumed to be 500 m. The porosity and permeability of the reservoir in both models were assumed to be 20% and 100 millidarcy (mD), respectively. CO_2 was injected at a primary rate constraint of 1,000 metric tonnes per day

(0.365 million metric tonnes per year) for 25 years with a secondary bottomhole pressure constraint of 31,457 kPa. The initial average reservoir pressure of 21,184.80, which is based on the brine density calculations, was used. The salinity used in the models as varied from 1 ppm (top of the model) to 195,000 ppm (base of the model) with depth as shown in Figure 4-1. These values of salinity are in the range reported in the published literature (Birkholzer et al., 2009; Bachu and Bennion, 2009; Gunter et al., 2000; Heinemann et al., 2012; Micheal et al., 2010; Zhou et al., 2010). The simulations were carried out for 1,000 years (25 years of CO_2 injection and 975 years of post injection). Figure 4-2 shows the assumed relative permeability curves used in this study (Tran et al., 2009). The intra-aqueous chemical-equilibrium reactions, mineral reactions, and percentage mineral volumes considered in this study are shown in Figure 4-3. The total surface area of each mineral per unit volume was assumed to be 10,000 m^2/m^3 (Nghiem et al., 2004; Xu et al., 2001). This section on the modeling of CO_2-brine-rock interaction is used to validate the geochemical response during CO_2 injection and the post injection period. A few modeling assumptions were made in this study as given below:

1. The reservoir layer is homogeneous and isotropic.
2. Injection well components do not react with CO_2. Issues related to corrosion and other chemical issues affecting well completion and surface facilities are not addressed.
3. Injected CO_2 is free from impurities such as H_2S, SO_x, NO_x, and O_2, which can dissolve into brine and is believed to affect pH and oxidation-reduction potential of brine (Jun et al., 2013).
4. The saline aquifer does not consist of any organic compounds. The presence of organic compounds can influence dissolution and precipitation (Yang et al., 2011).

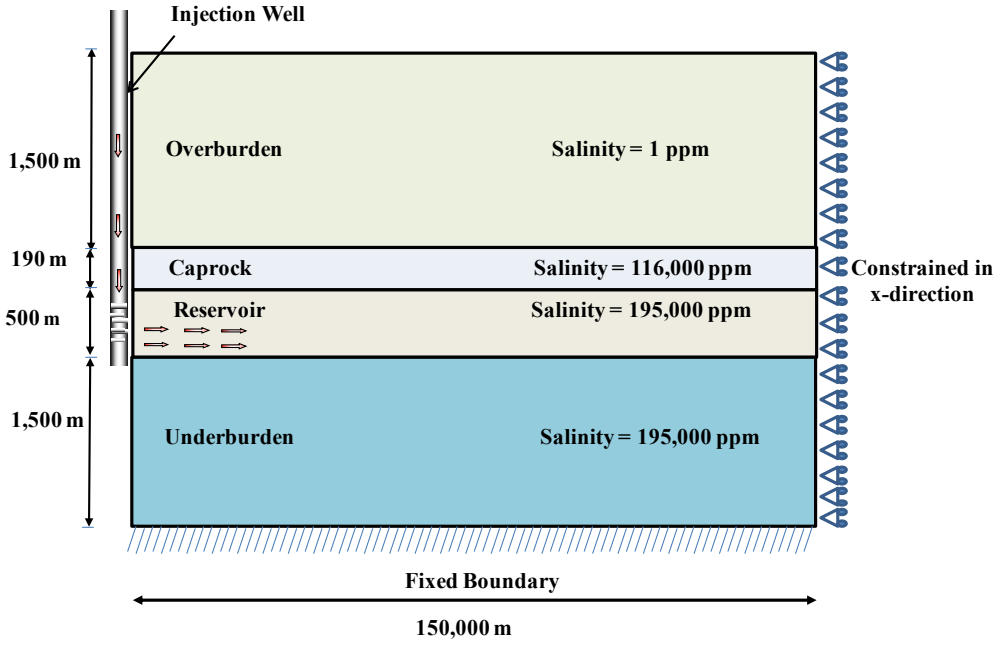

Figure 4-1: Schematic diagram of the hypothetical CO_2 storage site considered in this study.

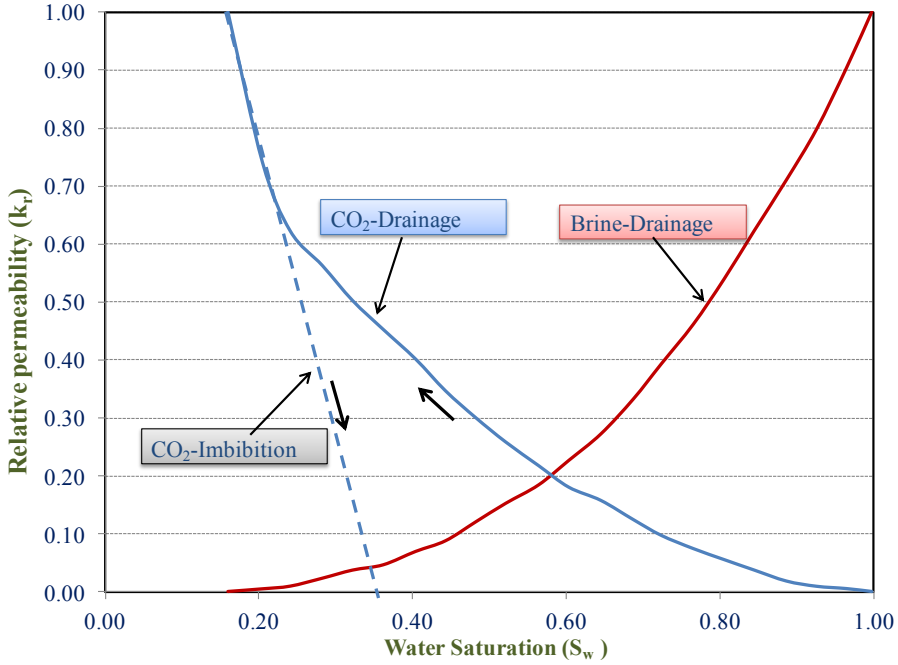

Figure 4-2: Assumed relative permeability curves (Modified from Tran et al., 2009).

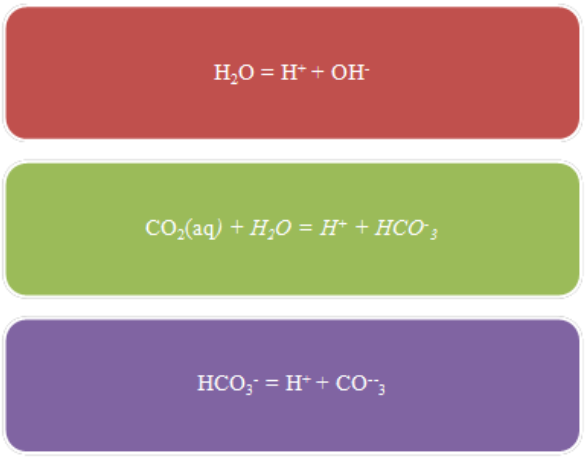

(a) Aqueous chemical equilibrium reactions

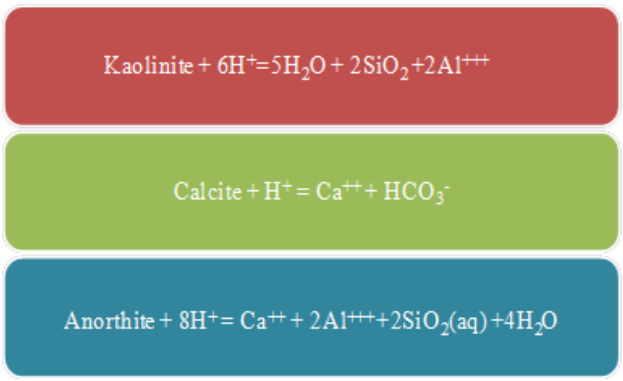

(b) Mineral dissolution/precipitation reactions

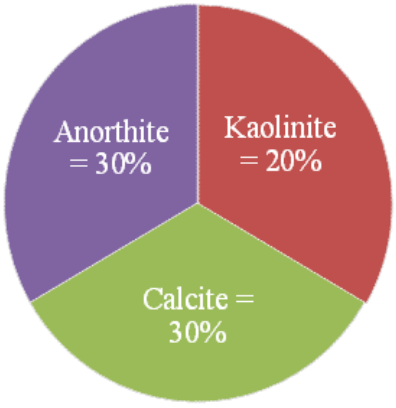

(c) Assumed reservoir mineral volume (%)

Figure 4-3: Intra-aqueous reactions, mineral reactions, and percentage mineral volume.

Table 4-1 provides the mineral dissolution and precipitation kinetic data that was used for the calculation of reaction rate constants at reservoir temperature (Johnson et al., 2004; Nghiem et al., 2004; Xu et al., 2001). As shown in Table 4-1, the reaction rate constants, k_β is at a reference temperature T_i (typically 298.15 K or 25° C).

Table 4-1:Mineral dissolution/precipitation reaction data (Johnson et al., 2004; Nghiem et al., 2004; Xu et al., 2001)

Mineral	Chemical Composition	Log(rate constant) (mol/m^2/s) @ 25^{0}C	Computed Reactive surface (m^2/m^3)	Activation Energy(J/mol)
Kaolinite	$Al_2Si_2O_5(OH)_4$	-13.0	200	62,760
Calcite	$CaCO_3$	-8.79588	300	41,870
Anorthite	$CaAl_2Si_2O_8$	-12.0	300	67,830

4.4 Geochemical Response

Modeling results show that when CO_2 is injected into the target formation, the free-phase CO_2 migrates to the top of the reservoir and is physically trapped by the overlying tight, low-permeability caprock layer. As some part of the injected CO_2 dissolves in the aqueous phase, density of brine increases and the aqueous CO_2 flows to the bottom of the reservoir. Results show that the evolution of CO_2 saturation is consistent with the migration of the CO_2 plume. Water saturation decreases initially and then increases, thus indicating the lateral migration of the CO_2 plume and the progressive dissolution of injected CO_2 in the formation brine. Figure 4-4 shows the water saturation at the end of 5, 10, 15, 20, and 25 years of injection. The pH value of formation brine changes from 7.07 (initially) to 5.0 (at the end of 25 years of injection) due to CO_2 dissolution as shown in Figure 4-5.

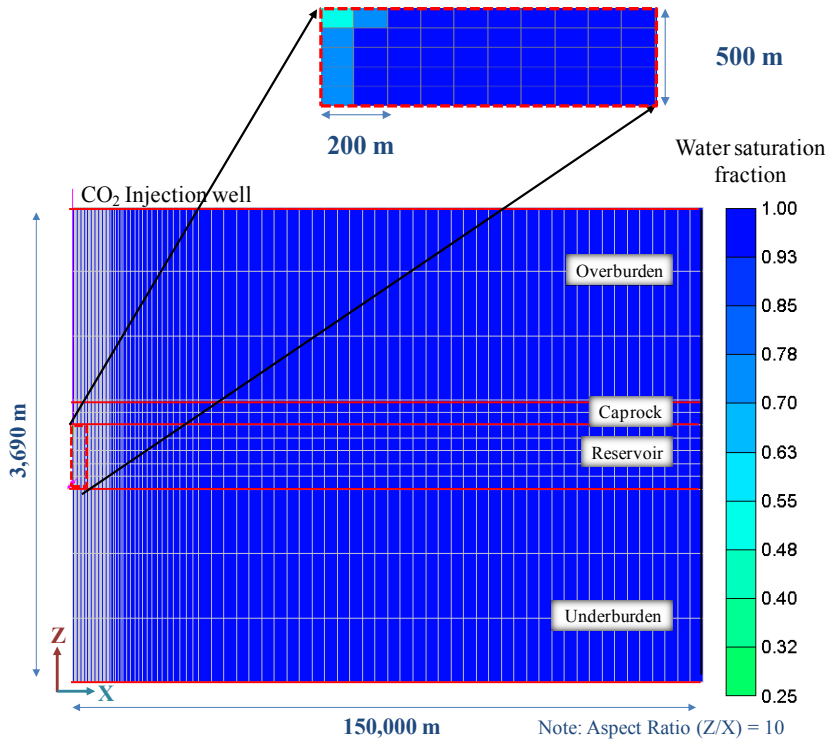

(a) 5 years

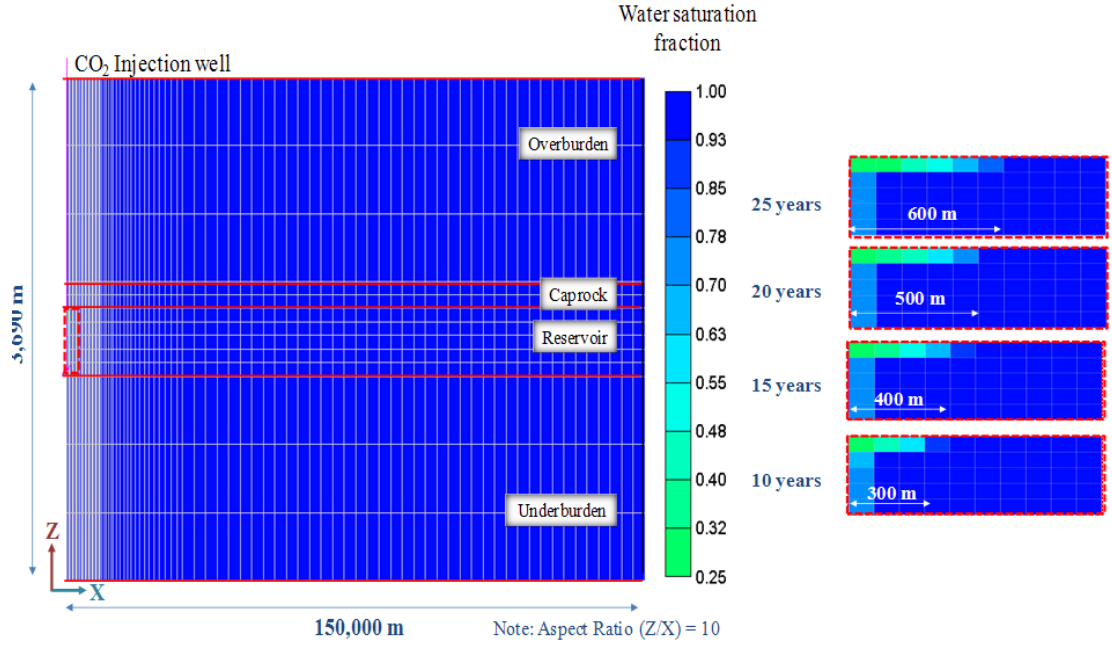

(b) 10 years to 25 years

Figure 4-4: Fluid migration during CO_2 injection.

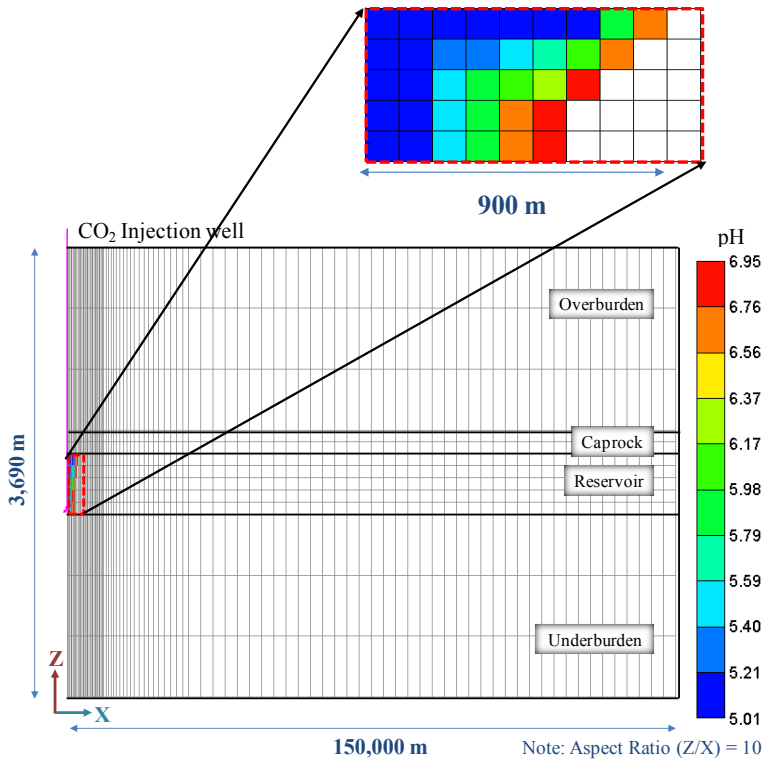

Figure 4-5: Computed pH at the end of CO_2 injection (25 years).

In the regions where high dissolution of CO_2 takes place, acidic nature of brine increases and causes dissolution of minerals such as Calcite and Anorthite. Precipitation of Calcite and Kaolinite occurs in the neighboring zone (where pH > 6) that surrounds the mineral dissolution. Anorthite is a non-carbonate, calcium-rich mineral, whose dissolution provides Calcium ions to the formation brine. With time, the Calcium ions (Ca^{2+}) in the formation brine react with the available bicarbonate ions to precipitate calcium carbonate ($CaCO_3$) or Calcite. In addition to Calcium ions (Ca^{2+}), Aluminum ions (Al^{3+}) and Silicate ions (SiO_2) aid in the precipitation of Kaolinite. Figure 4-6 shows the changes in mole concentration of Calcite, Anorthite, and Kaolinite after 1,000 years. The sign convention used in the numerical model is that the amount of mineral dissolution (kgs) is negative and mineral precipitation (kgs) is positive.

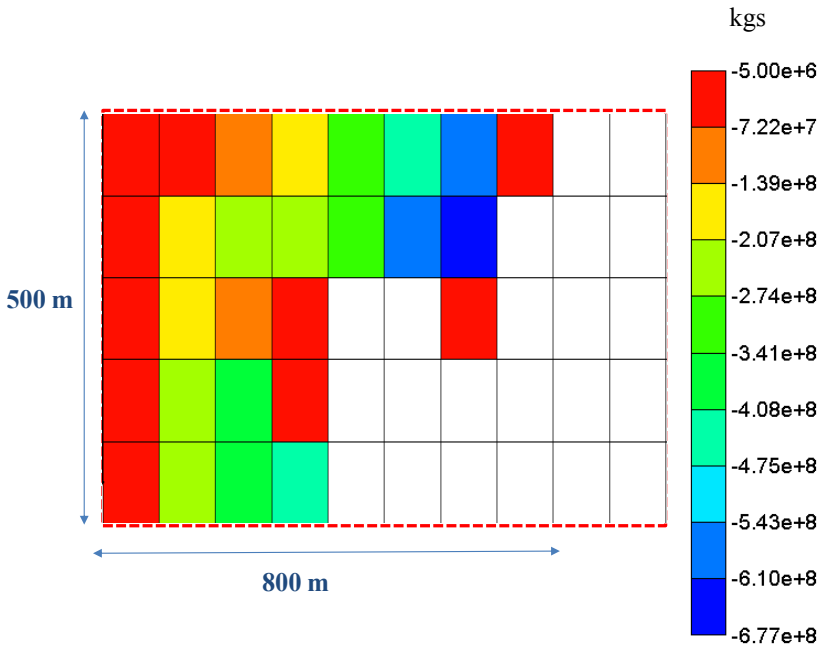

(a) Anorthite

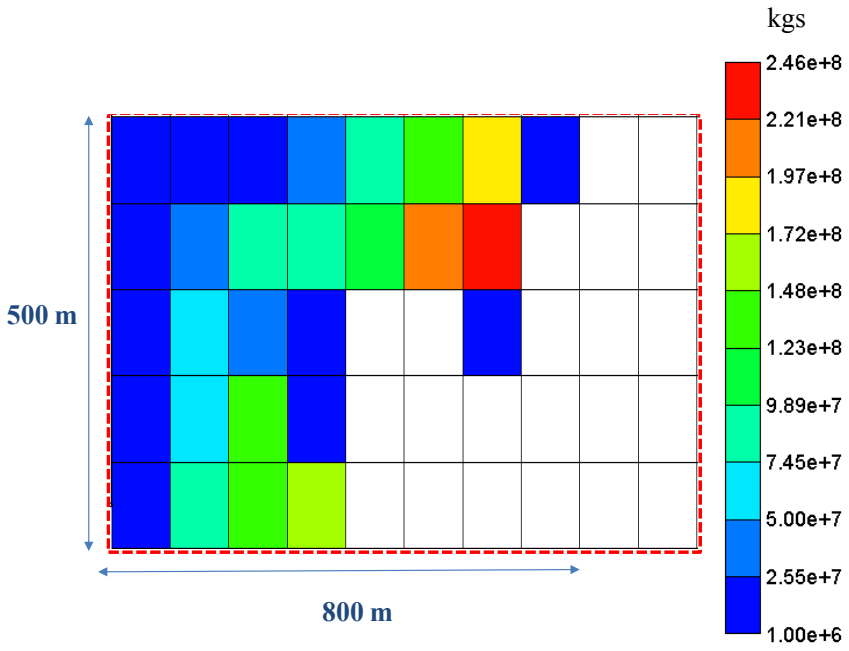

(b) Calcite

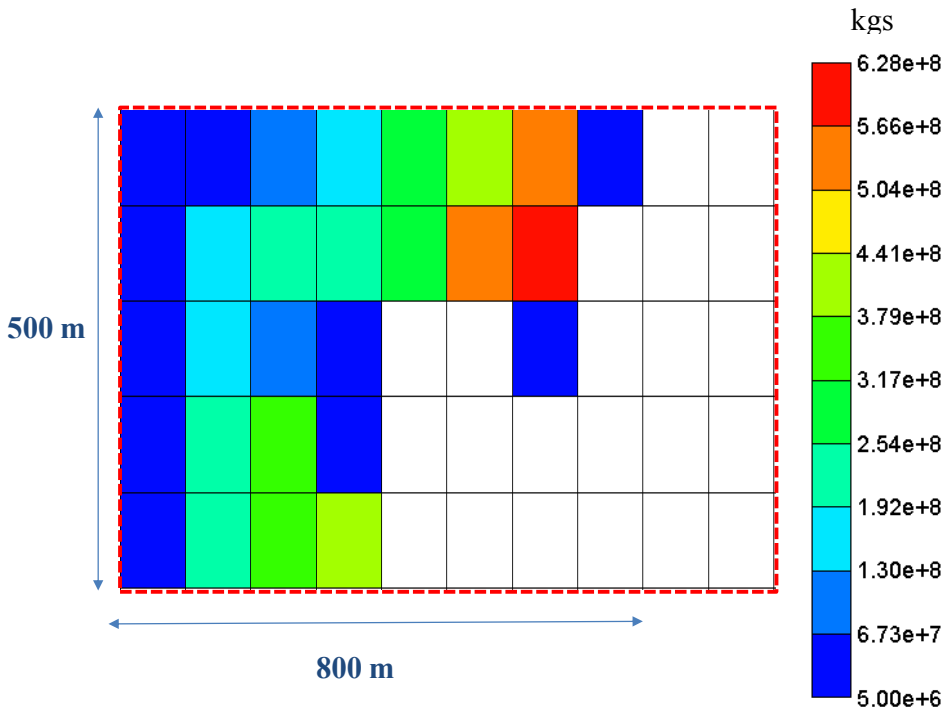

(c) Kaolinite

Figure 4-6: Computed mineral mass after 1,000 years.

Figure 4-7 shows the change in porosity due to geochemical reactions after 1,000 years (25 years of CO_2 injection and 975 years of post-injection). Modeling results show that the change is porosity due to geochemical reactions is not significant (~0.040 (fraction) shown in Figure 4-7), which translates to a 2% change in the original porosity.

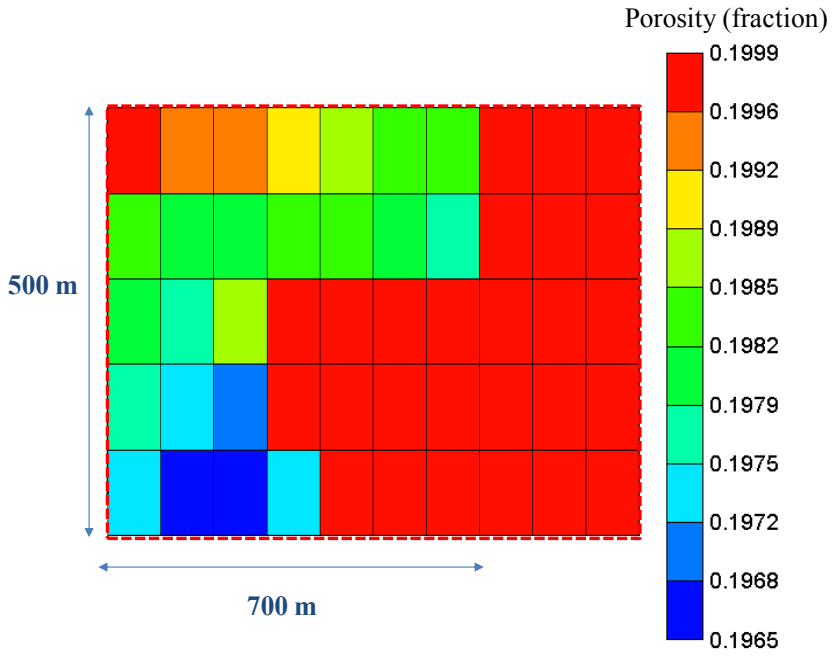

Figure 4-7: Computed reservoir porosity after 1,000 years.

4.5 Influence of mineral reaction rate constants on mineralization

The reaction rate constants of the rock minerals were modified to investigate their influence on mineralization and subsequently on rock porosity. The revised reaction rate constants are shown in Table 4-2. Based on the revised reaction rate constants, the maximum change in the computed porosity was observed to be 0.07 (fraction) after 1,000 years as shown in Figure 4-8. This change in porosity translates to a 35% change in the original porosity. The change in porosity and permeability in a selected block close to the injection well is shown Figure 4-9(a) and 4-9(b), respectively. The change in porosity as shown in Figure 4-9(a) is consistent with the cumulative change in mineral moles per bulk volume (Refer equation 4.8 for the porosity calculations).

Table 4-2: Mineral reaction data

Mineral	Chemical Composition	Log(rate constant) (mol/m^2/s) @ 25^{0}C	Assumed Log(rate constant) (mol/m^2/s) @ 25^{0}C	Computed Reactive surface (m^2/m^3)	Activation Energy (J/mol)
Kaolinite	$Al_2Si_2O_5(OH)_4$	-13.0	-10.0	200	62,760
Calcite	$CaCO_3$	-8.79588	-8.79588	300	41,870
Anorthite	$CaAl_2Si_2O_8$	-12.0	-10.0	300	67,830

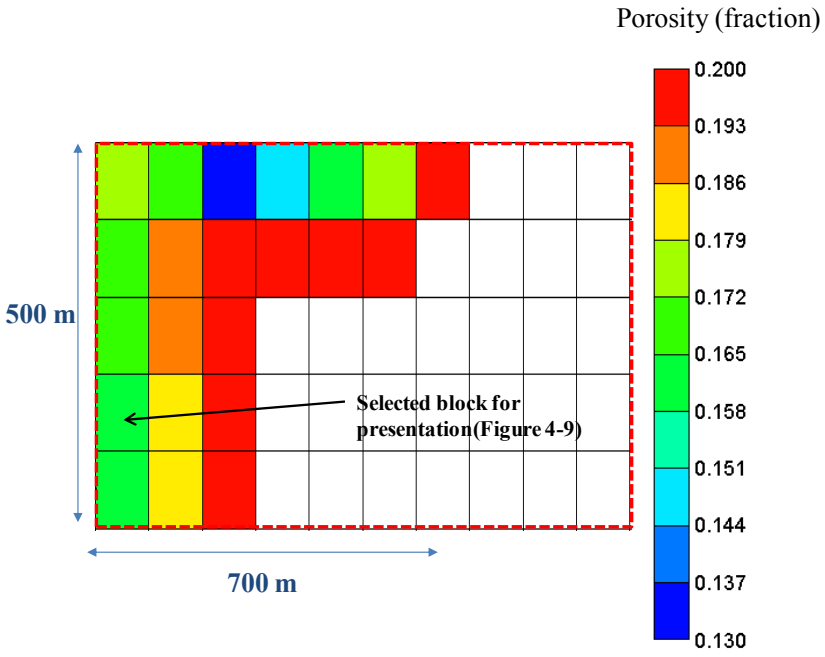

Figure 4-8: Computed reservoir porosity after 1,000 years.

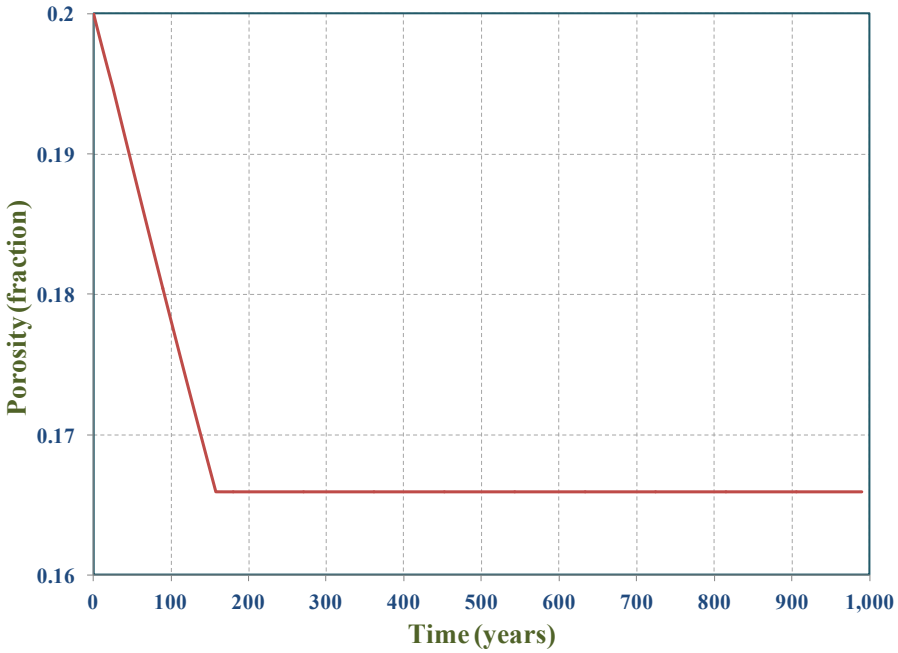

(a) Change in porosity in a selected block close to the injection well

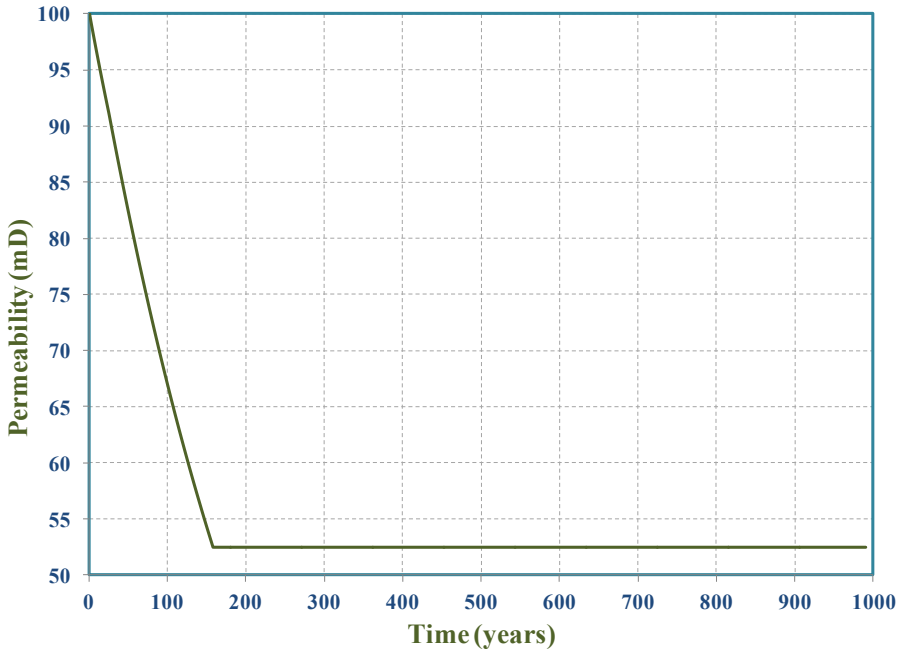

(b) Change in permeability in a selected block close to the injection well.

Figure 4-9: Computed changes in porosity and permeability with time due to mineralization.

Chapter 5: COUPLED MULTIPHASE FLUID FLOW AND GEOMECHANICS MODEL WITH GEOCHEMICAL REACTIONS

5.1 Introduction

In this study, coupled multiphase fluid flow and geomechanics models were constructed to investigate the behavior of fluid flow and ground response with the inclusion of geochemical reactions. In order to incorporate an iterative coupling of geomechanics with fluid flow (which includes geochemical processes), a modified equation-of-state compositional and GHG simulator is used (Trans et al., 2005; Trans et al., 2009). In the iterative coupled approach, geomechanics calculations are one step behind the reservoir flow calculations (Trans et al., 2005; Trans et al., 2009). The fluid flow module in CMG-GEM computes the amount of CO_2 dissolution fluid flow, geochemical reactions, changes in pressure, temperature, and compositions, and changes in porosity and permeability due to geochemical reactions (Trans et al., 2005; Trans et al., 2009). The values of pressure and temperature calculated at the end of every time step in the fluid flow module are passed on to the geomechanics module which computes stress changes and deformation in the formation and the surrounding layers. The solution from the geomechanics module is sent again to the fluid simulator through coupling variables which includes porosity (Tran et al., 2009). The porosity is a function of pressure, temperature, and total mean stress formula (Tran et al., 2004).This coupling variable is sent to the reservoir simulator to compute pressure and temperature values at time "t" (Tran et al., 2009). This iterative process continues in a given time step until the convergence criteria for pressure, stress, and porosity is satisfied (Tran et al., 2009). Figure 5-1 shows a flow chart of the process in a given step until a convergence criterion is satisfied.

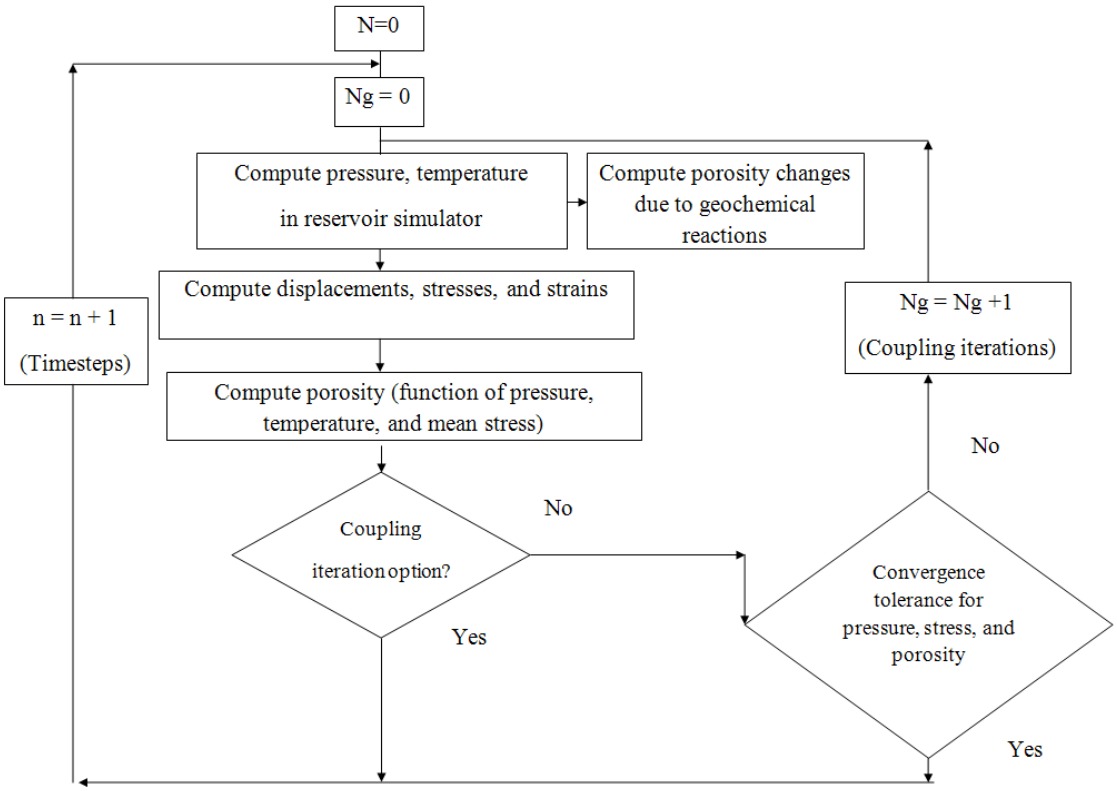

Figure 5-1: A general flow diagram for iterative coupling method used in this study (Modified from Tran et al., 2009).

The basic equations for reservoir fluid flow consist of mass balance equations, Darcy's law, and phase equilibrium models. Besides Darcy's law which governs the fluid flow in the reservoir, transport phenomenon such as dispersion and diffusion also contribute to the movement of components in the aqueous phase (Tran et al., 2009). The material-balance equations for multiphase fluid flow in a deformable reservoir can be found elsewhere (Chen et al., 2006; Tran et al., 2005; Tran et al., 2009).The basic equation for conservation of fluid in a deformable porous medium can be expressed as below (Tran et al., 2005):

.

$$\frac{\partial}{\partial t}\left[\phi\rho_f\left(1-\varepsilon_v\right)\right]-\nabla\left[\rho_f\frac{k}{\mu}\left(\nabla p-\rho_f b\right)\right]=Q_f \qquad \text{..... (5.1)}$$

where

b = body force per unit mass of fluid

k = permeability tensor

p_f = pressure at time "t"

Q_f = fluid flow rate

ε_v = volumetric strain

ϕ = porosity

μ = fluid viscosity

ρ_f = density of fluid

In a conventional flow simulator, bulk volume is assumed to be constant (Tran et al., 2005). However, the volumetric strain ε_v in eq 5.1, accounts for the change in pore volume and bulk volume of the porous media in the CMG-GEM geomechanics module (Tran et al., 2005). In order to model the changes in volumetric strain with a conventional simulator the reservoir porosity (ϕ_{res}) is defined as a function of true porosity (ϕ) and volumetric strain (ε_V) as shown in equation 5.2 (Tran et al., 2005).

$$\phi_{res} = \phi(1-\varepsilon_V) \qquad \text{..... (5.2)}$$

The constitutive equation for stress-strain relationship can be written as (Desai and Siriwardane, 1984; Siriwardane et al., 2013; Vilarrasa et al., 2011):

$$\sigma_{ij} = 2G\varepsilon_{ij} + (K - \frac{2G}{3})\varepsilon_{kk}\delta_{ij} + \alpha p\delta_{ij} \qquad \text{..... (5.3)}$$

where

σ_{ij} = stress tensor

G = shear modulus

K = bulk modulus

P = fluid pressure

α = Biot's constant ($\varphi \leq \alpha \leq 1$)

δ_{ij} = Kronecker delta

ε = strain tensor

The effective stress in the porous media can be expressed as (Martinez et al., 2013; Tran et al., 2005; Tran et al., 2009; Vilarrasa et al., 2011):

$$\sigma'_{ij} = \sigma_{ij} - \alpha p \delta_{ij} \quad \text{..... (5.4)}$$

5.2 Numerical Methodology

A coupled fluid flow and geomechanics model with the inclusion of geochemical reactions was constructed to investigate the behavior of the fluid flow and the ground response during CO_2 injection into a saline aquifer. Geomechanical calculations in CMG-GEM are based on an iterative coupling method as described in the previous section. The geomechanical calculations such as change in stresses and deformations are computed at every time step. In this model, material rock properties, fluid properties (salinity), and CO_2 injection constraints similar to the coupled fluid flow and geochemical model presented in section 4.3 were used. A constant elastic modulus of 40 GPa and a Poisson' ratio of 0.25 was used for all the rock layers. These values are within the range found in the literature (U.S.EPA, 2012).The bottom boundary of the model was constrained, and lateral boundaries were set on rollers. Figure 5-2 shows the assumed initial mineral volume percentages (%) in the reservoir. The baseline mineralogy for the sandstone aquifer was assumed based on reported values in the literature (Audigane et al., 2007; Balashov et al.,2013; Johnson et al., 2004; Liu et al., 2011; Nghiem et al., 2004). Generally, Quartz accounts for the maximum mineral volume in sandstone aquifers. Table 5-1 provides the input data for mineral dissolution and precipitation that was used for the calculation of reaction rate constants at reservoir temperature (Johnson et al., 2004; Palandri and Kharaka, 2004). The reaction rate constants are calculated internally within the simulator. Two models were constructed to determine the influence of

geochemical reactions on the geomechanical response of the rock system. These two models consist of: 1) Coupled fluid flow, geomechanics models, and geochemical models with geochemical reactions, 2) Coupled fluid flow and geomechanical models without geochemical reactions. Additionally, computer models were constructed to investigate the influence of salinity on CO_2 solubility, pressure response, and ground displacements. The models consist of: 1) Coupled fluid flow, geomechanics model with salinity and without geochemical reactions, 2) Coupled fluid flow and geomechanical model without salinity and geochemical reactions.

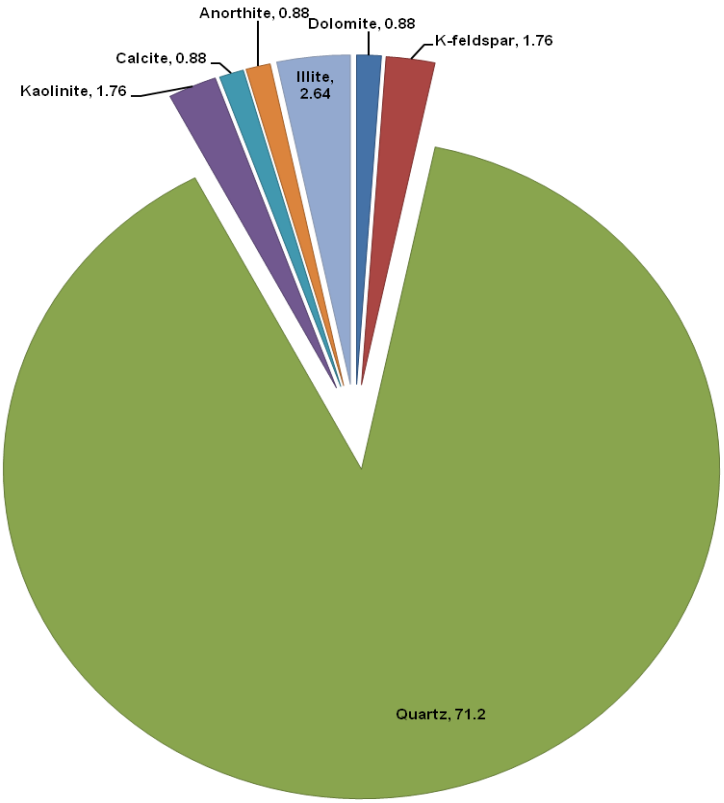

Figure 5-2: Mineral volumes in the reservoir.

Table 5-1: Mineral dissolution/precipitation reaction data (Johnson et al., 2004; Palandri and Kharaka, 2004)

Mineral	Chemical Composition	Molar weight (g/mol)	Density (kg/m^3)	Log K^m_{eq} (50 ^{0}C)	Log(rate constant) (mol/m2/s) @ 25^{0}C)	Reactive surface area (m^2/m^3)	E(J/mol)
Kaolinite	$Al_2Si_2O_5(OH)_4$	258	2,594	5.4706	-13.0	17,600	62,760
Calcite	$CaCO_3$	100	2,710	1.3560	-8.79588	88	41,870
Anorthite	$CaAl_2Si_2O_8$	116	4,047	23.0603	-12.0	88	67,830
Dolomite	$CaMg(CO_3)_2$	184	2,864	1.6727	-9.22180	88	41,870
Illite	$Mg_{0.25}K_{0.6}Al2.3Si_{3.5}O_{12}H_2$	384	2,763	7.4855	-14.0	26,400	58,620
Quartz	SiO_2	60	2,648	-3.6285	-13.9	7,128	87,500
K-feldspar	$KAlSi_3O_8$	278	2,655	-0.3439	-12.0	176	67,830

5.3 Geochemical response

The computed amount of mineral mass dissolved, and deposited over a period of 1,000 years is shown in Figure 5-3. The dissolution of minerals such as Dolomite, Calcite, Anorthite, Illite, and K-feldspar takes place initially at lower pH values. Dolomite dissolves initially and then precipitates due to availability of Mg^{++} ions from the dissolution of Illite. The Ca^{++} ions released from the dissolution of Anorthite and Dolomite react with the available bicarbonate ions (HCO_3^-) to precipitate Calcite. Quartz and Kaolinite precipitate due to the continuous availability of silicate and Al^{+++} ions from the dissolution of Illite. Figure 5-4 shows the amount of Quartz in-place as well as the amount of Quartz deposited after 1,000 years. Modeling results show that the amount of deposited Quartz mineral is insignificant when compared to the amount in-place. A similar behavior was shown by other reactive minerals. Table 5-2 shows the cumulative changes in mineral mass due to mineralization. Modeling results presented in this section show that the geochemical reactions do not have a significant influence on rock porosity due to the presence of an inert mineral such as Quartz (about 71% of mineral volume).

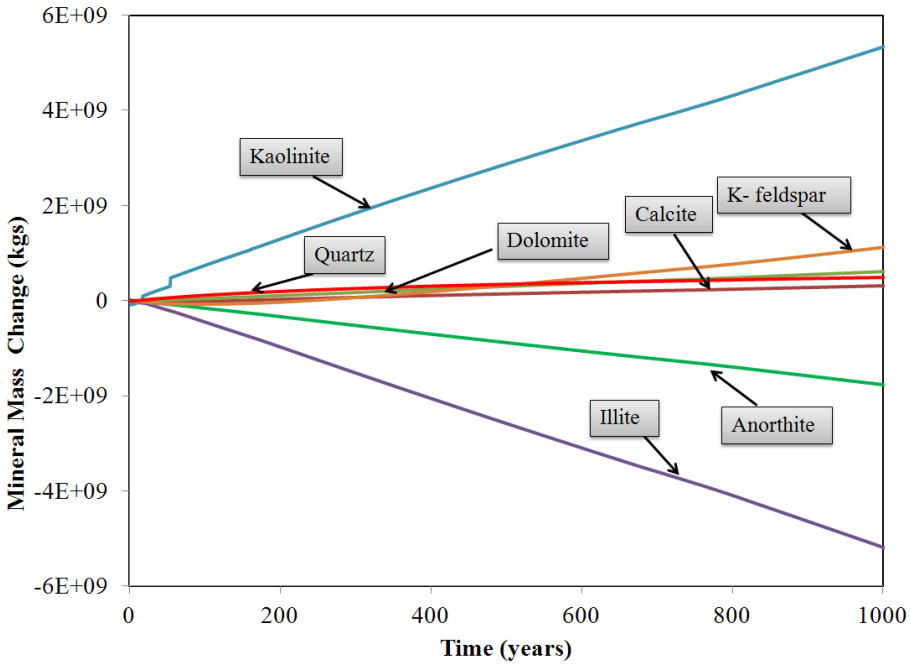

Figure 5-3: Computed amount of mineral dissolved and deposited after 1,000 years.

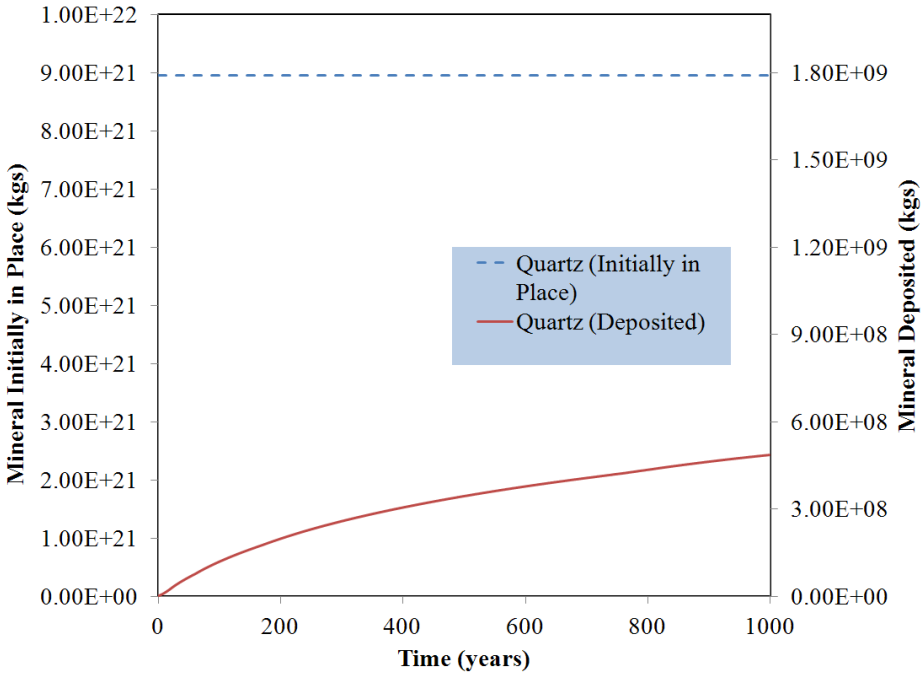

Figure 5-4: Computed amount of Quartz in-place and deposited due to geochemical reactions.

Table 5-2: Change in mineral mass due to mineralization.

Mineral	Mineral initially in place (kgs)	Cumulative Amount of Mineral Precipitation/Dissolution (kgs)	Cumulative percentage of mineral precipitation/dissolution (%)
Anorthite	4.83E+22	-7.38E+08	-1.53E-14
Calcite	1.13E+20	3.15E+08	2.78E-12
Dolomite	1.20E+20	6.14E+08	5.13E-12
Illite	3.47E+20	-5.19E+09	-1.49E-11
Kaolinite	2.17E+20	5.35E+09	2.46E-11
K-feldspar	2.14E+20	1.13E+09	5.30E-12
Quartz	8.94E+21	4.85E+08	5.42E-14

5.4 Pressure response

5.4.1 Coupled fluid flow and geomechanics model with geochemical processes and salinity

Figure 5-5 shows the brine density which was computed based on the assumed values of aqueous concentrations and salinity values. The brine density is computed in CMG-GEM using the Rowe and Chou (1970) correlations. Figure 5-6 shows the computed initial fluid pressure which is based on the brine density. The computed fluid pressure gradient in the reservoir is 10.86 kPa/m. Due to the high reservoir brine salinity assumed in this study (195,000 ppm), the computed fluid pressure gradient is higher than the fluid pressure gradient for freshwater (9.79 kPa/m). When CO_2 was injected at a primary injection rate of 0.365 million metric tonnes per year, and a secondary constraint of maximum bottomhole pressure of 31,457 kPa, the maximum change in reservoir pressure at the end of 25-year CO_2 injection was about 243 kPa. This change in pressure translates to an increase of 1.15% above the average initial reservoir pressure. The increase in pressure during CO_2 injection is very small due to the assumed value of high reservoir permeability (100 mD) and the infinite extent of the reservoir. Figure 5-7 shows the increase in fluid pressure after 25 years of CO_2 injection. Modeling results show that the reservoir pressure drops significantly during the first 10 years of the post-injection period.

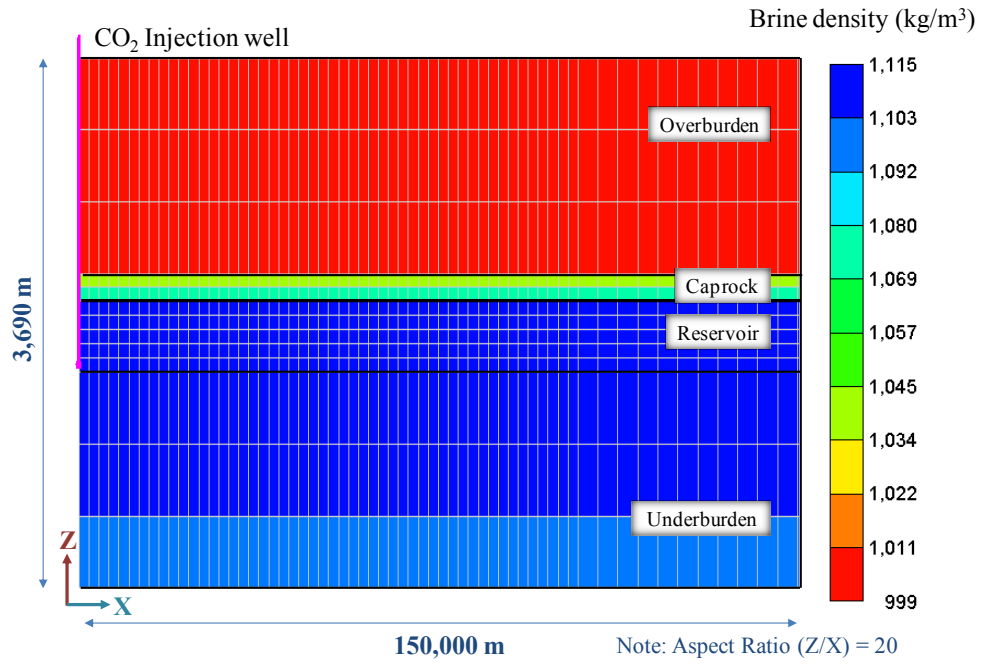

Figure 5-5: Brine density (kg/m^3).

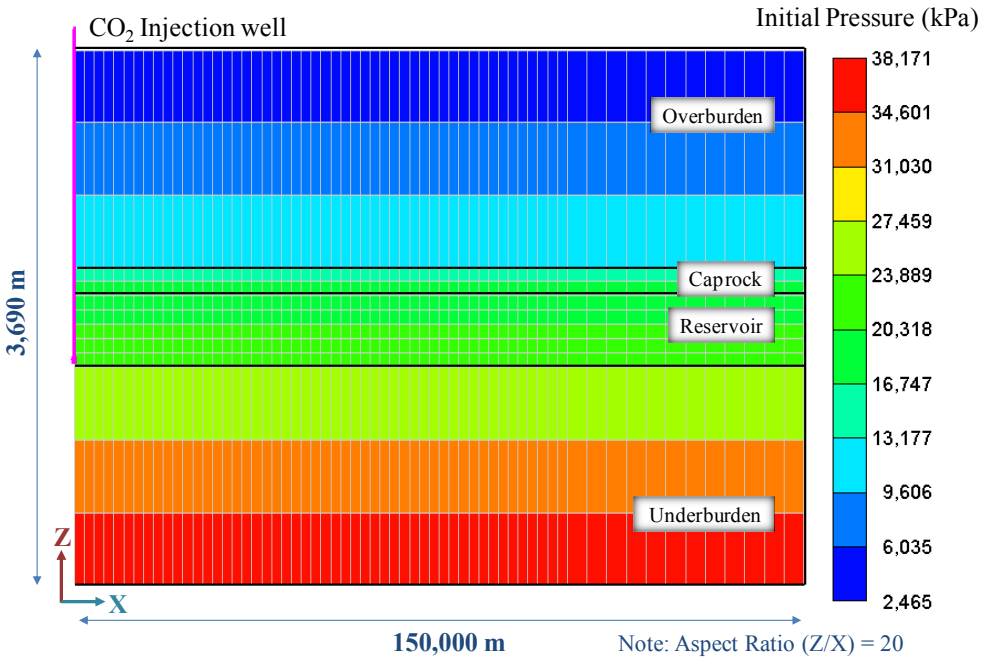

Figure 5-6: Initial fluid pressure distribution (kPa).

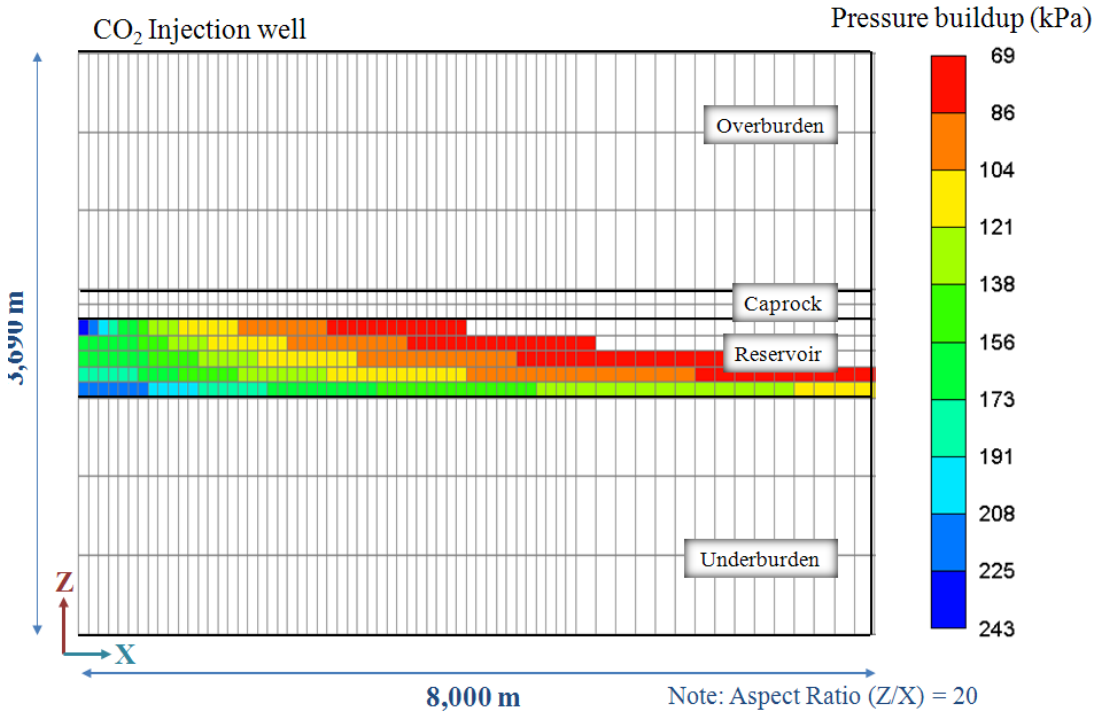

Figure 5-7:Pressure buildup (kPa) caused due to CO_2 injection.

5.4.2 Coupled fluid flow and geomechanics model with salinity and without geochemical processes

In this study a coupled fluid flow and geomechanics model without salinity and geochemical reactions was constructed to determine the influence of geochemical reactions on the pressure response. Modeling results show that the pressure response was similar to the coupled fluid flow and geomechanics model with salinity and geochemical reactions. Therefore, it can be concluded that geochemical reactions do not have any influence on the pressure response due to CO_2 injection.

5.4.3 **Coupled fluid flow and geomechanics model without geochemical reactions and salinity**

In this study, a coupled fluid flow and geomechanics model without salinity was constructed to determine the influence of salinity on the pressure response. Geochemical reactions were not included in the model as they do not have any significant influence on the pressure response during CO_2 injection. In the coupled fluid flow and geomechanical model without salinity, the aqueous mass density is calculated as a linear function of pressure (CMG, 2012). The computed density for the coupled fluid flow and geomechanics model with salinity, and the coupled fluid flow and geomechanics model without salinity are significantly different. Figure 5-8 shows the computed brine density for the coupled fluid flow and geomechanical model without salinity. Figure 5-9 shows computed initial fluid pressure based on the brine density calculations. Figure 5-10 shows the increase in fluid pressure after 25 years of CO_2 injection. When CO_2 was injected at a primary injection rate of 0.365 million metric tonnes per year, and a secondary constraint of maximum bottomhole pressure of 31,457 kPa, the maximum change in reservoir pressure at the end of 25-year CO_2 injection was about 216 kPa. This change in pressure translates to an increase of 1.02% above the average initial reservoir pressure.

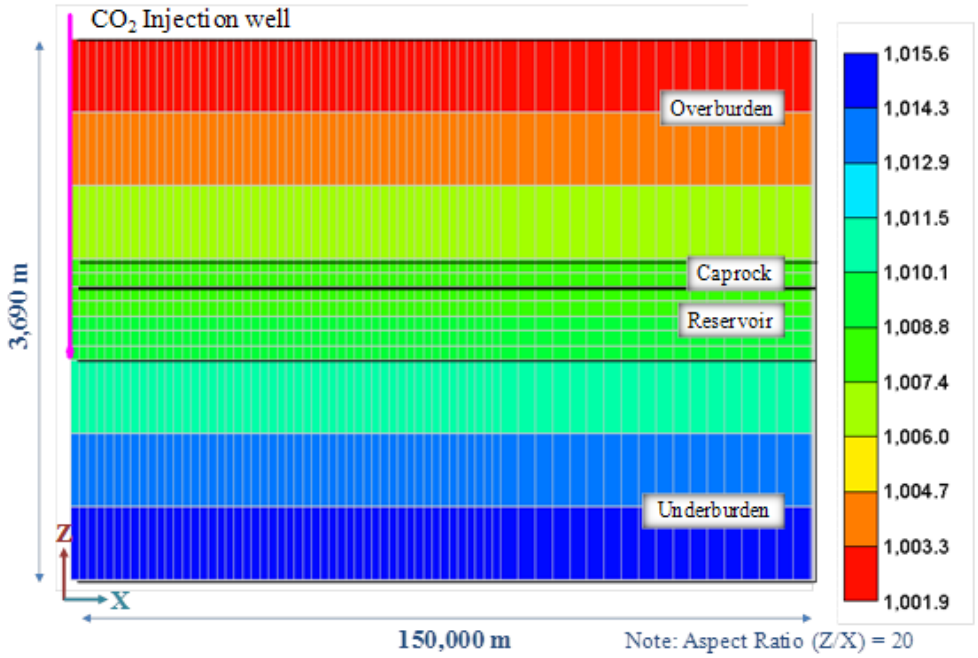

Figure 5-8:Aqueous mass density (kg/m^3).

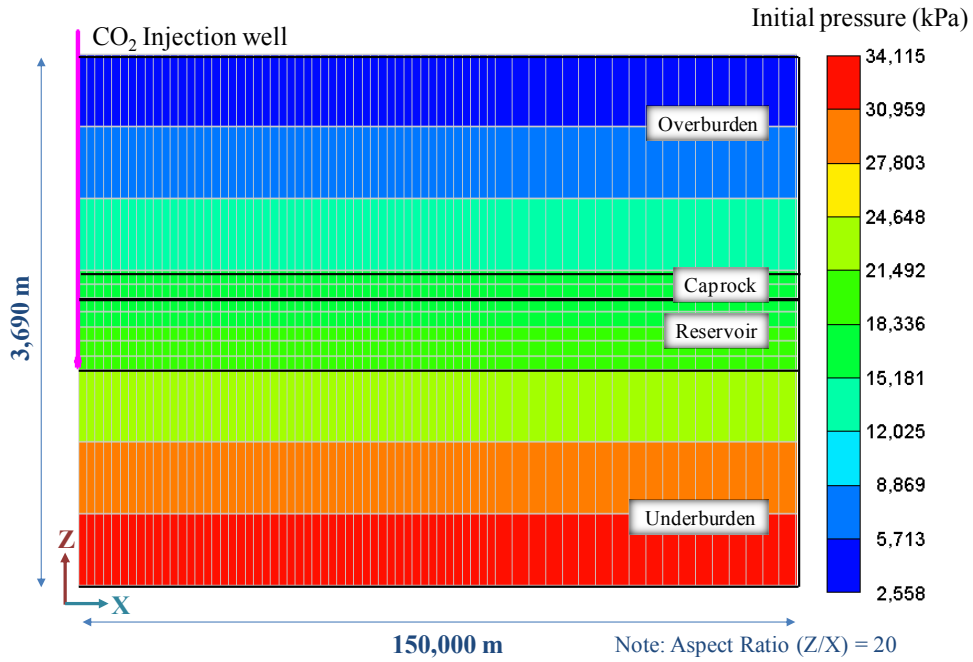

Figure 5-9: Initial fluid pressure distribution (kPa).

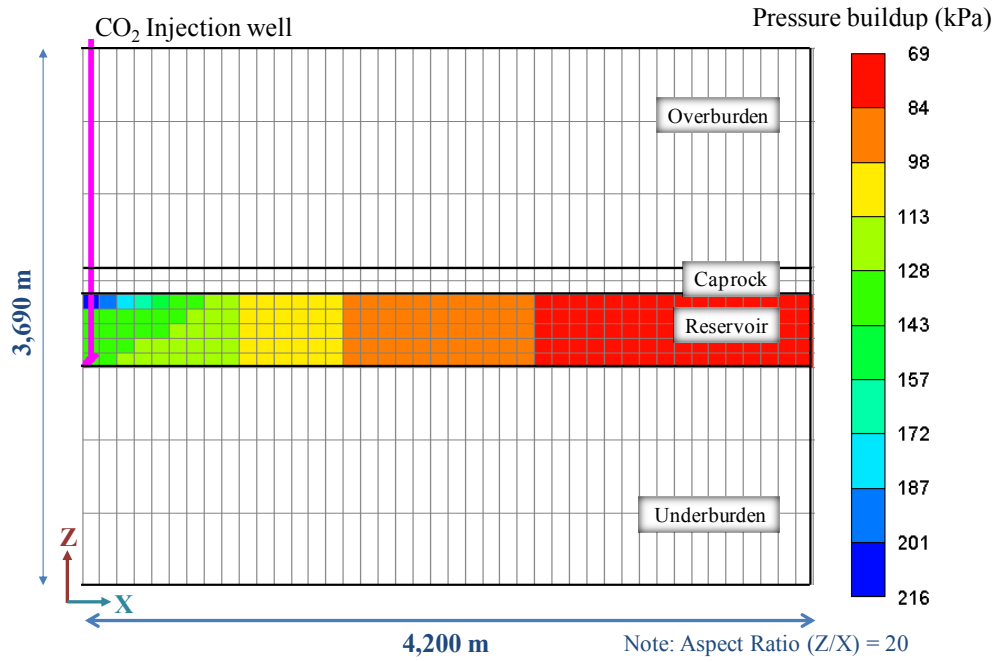

Figure 5-10: Pressure buildup (kPa) caused due to CO_2 injection.

5.5 Ground response

5.5.1 Coupled fluid flow and geomechanics model with geochemical reactions and salinity

Figure 5-11 shows the computed ground displacements at various time periods caused due to CO_2 injection. The maximum computed vertical displacement is about 0.16 cm after 25 years of injection.The magnitudes of ground displacement are small due to small changes in fluid pressure during injection.

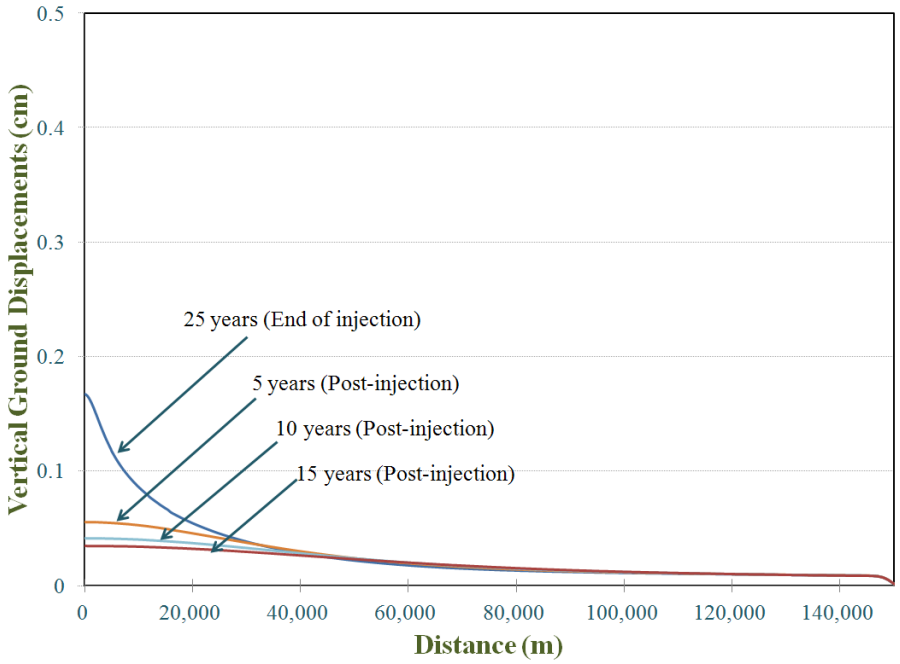

Figure 5-11: Computed vertical ground displacement at various time periods.

5.5.2 Coupled fluid flow and geomechanics model with salinity and without geochemical reactions

Figure 5-12 shows a comparison between the ground displacements at the end of 25 years of CO_2 injection for the coupled fluid flow and geomechanics model with salinity and no geochemical reactions and the coupled fluid flow and geomechanics model with salinity and geochemical reactions. The modeling results show that geochemical reactions do not any influence on the computed displacements.

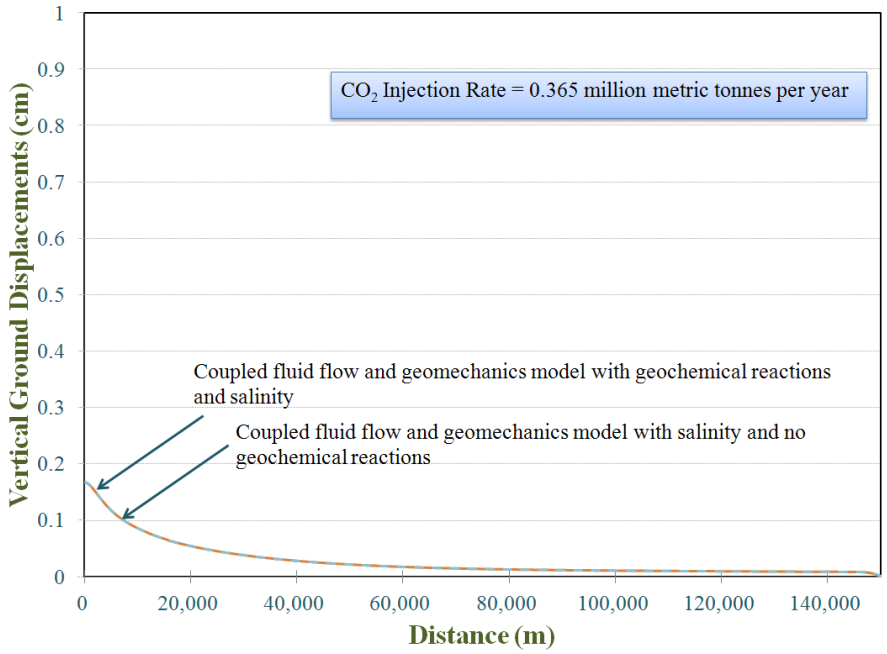

Figure 5-12: Comparison of computed ground displacement after 25 years of CO_2 injection.

5.5.3 Coupled fluid flow and geomechanics model without salinity

Figure 5-13 shows a comparison between the ground displacements at the end of 25 years of CO_2 injection for the coupled fluid flow and geomechanics model with salinity and the coupled fluid flow and geomechanics model without salinity. Modeling results show that salinity has an influence on the computed displacements. The maximum computed ground displacement in the coupled fluid flow and geomechanics model with salinity was about 0.16 cm after 25 years of injection.The maximum computed ground displacement in the coupled fluid flow and geomechanics model without salinity was about 0.115 cm after 25 years of injection. This difference in the ground displacements can be related to the difference in the magnitude of fluid pressure buildup due to CO_2 injection in the coupled fluid flow and geomechanics model with and without salinity.

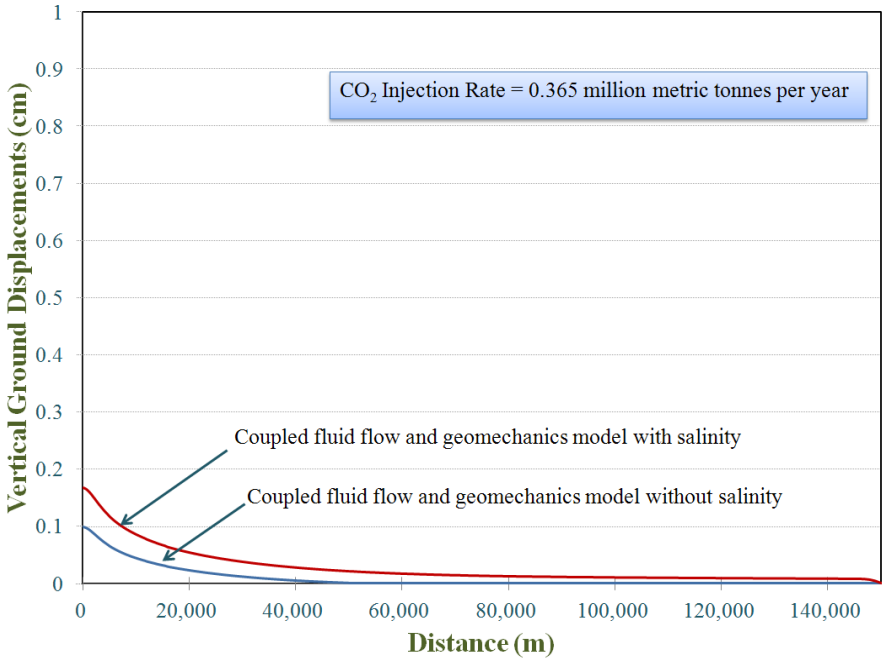

Figure 5-13: Comparison of computed ground displacement after 25 years of CO_2 injection.

CO_2 dissolution or solubility in brine decreases with salinity. Under such circumatances the displacement of the highly viscous brine during CO_2 injection by the less viscous CO_2 requires more effort thus leading to an increase in fluid pressure. The increase in fluid pressure results in an increase of the ground dispalcements. In order to investigate the influence of CO_2 solubility on the ground displacements, a coupled fluid flow and geomechanics models with different values of brine salinity were constructed. Table 5-3 shows the computed amount of CO_2 dissolved in brine for different values of salinity. Modeling results show that the maximum reduction in CO_2 dissolution was about 44% when compared to the coupled fluid flow and geomechanics model without salinity. Figure 5-14 shows the changes in ground displacement for different salinity values. From modeling results shown in Figure 5-14, it can be concluded that brine salinity and CO_2 solubility in brine have an influence on the computed ground displacements.

Table 5-3: Change in CO_2 dissolution with brine salinity.

Salinity (ppm)	Amount of CO_2 dissolved in Brine (tons) after 25 years of injection	% reduction in CO_2 dissolution with respect to CO_2 dissolution at zero salinity	Comments
0	1.94e+06	--	Solubility decreases with increase in salinity
50,000	1.76e+06	9.27%	
100,000	1.50e+06	22.68%	
150,000	1.26e+06	35.05%	
195,000	1.09e+06	43.81%	
Total Injection Mass = 9.28e+06 tons			

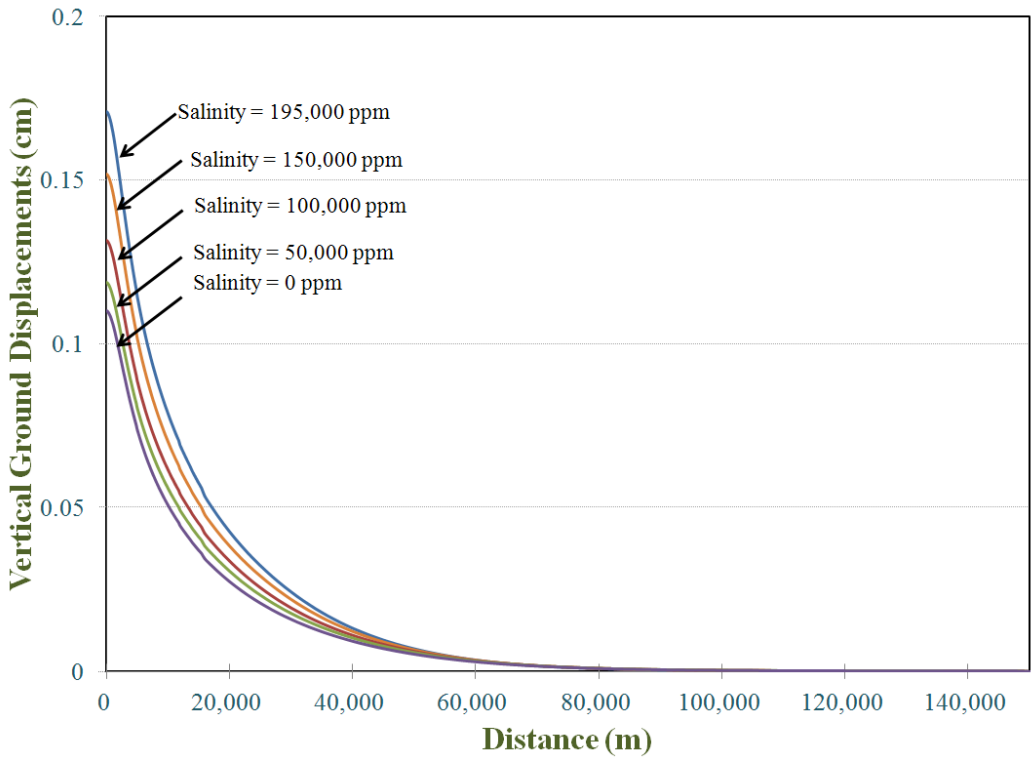

Figure 5-14: Change in ground displacements for different brine salinity values.

Chapter 6: MODEL VALIDATION

In this chapter, the coupled fluid flow, geomechanical and geochemical methodology presented in Chapter 4 and Chapter 5 is validated by performing numerical modeling using data reported in the literature and comparing the modeling results.

6.1 Validation of Coupled Fluid Flow and Geochemical Modeling (Example 1)

Nghiem et al., (2004) performed coupled multiphase fluid flow and geochemical modeling which involves the solution of the component transport equations, the thermodynamic equilibrium between gas and aqueous phase, and the equations of geochemistry. Numerical modeling was performed using CMG-GEM. A three dimensional model with both aqueous phase reactions and mineral reactions was used to illustrate the phenomenon of mineral trapping on CO_2 sequestration in an aquifer. In this study, the Peng-Robinson equation of state was used to calculate the PVT properties of CO_2 (Peng and Robinson, 1976). Henry's Law was used to calculate solubility of CO_2 in the aqueous phase (Li and Nghiem, 1986). The aqueous phase density was calculated using Rowe and Chou (1970) correlation, which is function of pressure, temperature and salinity.

In the current study, both three dimensional (3D) and axisymmetric, coupled fluid flow and geochemical models were constructed using the modeling details available in the literature (Nghiem et al., 2004). Figure 6-1 shows the schematic diagram of the hypothetical injection site. A no-flow boundary was assumed along the top and bottom of the model to account for the impermeable seal layers for both the models. A no-flow boundary condition was also assumed at the left boundary of the axisymmetric model due to the radial symmetry of the CO_2 injection point. A constant pressure boundary was used at the right end of the axisymmetric and the 3D models to simulate an infinite radius reservoir condition. A reservoir thickness of 250 m was used in the models. The porosity and permeability of the reservoir was 38% and 2000 mD, respectively. CO_2 was injected for 25 years at a primary rate constraint of 2,568 metric tonnes per day. Table 6-1 shows

the initial aqueous concentrations values used in this study. Table 6-2 shows the mineral and the reaction kinetic data obtained from the literature (Nghiem et al., 2004). Figure 6-2 and Figure 6-3 show the computed pH and the aqueous mass density, respectively. The numerical modeling results shown in Figure 6-2 and Figure 6-3 show that the axisymmetric model and 3D model provide a good match with the results reported by Nghiem et al.,(2004).

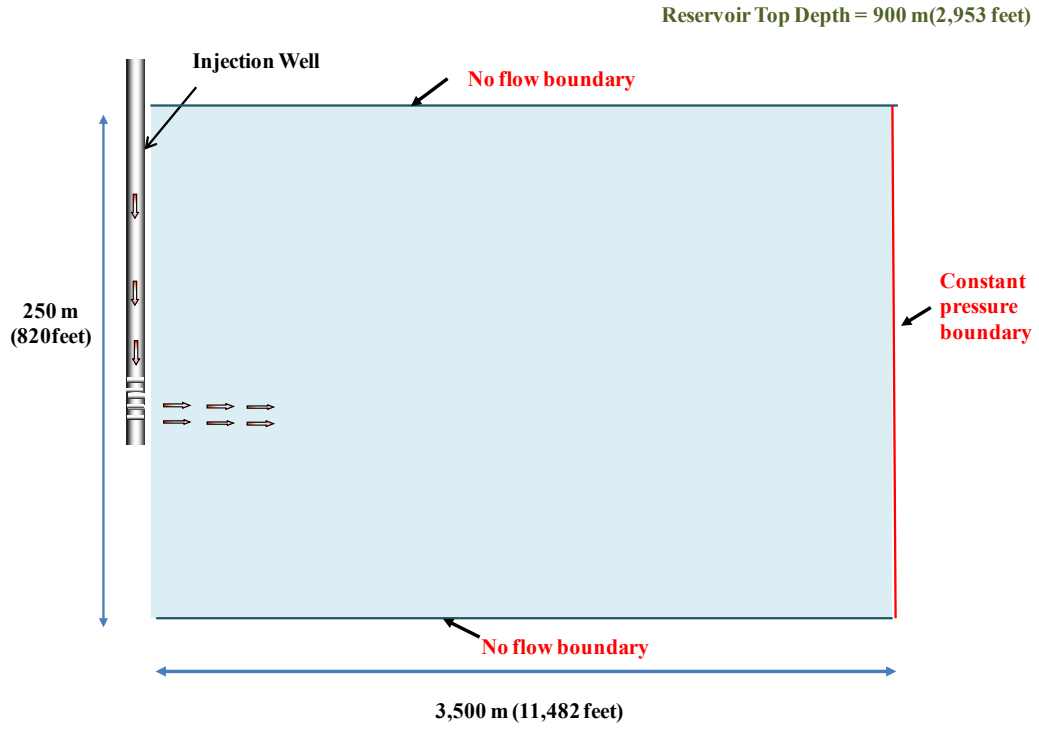

Figure 6-1: Model geometry and boundary conditions.

Table 6-1: Initial aqueous phase concentrations

Aqueous species	Molality (mg/l)
H^+	5.10e-08
Ca^{++}	9.118492e-05
SiO_2 (aq)	2.345433e-08
Al^{+++}	2.317806e-11
OH^-	5.456322e-07
HCO_3^-	2.489299e-02
CO_3^{2-}	1.170273e-05

Table 6-2: Mineral reaction data

Mineral	Chemical Composition	Log K^m_{eq} (50 ^{0}C)	Log(rate constant) (mol/m2/s) @ 25^{0}C)	Reactive surface area (m^2/m^3)	E(J/mol)	Volume fraction
Kaolinite	$Al_2Si_2O_5(OH)_4$	5.4706	-13.0	17,600	62,760	0.0176
Calcite	$CaCO_3$	1.3560	-8.79588	88	41,870	0.0088
Anorthite	$CaAl_2Si_2O_8$	23.0603	-12.0	88	67,830	0.0088

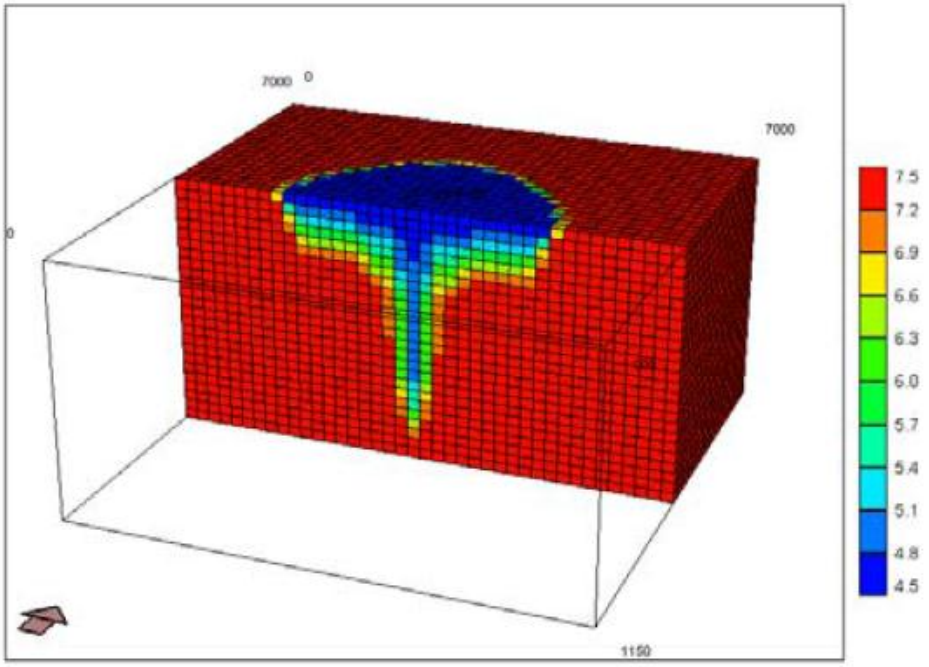

(a) 25 years (Nghiem et al., 2004)

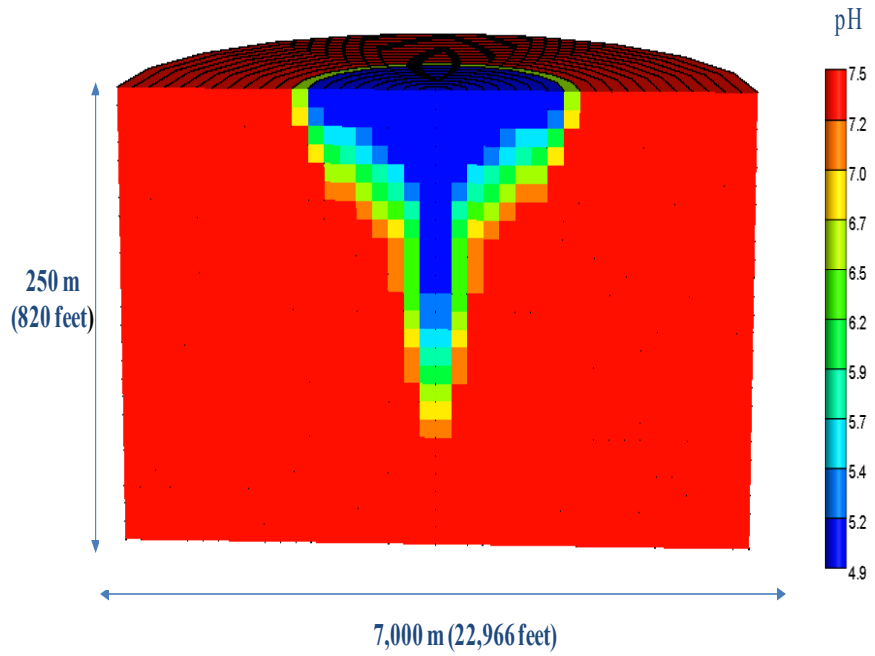

(b) 25 years (Axisymmetric model)

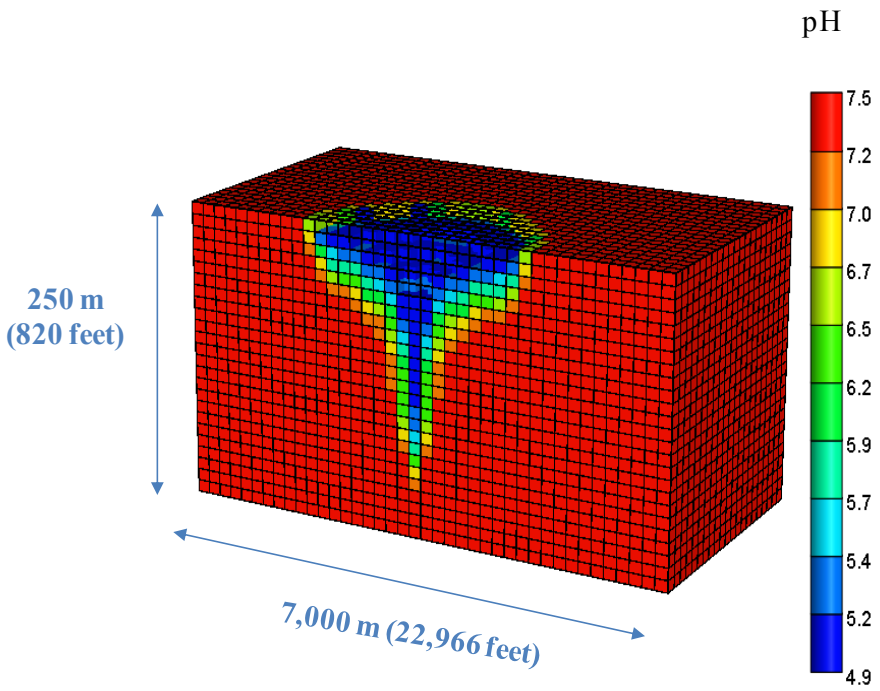

(c) 25 years (3D model)

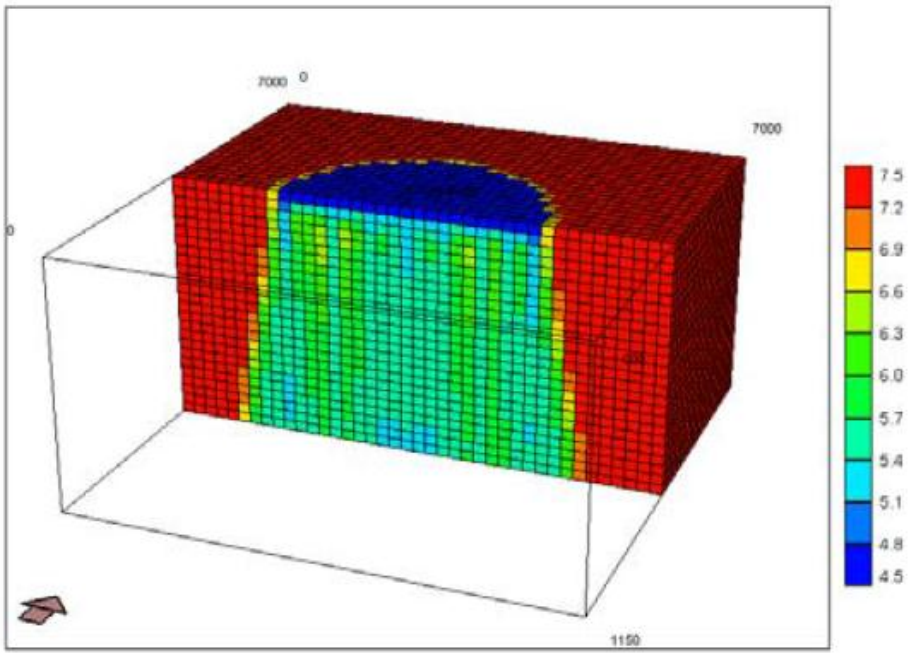

(d) 500 years (Nghiem et al., 2004)

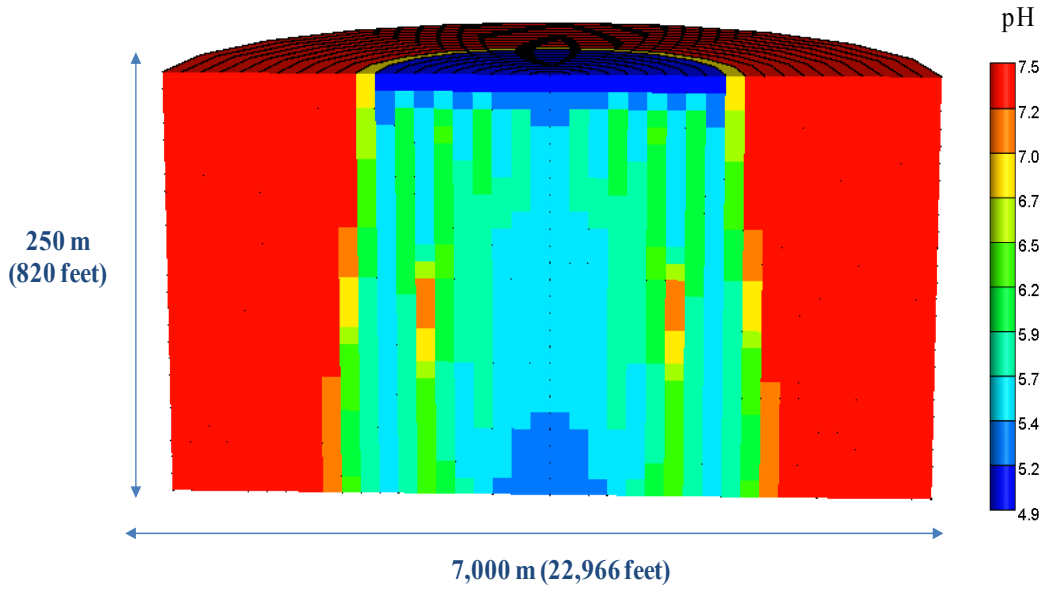

(e) 500 years (Axisymmetric model)

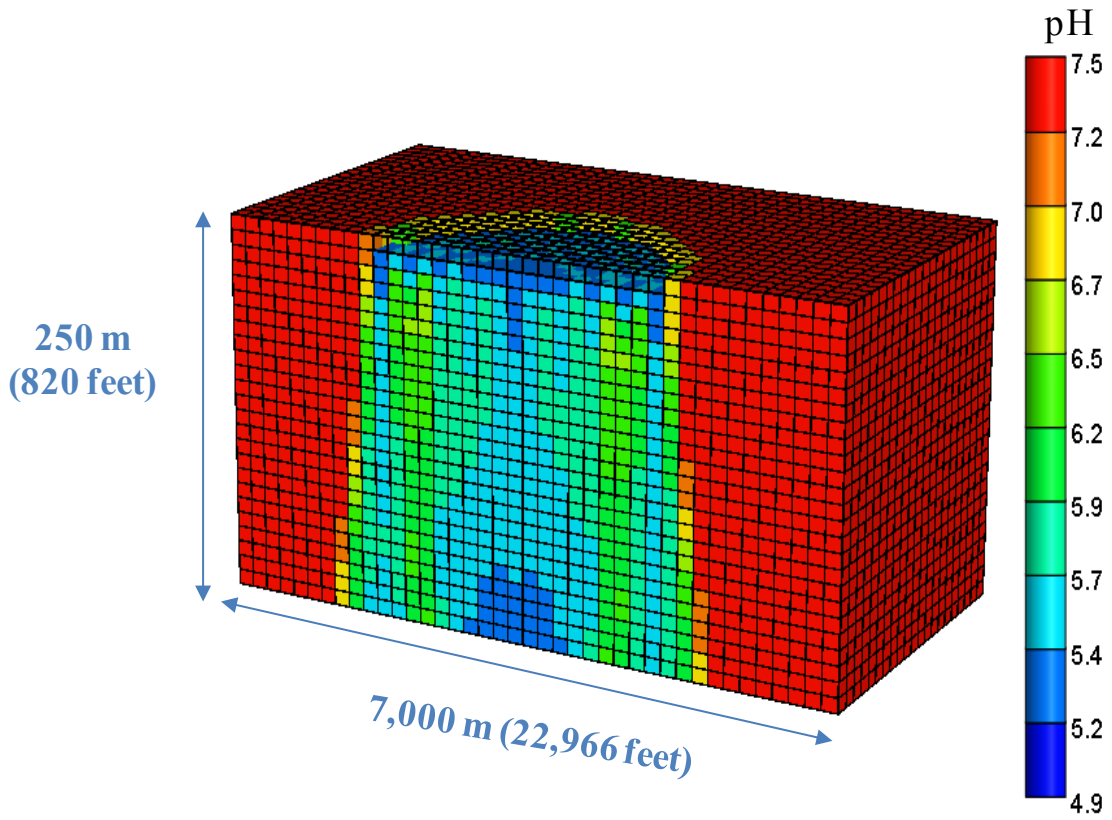

(f) 500 years (3D model)

Figure 6-2: Computed pH.

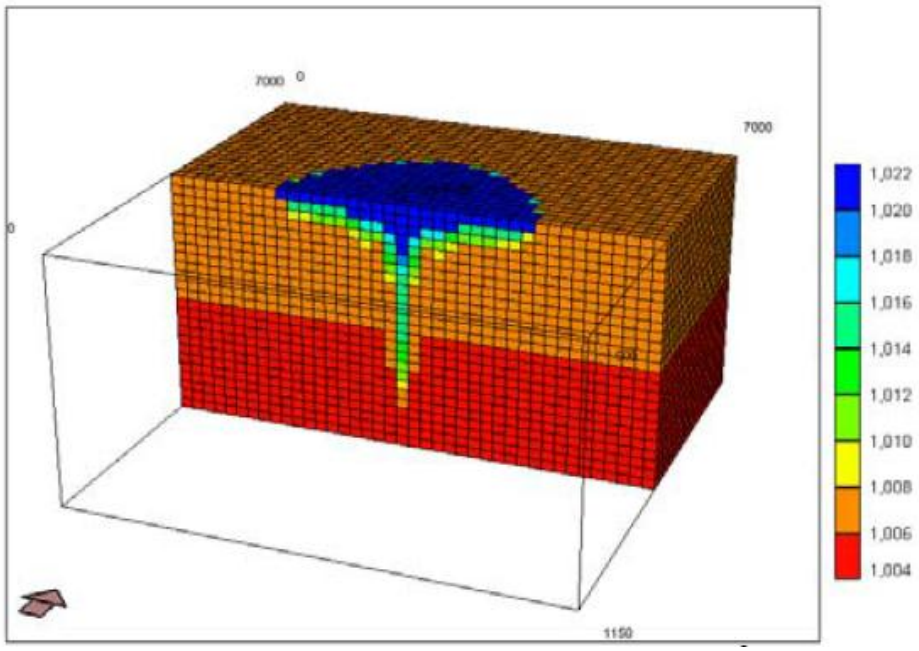

(a) 25 years (Nghiem et al., 2004)

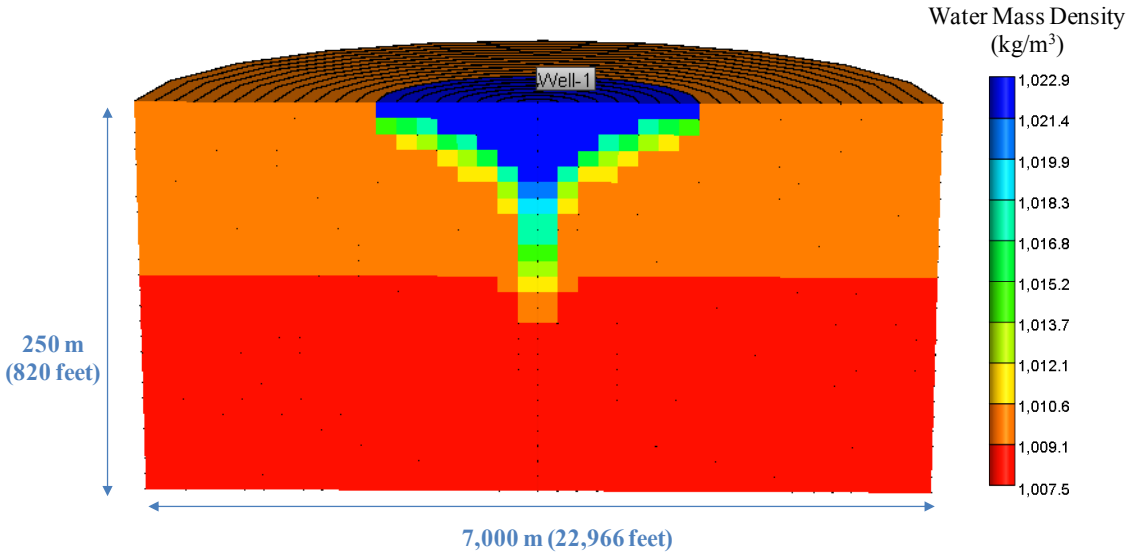

(b) 25 years (Axisymmetric model)

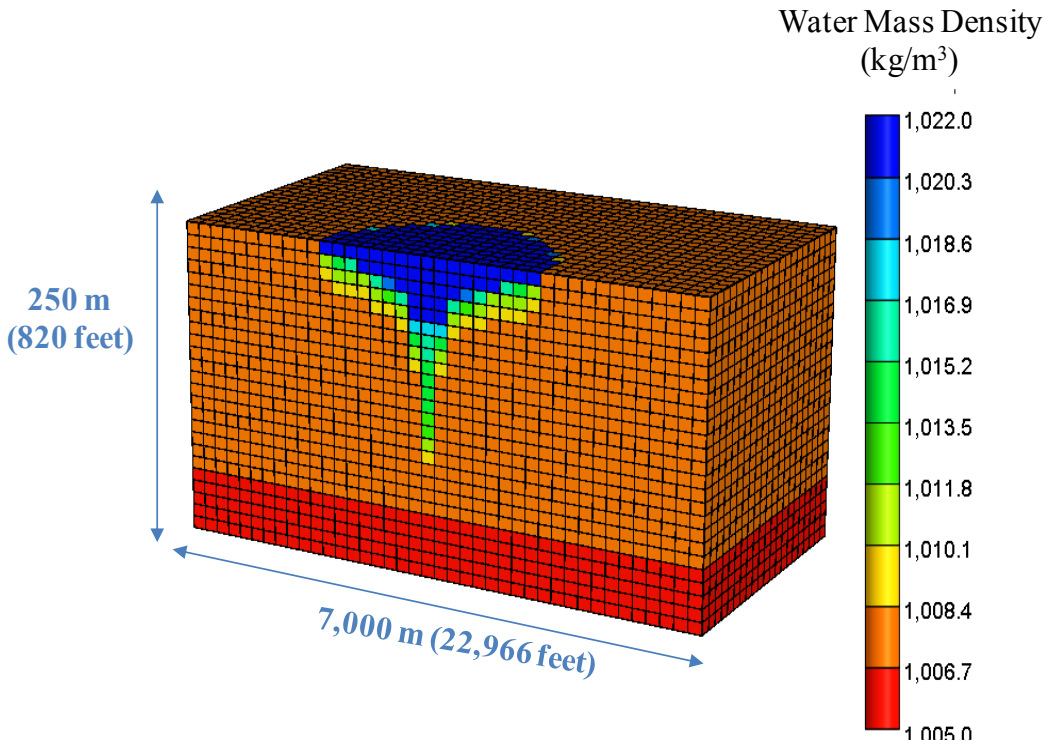

(c) 25 years (3D model)

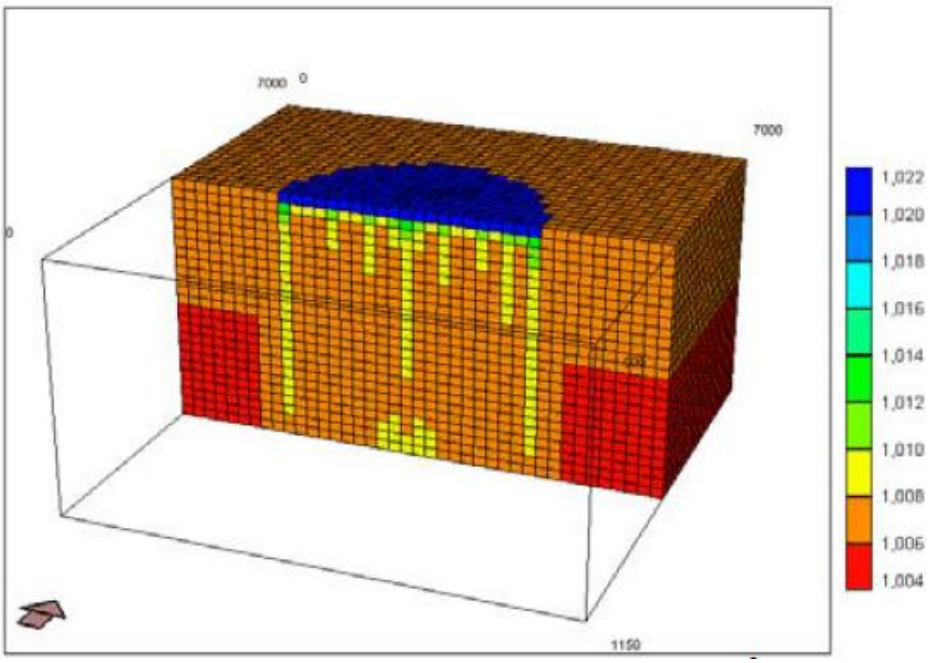

(d) 500 years (Nghiem et al., 2004)

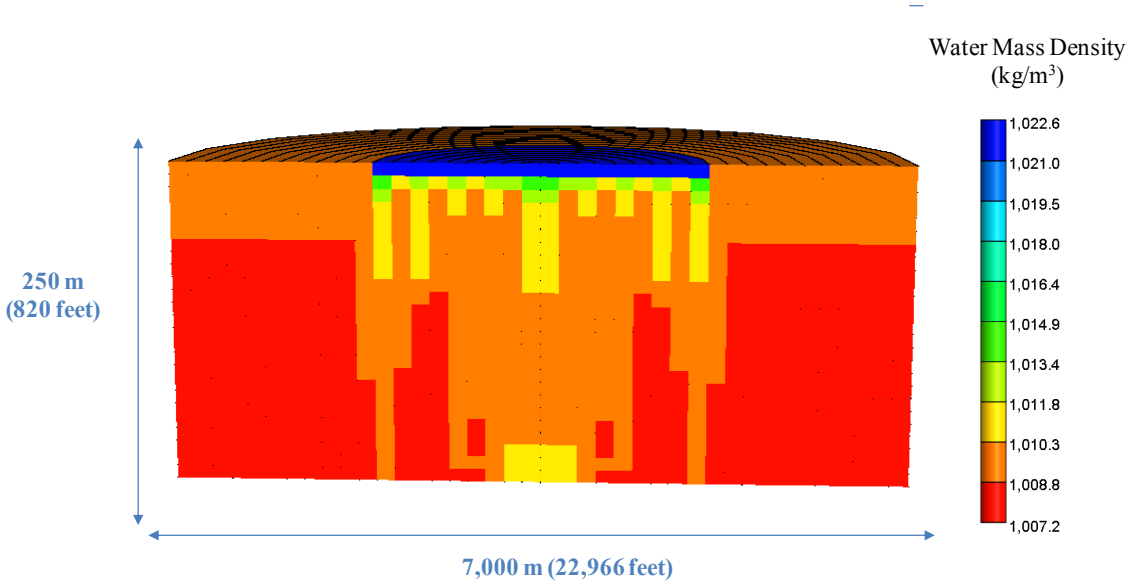

(e) 500 years (Axisymmetric model)

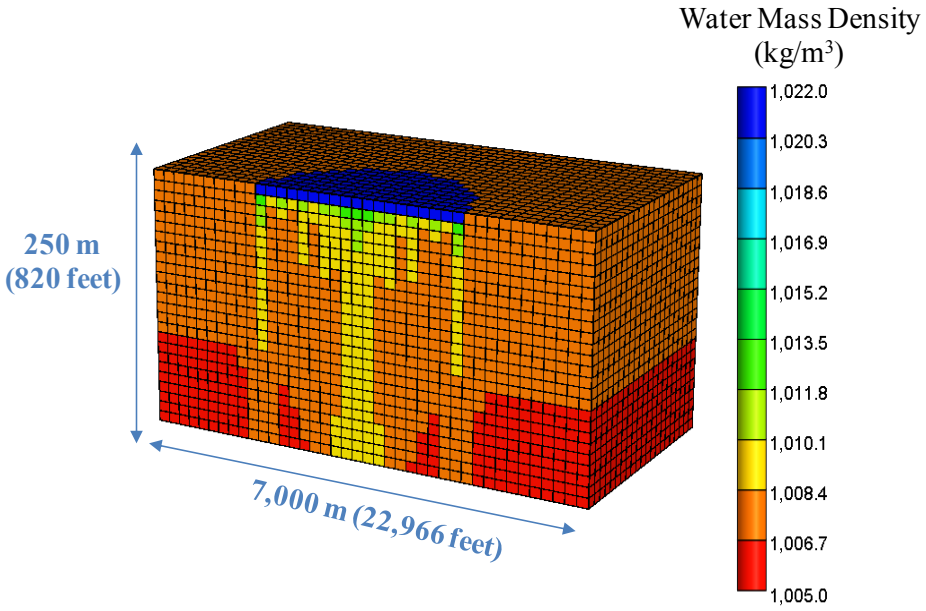

(f) 500 years (3D model)

Figure 6-3: Computed water mass density.

6.2 Comparison of Coupled Fluid Flow and Geochemical Modeling (Example 2)

Ranganathan et al.,(2011) performed coupled fluid flow and geochemical modeling to evaluate the viability of CO_2 storage within the Rotliegend sandstone formation,located in the Netherlands. The thickness of the sandstone formation was reported to be 50 m. CO_2 injection was carried out at a rate of 1 millon metric tonne per year for a period of 16 years. The total simulation run time was 10,000 years. A three dimensional cartesian grid which consists of 50 (i-direction) x 50 (j-direction) x 10 (z-direction) blocks encompassing an area of 15,000 m x 15,000 m x 50 m was used in the study performed by Ranganathan et al., (2011). In the current study, an axisymmetric, multiphase, coupled fluid flow and geochemical model as shown in Figure 6-4 was constructed to simulate the CO_2 injection and the process of mineral dissolution and precipitation that takes place due to CO_2 dissolution in brine. A no-flow boundary was assumed along the top and bottom of this model to account for the impermeable seal layers. A no-flow boundary condition was also assumed at the left boundary due to the radial symmetry. However, a constant pressure boundary was used at the right end of the model to simulate an infinite radius reservoir condition. The formation porosity and permeability was reported to be 18% and 200 mD, respectively (Ranganathan et al., 2011). The mineral reaction data shown in Table 6-3 was reported in the study performed by Ranganathan et al., (2011). Table 6-4 shows the aqueous concentration of the brine.

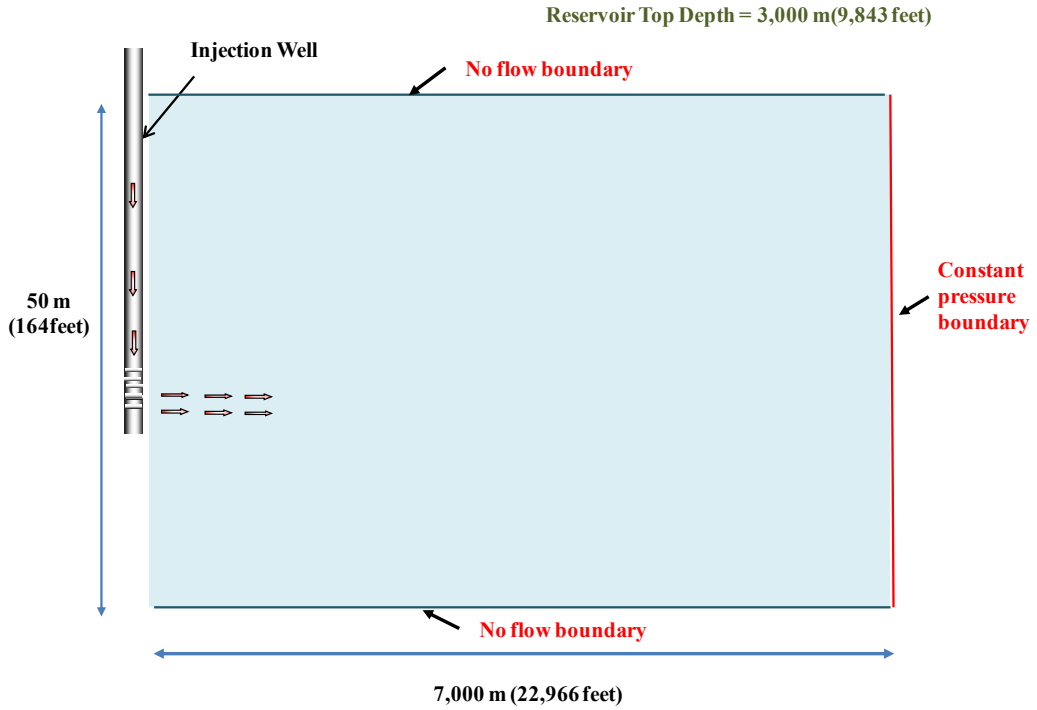

(a) Schematic diagram of the hypothetical injection zone

Figure 6-4: Model geometry and boundary conditions.

Table 6-3: Mineral reaction data (Ranganathan et al., 2011)

Mineral	Chemical Composition	Log K^{m}_{eq} (50 ^{0}C)	Log(rate constant) (mol/m2/s) @ 25^{0}C)	Reactive surface area (m^2/m^3)
Kaolinite	$Al_2Si_2O_5(OH)_4$	5.4706	-12.0	17,600
Quartz	SiO_2	-3.629	-13.9	7,128
K-feldspar	$KAlSi_3O_8$	-0.344	-13.00	176
Dolomite	$CaMg(CO_3)_2$	1.6727	-9.22	88
Illite	$Mg_{0.25}K_{0.6}Al2.3Si_{3.5}O_{12}H_2$	7.4855	-14.00	26,400

Table 6-4: Aqueous molality concentration in formation brine (Ranganathan et al., 2011)

Aqueous species	Molality (mol/kg of water)
H^+	1.64e-08
Ca^{2+}	6.11e-03
SiO_2	8.64E-04
Al^{3+}	5.57e-07
K^+	5.09e-01
Mg^{2+}	3.44e-02
OH^-	5.66e-05
HCO_3^-	1.44e-02
CO_3^{2-}	1.47e-07

A comparison of the computed changes in the mineral mole concentrations for different minerals with the reported values by Ranganathan et al., (2011) is shown in Figures 6-5(a) through 6-5(e). Modeling results show that the computed amount of Dolomite that has been deposited is significantly lower than Kaolinite, K-feldspar, and Quartz. Although, Dolomite has a significantly higher rate of reaction compared to Quartz, Kaolinite and K-feldspar, the computed amount of Dolomite that has been deposited is significantly lower due to insignificant amounts of Ca^{2+} and Mg^{2+} ions available in the brine. The coupled fluid flow and geochemical model used in the current study underestimates the amount of Quartz deposited and overestimates the amount K-feldspar mineral deposited as shown in Figure 6-5 (d) and Figure 6-5(e), respectively. It has been reported by Ranganathan et al., (2011) that the computed amount of Quartz and Kaolinite that is deposited during the storage period is about the same. In order to match the modeling results reported by Ranganathan et al., (2011), a parametric analyses was performed by changing the mineral reaction rate of K-feldspar. A mineral reaction value of -14.00 mol/m^2/s gave a good match for the change in mineral moles for different mineral that were reported by Ranganathan et al., (2011). Figures 6-6(a) through Figure 6-6(e) show the comparison of the computed changes in the mineral mole concentrations for different minerals with the reported values by Ranganathan et al., (2011)

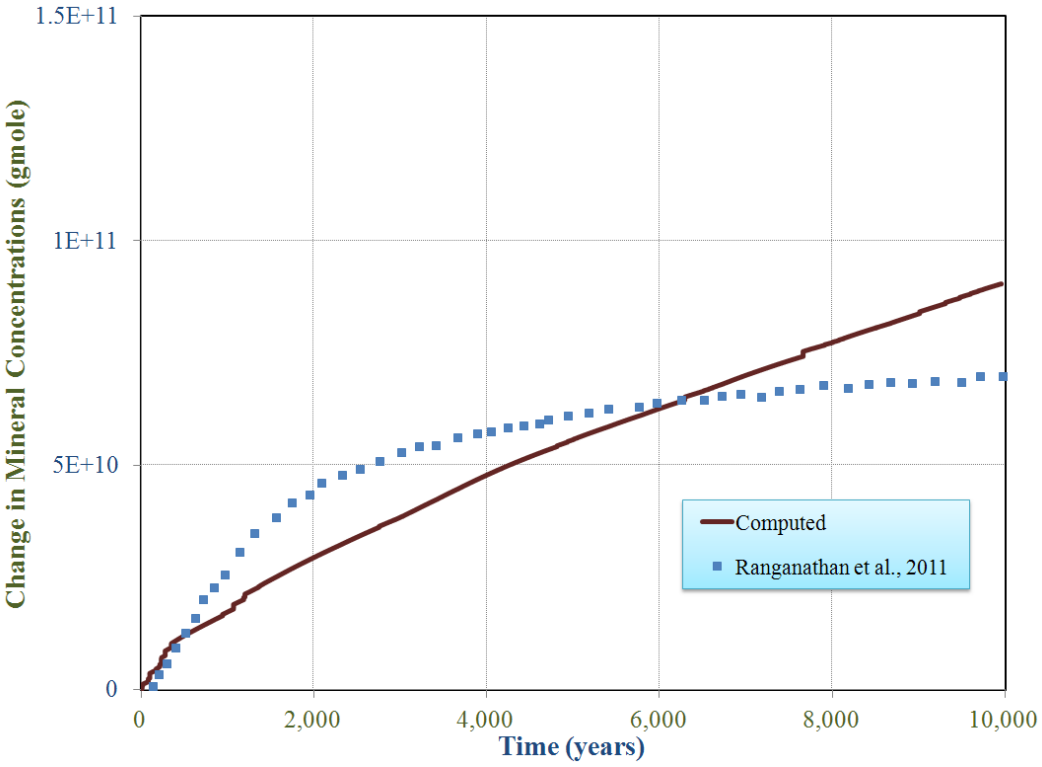

(a) Kaolinite

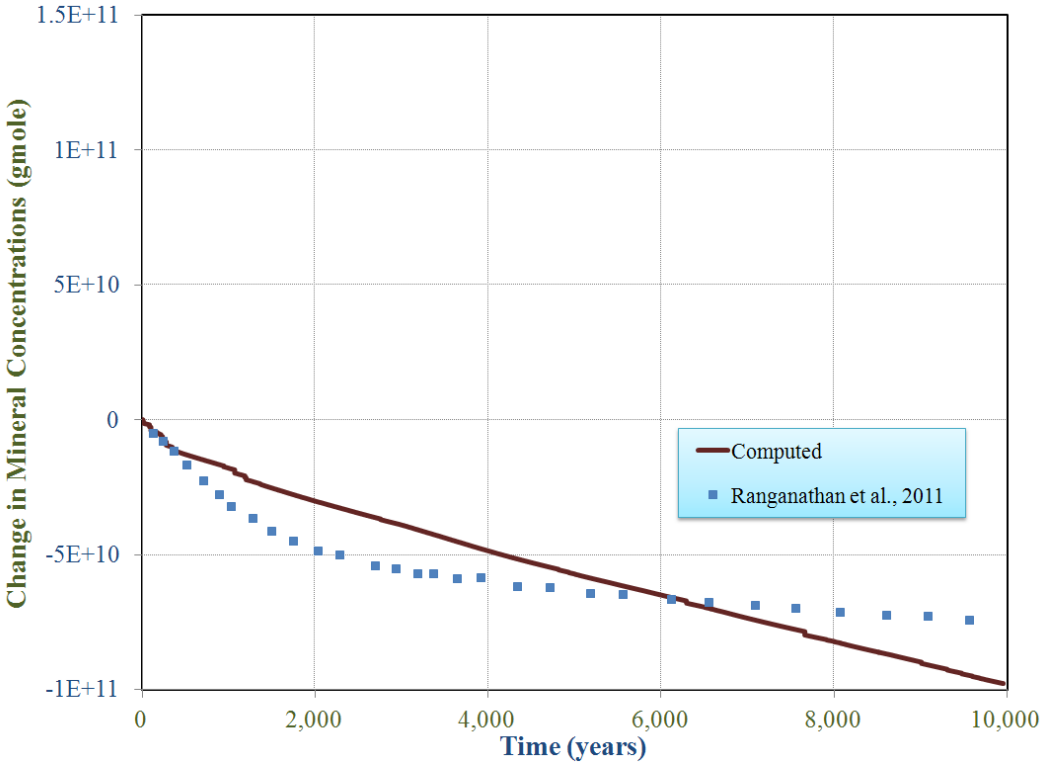

(b) Illite

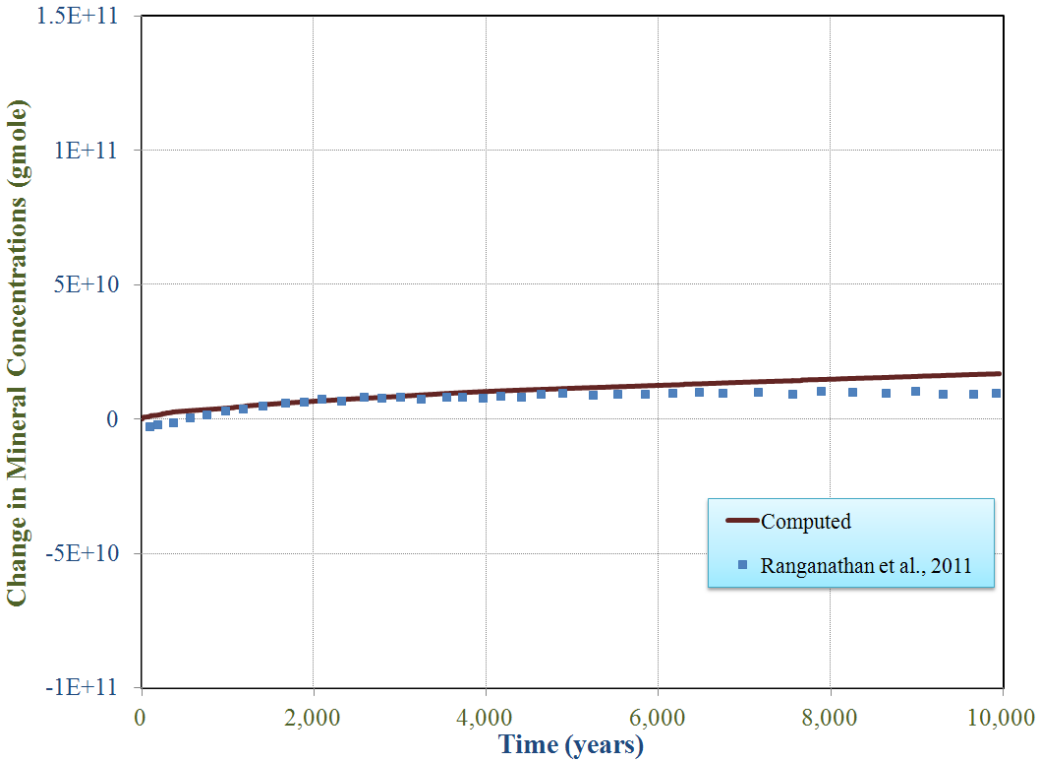

(c) Dolomite

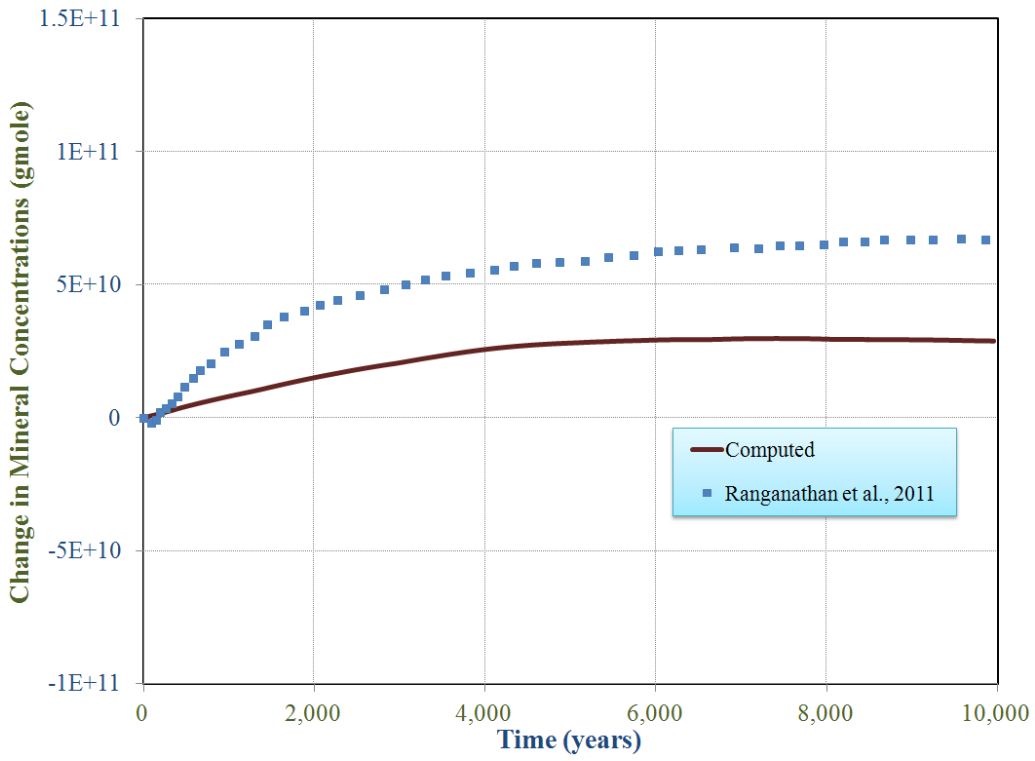

(d) Quartz

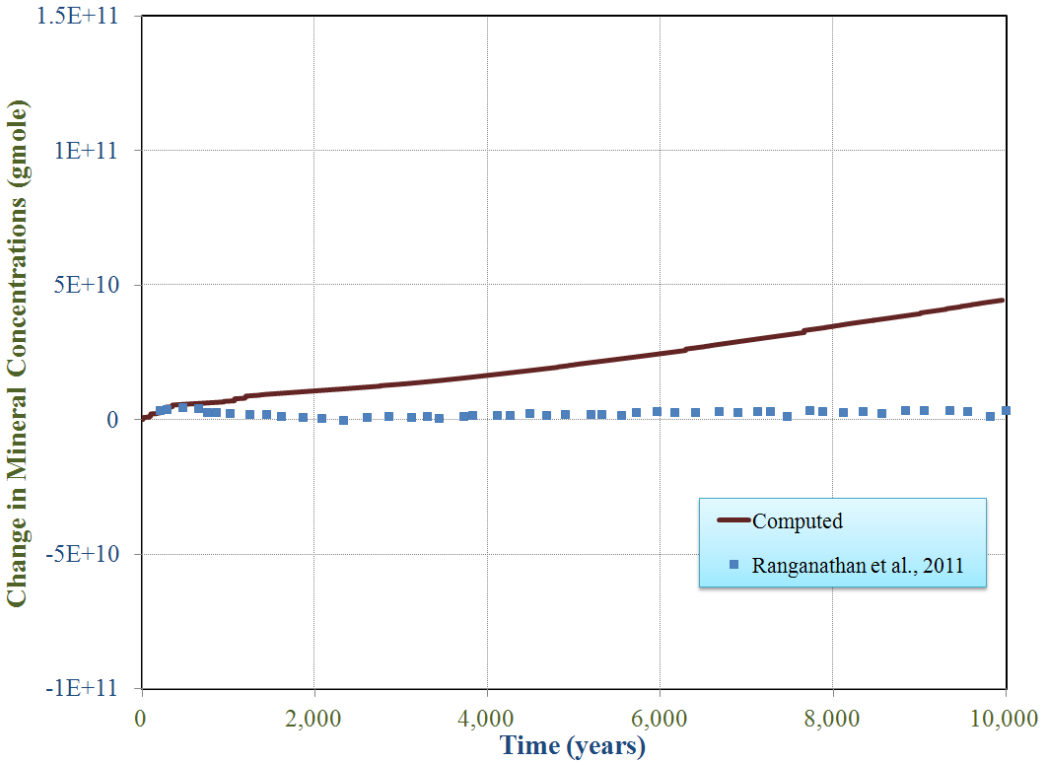

(e) K-feldspar

Figure 6-5: Change in mineral mole concentrations using the mineral reaction data reported by Ranganathan et al., 2011.

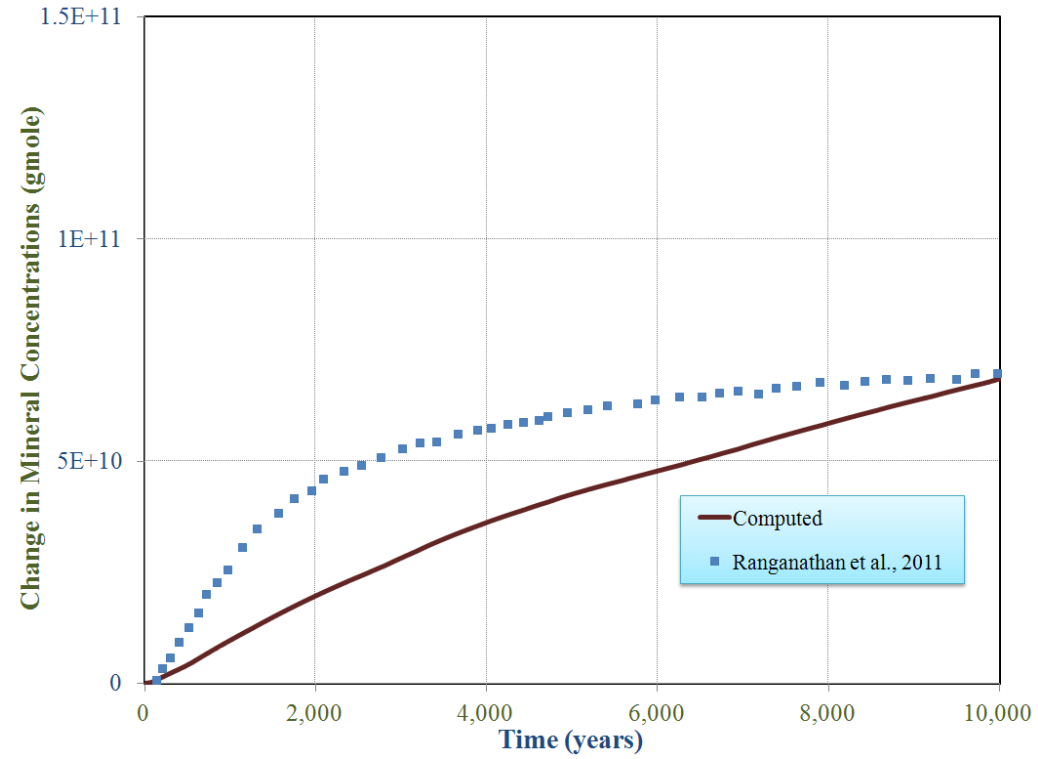

(a) Kaolinite

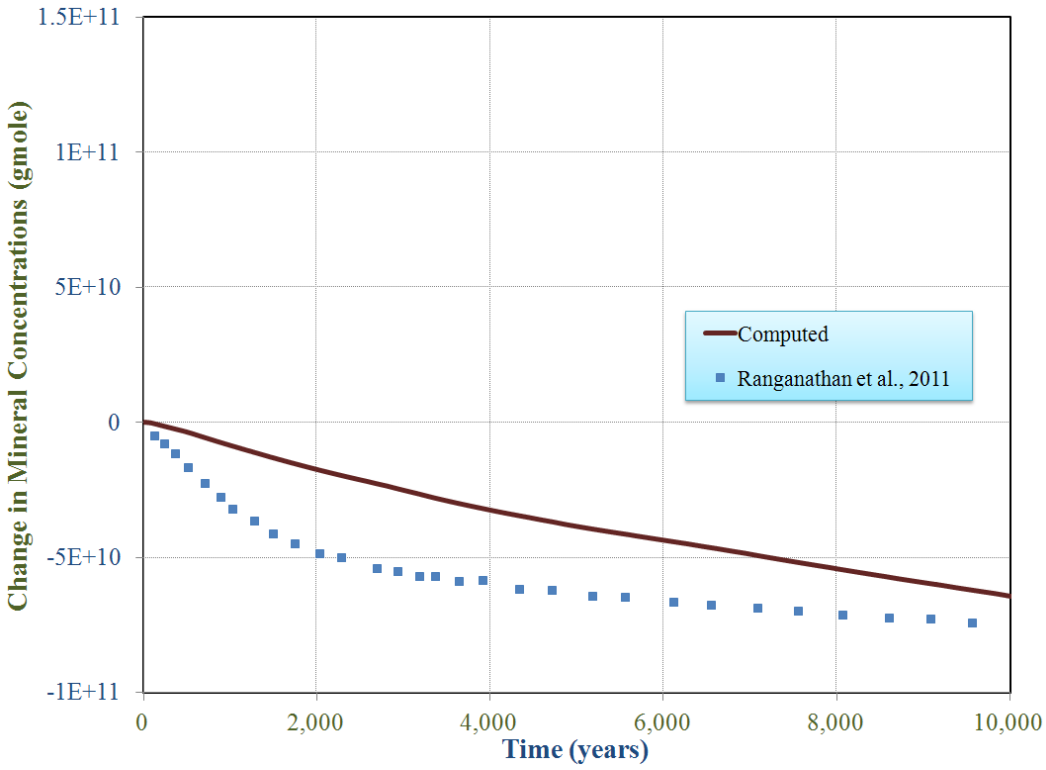

(b) Illite

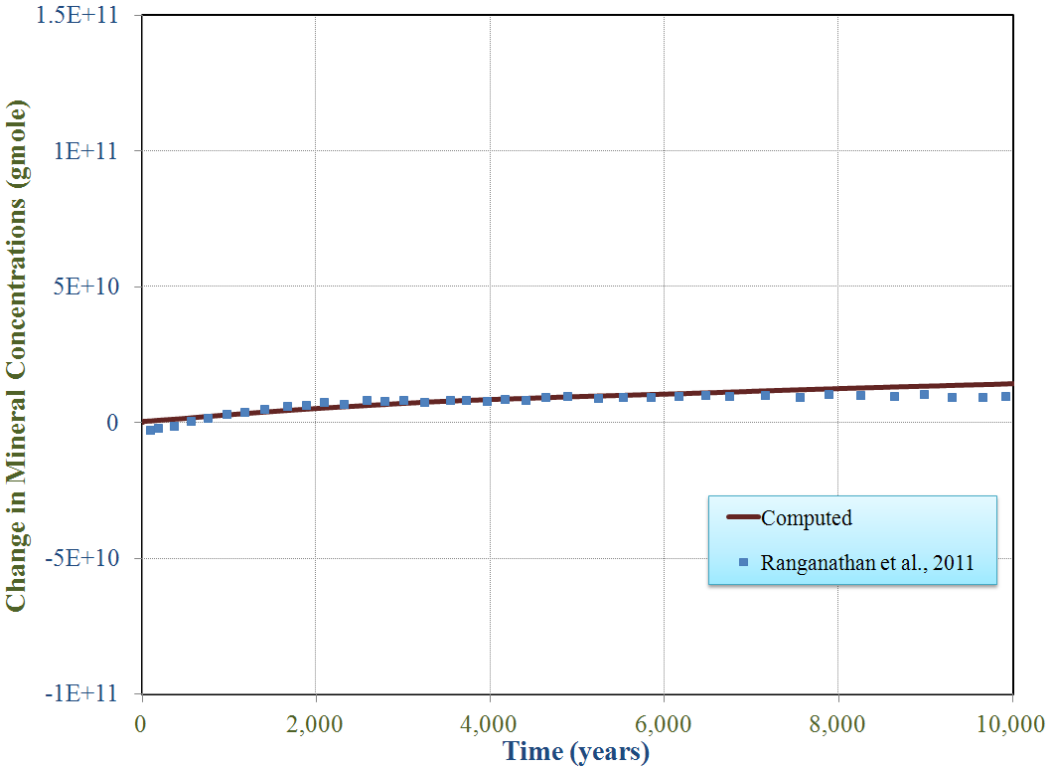

(c) Dolomite

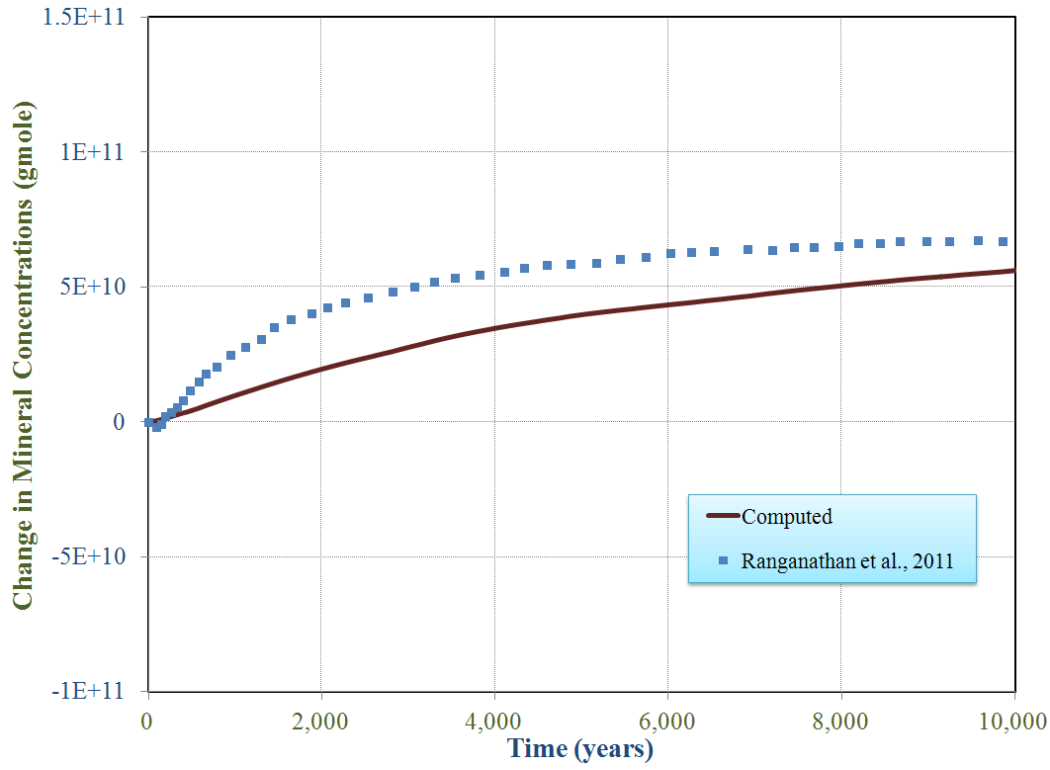

(d) Quartz

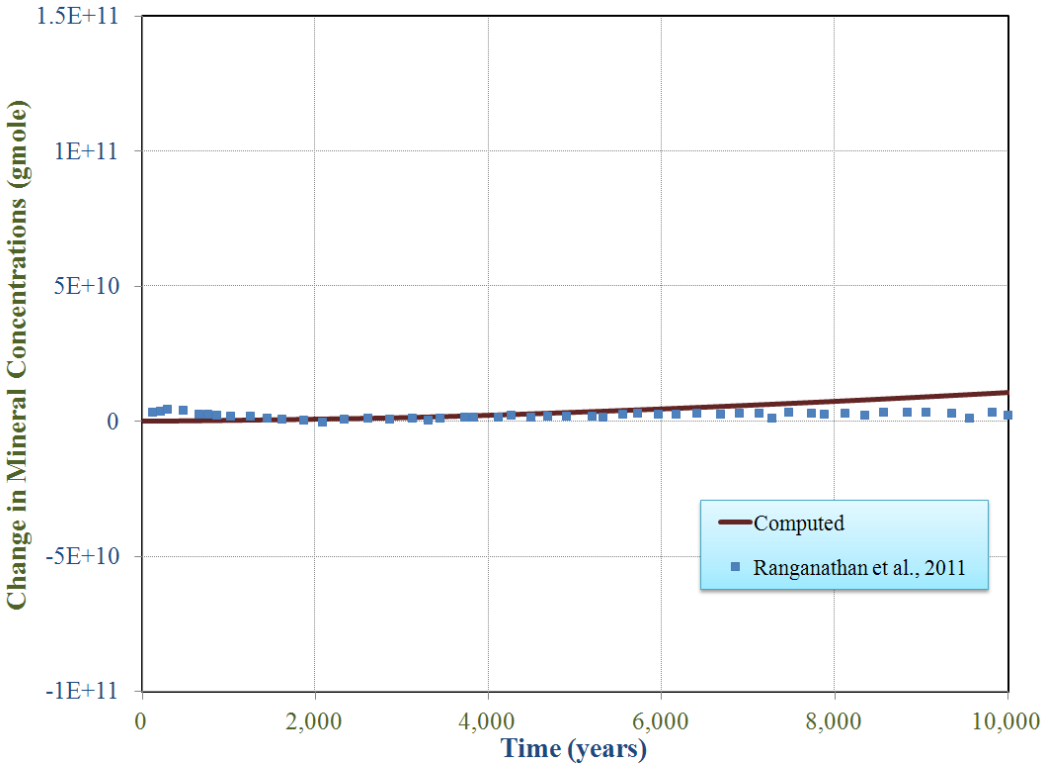

(e) K-feldspar

Figure 6-6: Comparison of the change in mineral mole concentrations with reduced mineral reaction rate for K-feldspar.

There seems to be an inconsistency between the rate of reactions reported by Ranganathan et al., (2011) and amount of mineral deposition that is taking place. Since the mineral rate reaction of Kaolinite is about two orders of magnitude greater than Quartz, a lesser amount of Quartz deposition should have occurred. Also, Ranganathan et al., (2011) assumed that the reaction rate of Kaolinite (-12.00 mol/m^2/s) is greater than K-feldspar (-13.00 mol/m^2/s) and Quartz (-13.90 mol/m^2/s). However, the reaction rate constants reported by Nghiem et al., (2004) and Xu et al., 2003, suggest that the reaction rate of Kaolinite (-13.00 mol/m^2/s) is lower than K-feldspar (-12.00 mol/m^2/s). Based on the magnitude of the mineral reaction rate constant, the SiO_2 ions available from the dissolution of Illite, are consumed primarily by Kaolinite, and followed by K-feldspar and Quartz, respectively. However, the computed amount of K-feldspar reported by Ranganathan et al., (2011) is significantly lower than the amount of Quartz deposited. In order to investigate the influence of the mineral reaction rate on mineralization, a study was performed using the mineral reaction rate constants reported by Nghiem et al., (2004). Table 6-5 shows the mineral reaction data reported by Nghiem et al., (2004). Figure 6-7 shows the change in mineral mole concentrations using the mineral reaction data reported by Nghiem et al., (2004). Table 6-6 shows a comparison of the computed cumulative changes in mineral concentration for different mineral reaction rate values. Modeling results show that there is a significant reduction in the precipitation of Quartz when the mineral reaction rate data reported by Nghiem et al., (2004) was used.

Table 6-5: Mineral reaction data (Nghiem et al., 2004)

Mineral	**Chemical Composition**	**Log K^m_{eq} (50 ^{0}C)**	**Log(rate constant) (mol/m^2/s) @ 25^{0}C)**	**Reactive surface area (m^2/m^3)**
Kaolinite	$Al_2Si_2O_5(OH)_4$	5.4706	-12.0	17,600
Quartz	SiO_2	-3.629	-13.9	7,128
K-feldspar	$KAlSi_3O_8$	-0.344	-13.00	176
Dolomite	$CaMg(CO_3)_2$	1.6727	-9.22	88
Illite	$Mg_{0.25}K_{0.6}Al_2.3Si_{3.5}O_{12}H_2$	7.4855	-14.00	26,400

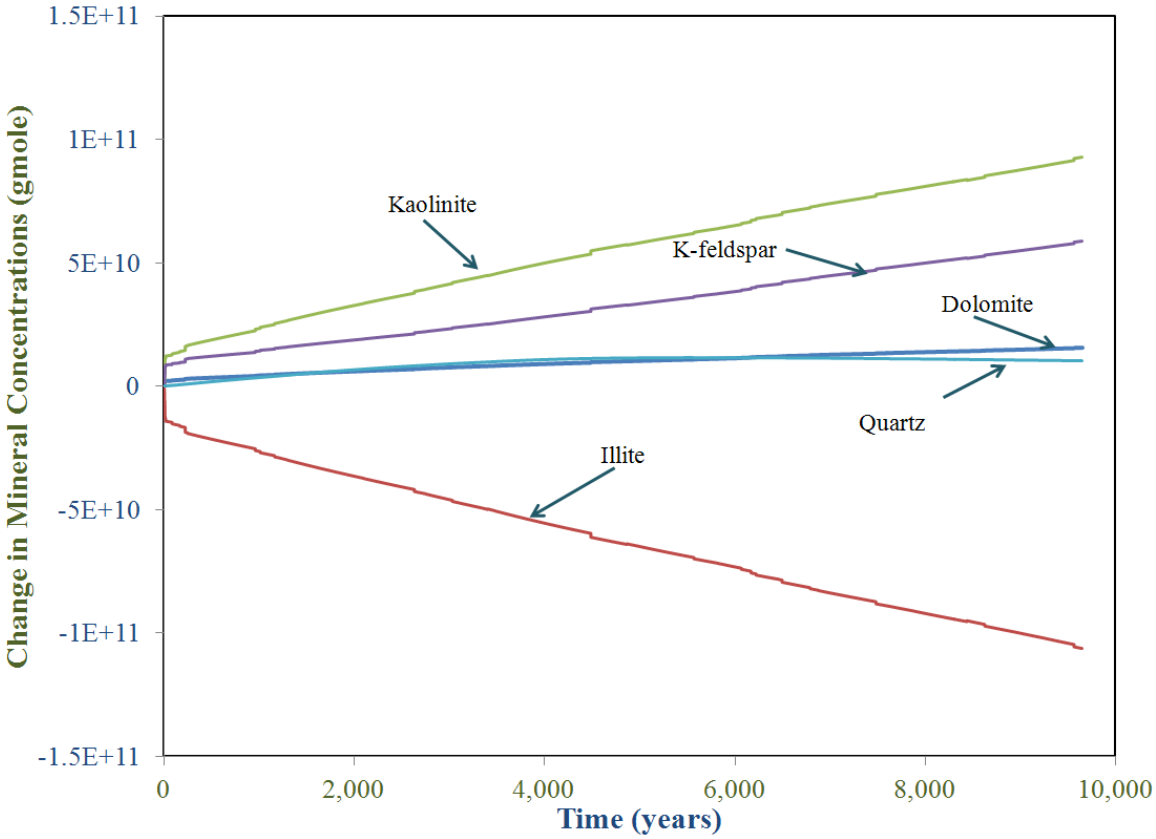

Figure 6-7: Change in mineral mole concentrations using the mineral reaction data reported by Nghiem et al., 2004.

Table 6-6: Comparison of mineral mole change due to mineralization.

Mineral	Cumulative change in mineral concentration (gmole)		% Difference in mineral molar change with respect to Ranganathan et al., 20011 data
	Ranganathan et al., (2011) reaction rate data	Nghiem et al., (2004) reaction rate data	
Dolomite	1.68E+10	1.62E+10	-3.81
Illite	-9.83E+10	-1.09E+11	10.72
Kaolinite	9.07E+10	9.50E+10	4.74
K-feldspar	4.46E+10	6.04E+10	35.32
Quartz	2.88E+10	9.97E+09	-65.39

6.3 Validation of Single-Phase Coupled Fluid Flow and Geomechanical Modeling

In order to validate the iterative coupled approach used in the coupled fluid flow and geomechanical modeling using CMG-GEM (refer to section 5-1), a comparison of the ground displacements due to fluid injection into a hypothetical injection site was performed with the results obtained from ABAQUS (2012). ABAQUS is a commercially available finite element software. Figure 6-8 shows the schematic diagram of the hypothetical injection site considered in this study. Four geologic layers were considered, including the overburden layer, the caprock layer, the target reservoir, and the underburden layer. Table 6-7 shows the assumed reservoir and geomechanical properties for each layer which were based on the values reported in published literature (Rutqvist and Tsang. 2002). An axisymmetric model was constructed using CMG-GEM and

Abaqus, and the ground responses are presented in this section. The model extends vertically from 0 to 3,000 m and horizontally far enough from the injection zone (30,000 m). Reservoir temperature of 47.50 °C was assumed using a gradient of 1.82°C/100 m (Rutqvist and Tsang, 2002). Initial fluid pressure was computed by assuming a fluid pressure gradient of 9.81 kPa/m.

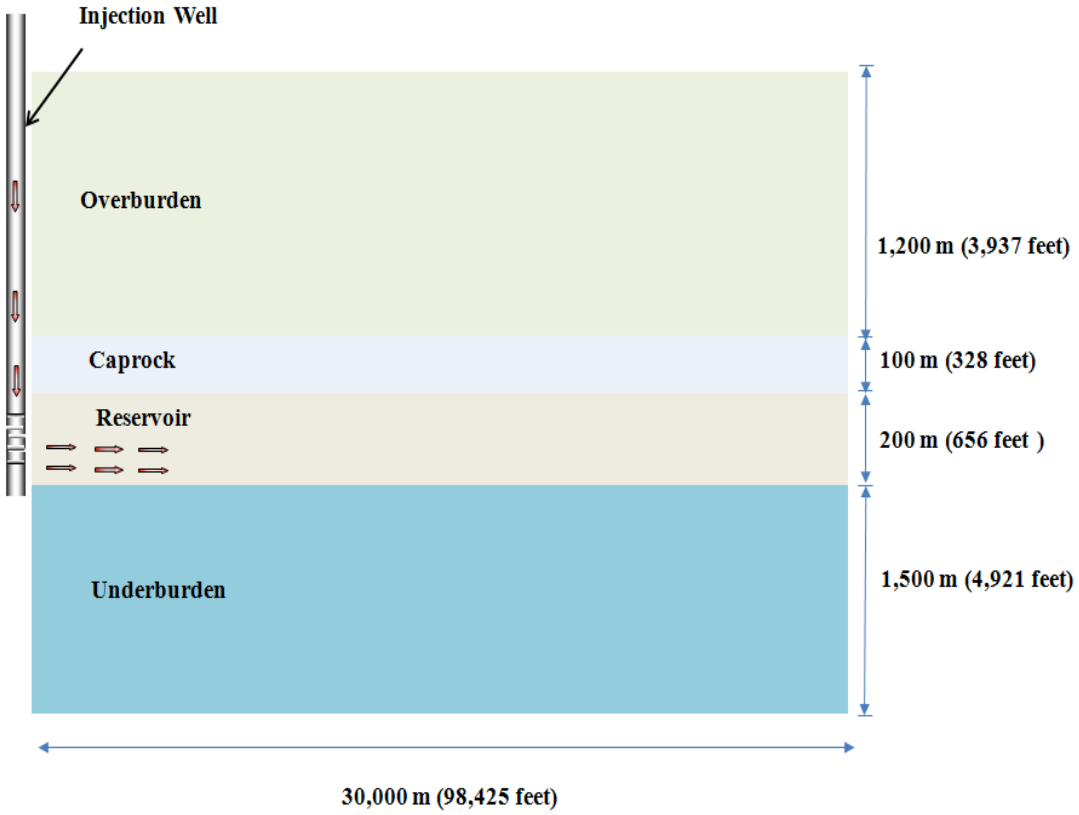

(a) Schematic diagram of the hypothetical injection site

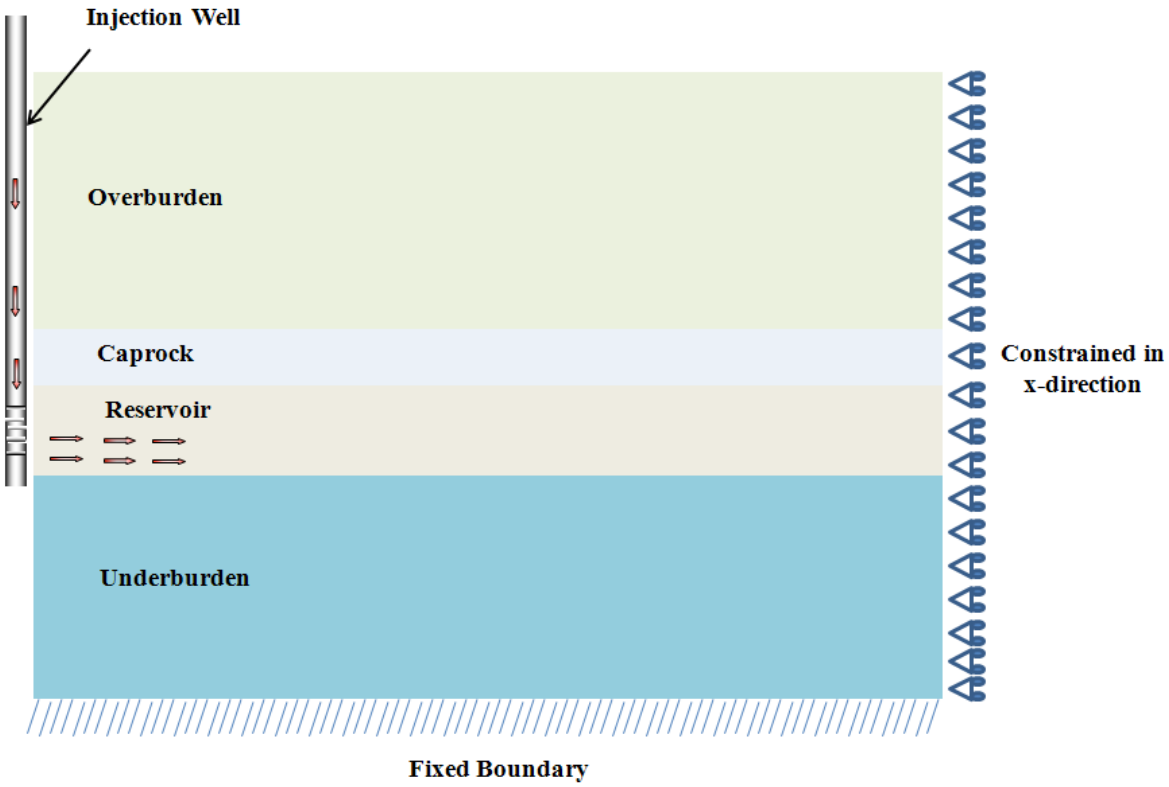

(b) Boundary conditions

Figure 6-8: Model geometry and boundary conditions.

Table 6-7 : Material Properties (Rutqvist and Tsang., 2002)

Material Property	Overburden Layer	Caprock	Reservoir	Underburden
Elastic Modulus (kPa)	5e+06	5e+06	5e+06	5e+06
Poisson's ratio	0.25	0.25	0.25	0.25
Permeability (mD)	1	1e-02	1e+02	1e-06
Porosity (%)	10	10	10	10

6.3.1 **Axisymmetric modeling using CMG-GEM**

Based on the hypothetical injection site as shown in Figure 6-8, an axisymmetric, coupled fluid flow and geomechanical model (300 x 1 x 20 blocks) was constructed. Since CMG-GEM is a multi-phase fluid flow simulator, water and CO_2 were selected as two components in the fluid flow model. A fully water saturated (99.999%) reservoir was considered in the model. However, a small fraction of CO_2 (0.001) was considered in the initialization of the fluid components in the model. Idealized relative permeability curves were used in the model as shown in Figure 6-9. In order to simulate an infinite lateral extent of the geologic layers; a constant pressure boundary was prescribed using large volume multipliers for the grid blocks of the boundary elements. The bottom boundary of the model was constrained in the z-direction, and the lateral boundaries were set on rollers. Water injection was carried out at a depth of 1,400 m at a differential pressure of 13,788 kPa for a time period of five years.

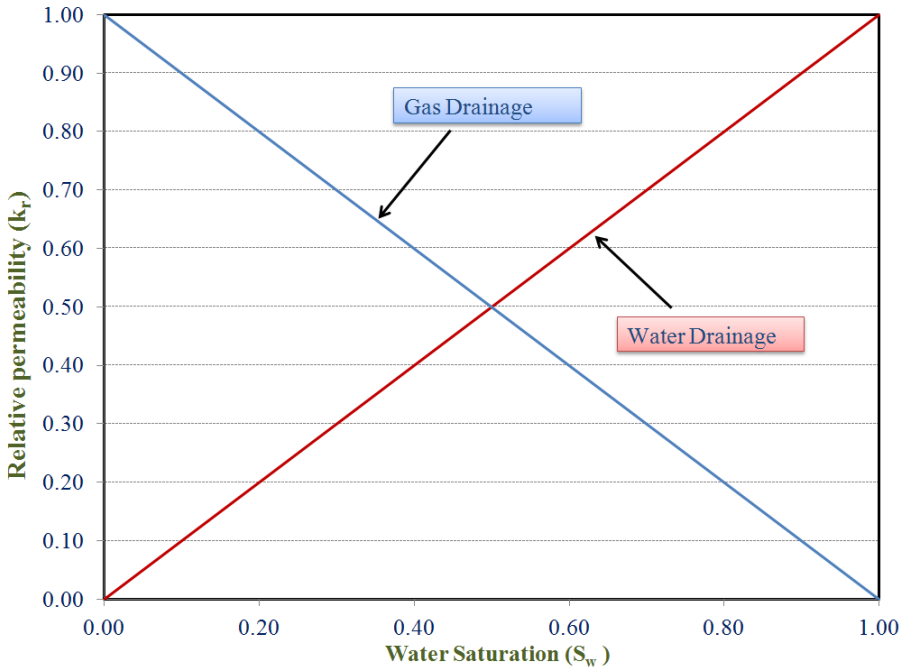

Figure 6-9: Idealized relative permeability curves.

6.3.2 **Axisymmetric modeling using Abaqus**

Based on the hypothetical injection site as shown in Figure 6-8, an axisymmetric, coupled fluid flow and geomechanical model with the same grid configuration used in the CMG-GEM model (300 x 1 x 20 blocks) was constructed to simulate water injection into the hypothetical reservoir. A fully-saturated reservoir was considered in the model. In order to simulate an infinite lateral extent of the geologic layers, a constant pressure boundary was prescribed for the lateral boundary elements. The bottom boundary of the model was constrained in the z-direction, and the lateral boundaries were set on rollers. Water injection was carried out at a depth of 1,400 m at a differential pressure of 13,788 kPa for a time period of five years. Figure 6-10 shows the comparison between the computed ground displacements along the radial distance from the CMG-GEM and Abaqus models. Modeling results show that the finite element model (Abaqus) yields smaller vertical ground displacements (0.058 m) as supposed to CMG-GEM (0.063 m).The difference in magnitudes of ground displacements is about 9%. This difference in vertical displacements can be considered insignificant.

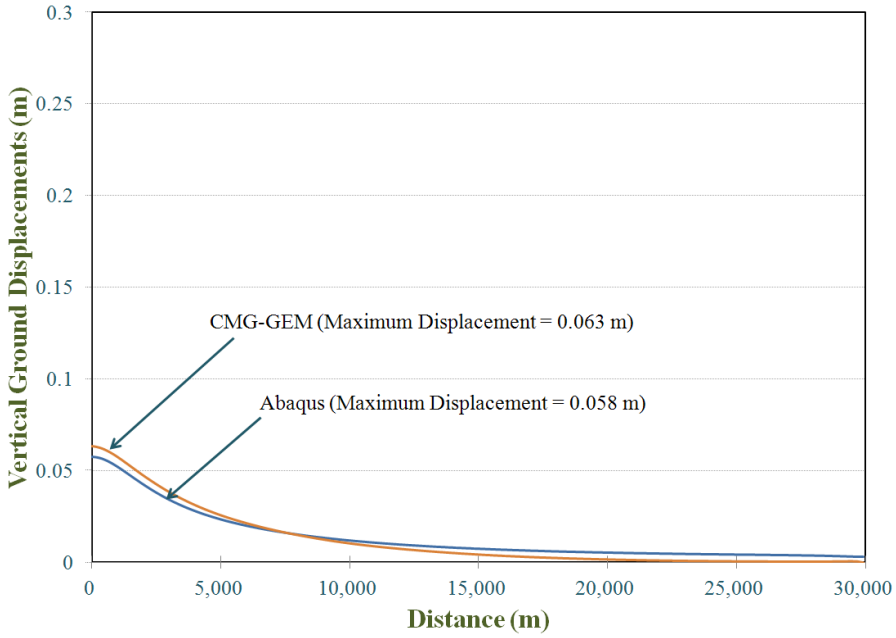

Figure 6-10: Comparison of computed ground displacements.

6.4 Validation of Multiphase Coupled Fluid Flow and Geomechanical Modeling

In order to validate the multi-phase coupled fluid flow and geomechanical modeling using CMG-GEM, a study was performed to compare the ground displacements due to CO_2 injection with the values reported by Rutqvist et al., (2010). A study was performed by Rutqvist et al., (2010) to investigate the effectiveness of multiphase, coupled fluid flow and geomechanical modeling in evaluating the geomechanical response due to CO_2 injection into a low- permeability formation at the In Salah Gas Project site, Algeria. The numerical modeling results were compared with the available field data which included the ground deformations obtained from a satellite-based inferrometry (InSAR). TOUGH-FLAC was used in the study performed by Rutqvist et al., (2010). In the current study, an axisymmetric, coupled fluid flow and geomechanical model was constructed using CMG-GEM. Geometric details similar to that reported in the study performed by Rutqvist et al., (2010) were used in this study. Figure 6-11 shows the geometric details and a schematic diagram of the injection site considered in this study. Four geologic layers were considered, including the overburden layer, the caprock layer, the target reservoir, and the underburden layer. Table 6-8 shows the assumed reservoir and geomechanical properties for each layer which were based on values reported in published literature (Rutqvist et al., 2010). The vertical extent of the model is 3,640 m and the horizontal extent is 5,000 m. Reservoir temperature of 90 °C was assumed. The initial reservoir pressure was assumed to be 17,900 kPa. The reservoir temperature and initial reservoir pressure values were obtained from the literature (Rutqvist et al., 2010).

Based on the hypothetical injection site as shown in Figure 6-11, an axisymmetric, multiphase, coupled fluid flow and geomechanical model (40 x 1 x 13 blocks) was constructed to simulate CO_2 injection into the hypothetical reservoir. A fully-saturated reservoir was considered in the model. However, a small fraction of CO_2 (0.001) was considered in the initialization of the fluid components in the model. The bottom boundary of the model was constrained in the z-direction, and the lateral boundaries were set on rollers. CO_2 injection was carried out at a depth of 1,810 m at a

primary rate constraint of 780 metric tonnes per day and a secondary bottom-hole pressure constraint 27,900 kPa for a time period of three years. The CO_2 injection parameters were consistent with the average injection rates at the In Salah Project site (Rutqvist et al., 2010).

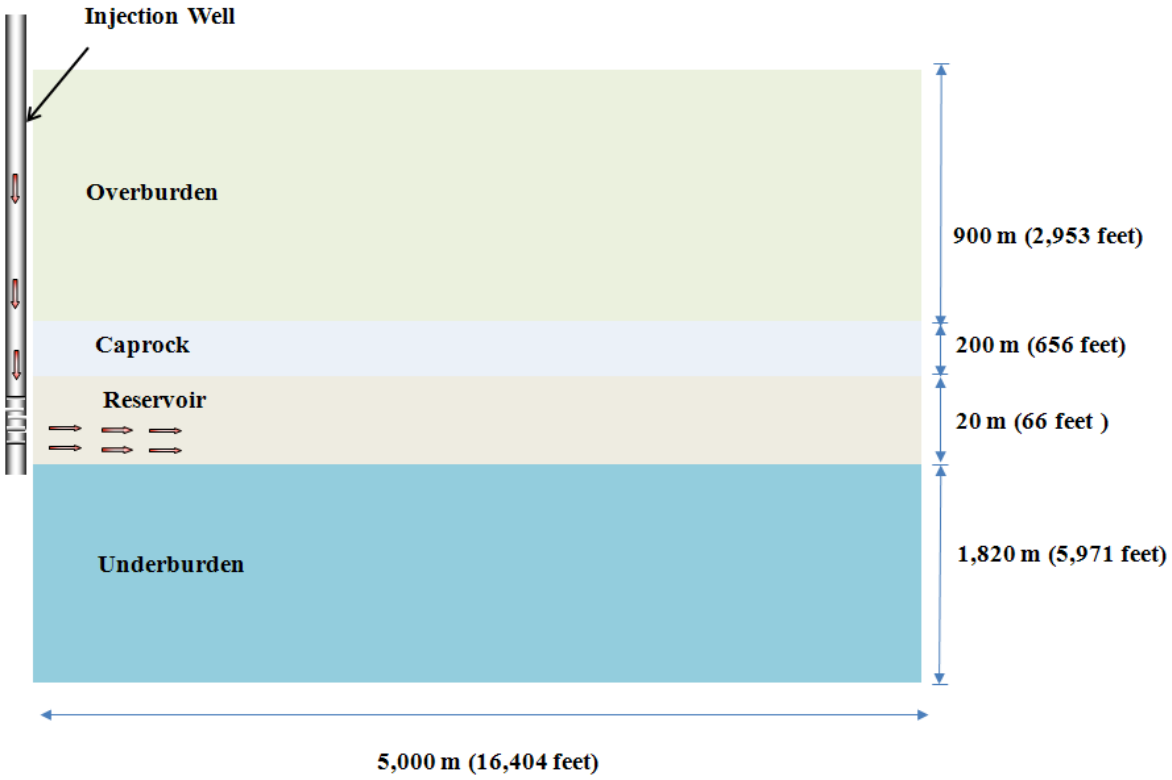

(a) Schematic diagram of the hypothetical injection site

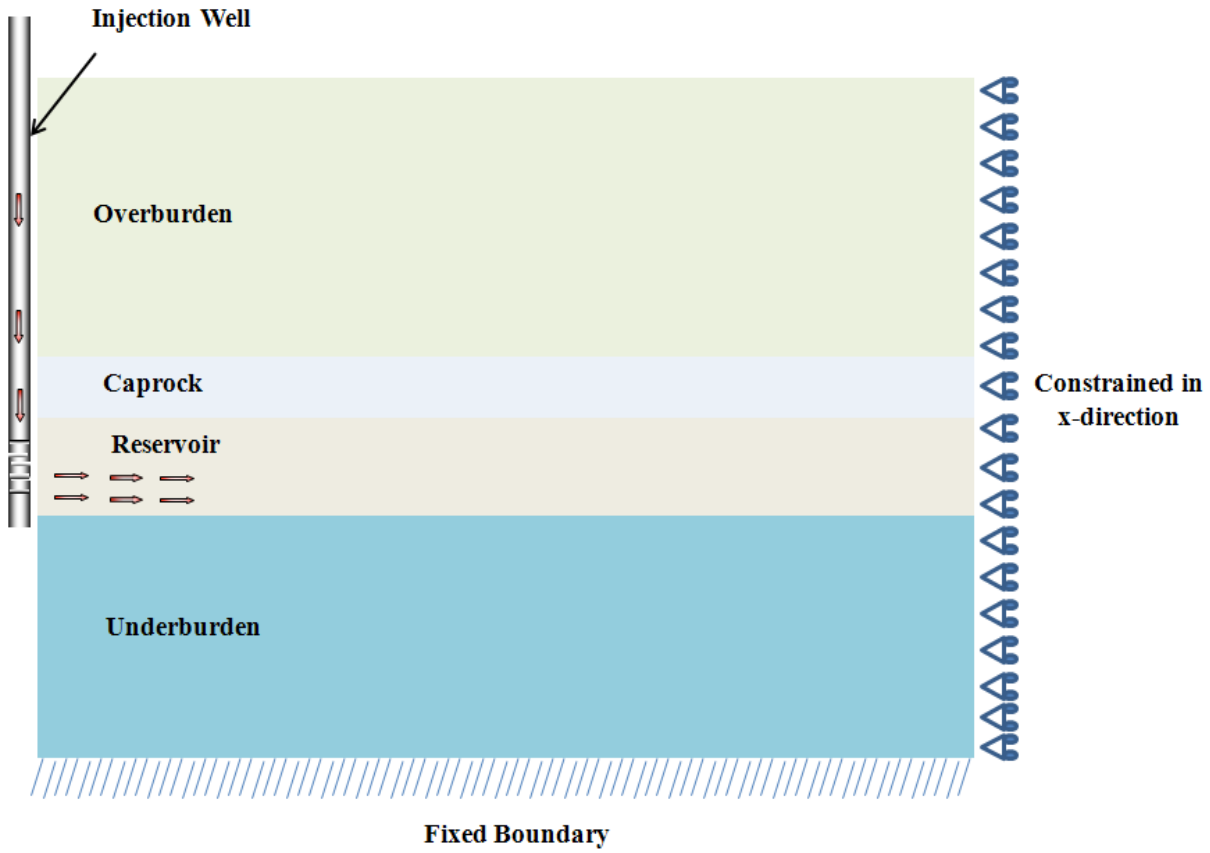

(b) Boundary conditions

Figure 6-11 : Model geometry and boundary conditions.

Table 6-8: Material Properties (Rutqvist et al., 2010)

Material Property	Overburden Layer	Caprock	Reservoir	Underburden
Elastic Modulus (kPa)	1.50e+06	20.0e+06	6.00e+06	20.00e+06
Poisson's ratio	0.25	0.25	0.25	0.25
Permeability (mD)	1e-02	1e-04	13	1e-04
Porosity (%)	10	1	17	1

Figure 6-12 shows the computed ground displacements at different time periods due to CO_2 injection. Figure 6-12 also shows the comparison of the computed displacements from this study with the InSAR data (Rutqvist et al., 2010) and the computed results obtained by Rutqvist et al., (2010). Modeling results show that the computed displacements provide a good match with the data available in the literature (Rutqvist et al., 2010).

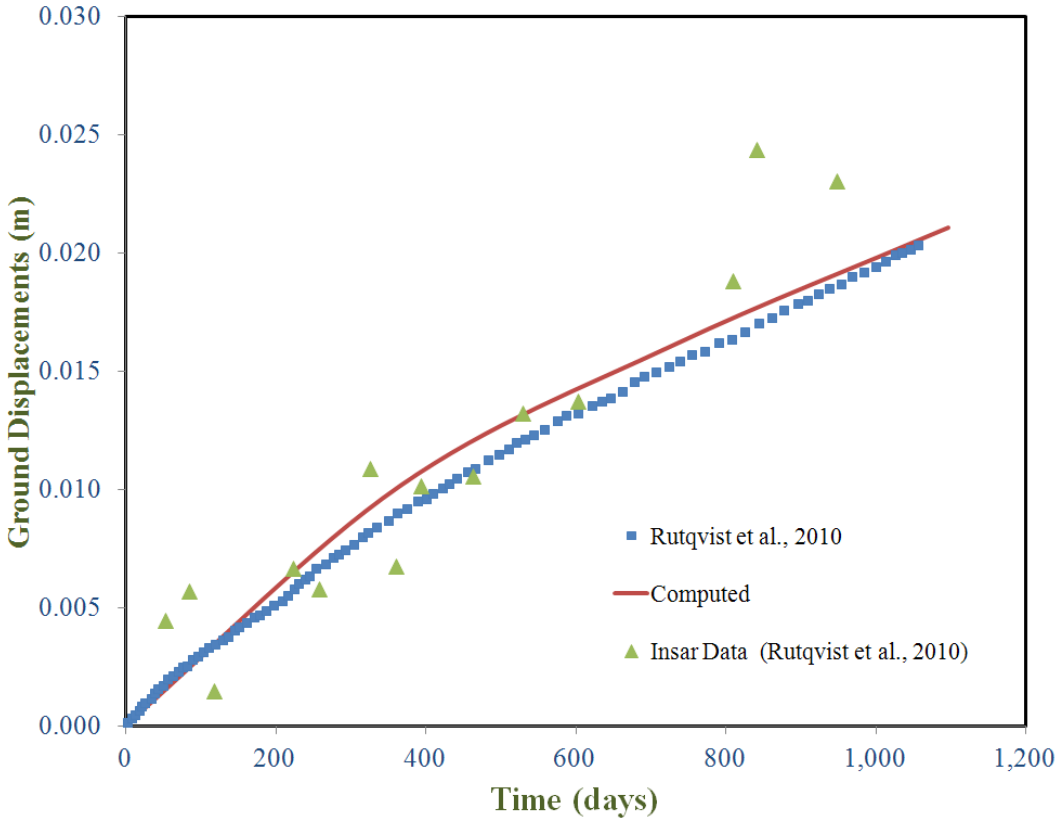

Figure 6-12: Comparison of ground displacements with data available from the literature.

6.1 Comparison of Multiphase Coupled Fluid Flow and Geomechanical Modeling with Geochemical Reactions

In order to validate the multiphase, coupled fluid flow and geomechanical modeling with geochemical reactions, a study was performed to compare the geochemical and geomechanical response of the reservoir and overburden with available data in the literature (Zhang, 2013).Zhang (2013) performed a fully coupled thermal hydrological mechanical and chemical (THMC) modeling to investigate the CO_2 transport phenomenon, the geochemical response, and the geomechanical response during CO_2 injection into a hypothetical saline reservoir. TOUGHREACT simulator was used in the study performed by Zhang (2013). Figure 6-13 shows the geometric details and a schematic diagram of the hypothetical injection site considered in this study. Four geologic layers were considered, including the overburden layer, the caprock layer, the target reservoir, and the underburden layer. Table 6-9 shows the assumed reservoir and geomechanical properties for each layer which were based on values reported in published literature (Zhang, 2013; Rutqvist and Tsang, 2002). The vertical extent of the model is 3,000 m and the horizontal extent is 70,000 m. A temperature gradient of 25 ° C/ 1000 m was assumed in the study. No-flow boundaries were assumed in the model as shown in Figure 6-13. The right and left boundaries in the model were not fixed, and were allowed to move in the z-direction (Zhang, 2013). It was assumed that the mineral composition was the same in all the rock domains. The mineralogical composition of the rock was representative of a typical combination of a shale and sandstone formation. More of the study and modeling results can be found elsewhere (Zhang, 2013).

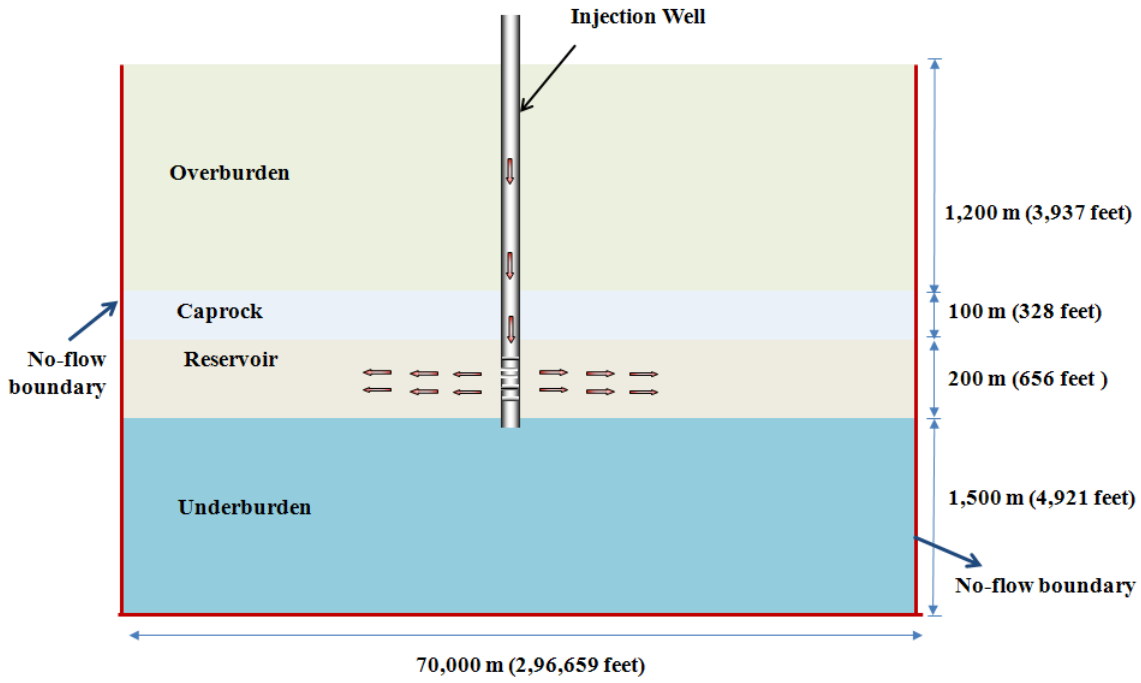

Figure 6-13: Schematic diagram of a hypothetical injection site.

Table 6-9: Material Properties (Zhang, 2013)

Material Property	Overburden Layer	Caprock	Reservoir	Underburden
Elastic Modulus (kPa)	5+06	5e+06	5e+06	5e+06
Poisson's ratio	0.25	0.25	0.25	0.25
Permeability (mD)	1e-02	1e-04	100	1e-04
Porosity (%)	10	1	10	1

Based on the hypothetical injection site described above, a two dimensional, multiphase, coupled fluid flow and geomechanical model (91 x 1 x 15 blocks) was constructed to simulate CO_2 injection into the hypothetical reservoir. A reservoir permeability of 100 mD and constant porosity of 10% was assumed for all rock layers.

Geomechanical rock properties such as Elastic Modulus and Poisson's ratio as shown in Table 6-9 were used in this study. A fully water saturated reservoir was considered in the model. However, a small fraction of CO_2 (0.001) was considered in the initialization of the fluid components in the model. CO_2 injection was carried out at a depth of 1,475 m at a rate of 4.32 metric tonnes per day for a time period of 30 years (Zhang, 2013).This injection rate was consistent with the values reported in the literature (Zhang, 2013; Rutqvist and Tsang, 2002). Table 6-10 shows the list of minerals that were used in this study. Oligoclase is a form of plagioclase feldspar and has crystallographic and physical characteristics between that of albite and anorthite. Due to the unavailability of Oligoclase within the database of CMG, albite and anorthite were used in this study. Similarly Chamosite was used instead of Chlorite. There seems to be some inconsistency between the porosity specified for different rock layers and the mineral volume fractions reported by Zhang (2013). The sum of all mineral volume (%) should be equal to (100-porosity %) (Xu et al.,2003). However, the sum of mineral volume (%) reported by Zhang (2013) was 100%. Thus, a constant porosity of 10% was used in the current study for simplicity. Table 6-11 shows the initial concentrations of primary chemical species that were used in the study. The initial concentration of H^+ ions (4.32e-01 mol/l) reported by Zhang (2013) results in a pH of 1.36. Such a low pH corresponds to a highly acidic environment which is not typical for a saline reservoir. Thus, the initial concentration of H^+ ions was assumed to be 4.32e-09 mol/l in this study. Table 6-12 shows the mineral reaction data that was used in this study. A total surface area of each mineral was assumed to be 6,500 m^2/m^3 (Xu et al., 2003).

Table 6-10: Rock mineral composition

Zhang (2013)		Current Study		Comments
Mineral	**Volume Fraction**	**Mineral**	**Volume (%)**	
Primary Minerals				
Quartz	59.181	Quartz	58.078	
Calcite	5.929	Calcite	5.929	
Oligoclase	10.662	Albite	5.331	Albite and Anorthite were substituted for Oligoclase
		Anorthite	5.331	
Smectite-Na	8.897	Smectite-Na	--	Not available in CMG database
Chlorite	15.331	Chamsonite	15.331	Chamosite was substituted for Chlorite
Total	100%	Total	90%*	
Secondary Minerals				
Kaolinite	0.0	--	--	Secondary minerals were not considered in this study.
Illite	0.0	--	--	
Hematite	0.0	--	--	
Anorthite	0.0	--	--	
Pyrite	0.0	--	--	
K-feldspar	0.0	--	--	
Gypsm	0.0	--	--	
Magnesite	0.0	--	--	
Dolomite	0.0	--	--	
Low-albite	0.0	--	--	
Siderite	0.0	--	--	
Ankerite	0.0	--	--	
Dawsonite	0.0	--	--	
Smectite-Ca	0.0	--	--	
Goethite	0.0	--	--	
Porosity	--	Porosity	10	
Total	100%	Total	100%	

*The sum of all mineral volume (%) should be equal to (100- porosity %) (Xu et al., 2003). However, the sum of mineral volume (%) reported by Zhang (2013) was 100%. Therefore the mineral volumes (%) in the current study were adjusted to account for porosity (%)

Table 6-11: Initial aqueous phase concentrations

Zhang (2013)		Current study
Aqueous species	**Molality (mg/l)**	**Molality (mg/l)**
H^{+}	4.32e-01	4.32e-09
Na^{++}	9.89e-01	9.89e-01
$SiO_{2(Aq)}$	1.03e-02	1.03e-02
K^{+}	5.96e-03	5.96e-03
Ca^{++}	4.73e-03	4.73e-03
Mg^{++}	2.67e-05	2.67e-05
HCO_3^{-}	4.56e-02	4.56e-02
CO_3^{2-}	--	1.17e-05*
Al^{+++}	--	2.32e-11*
Cl^{--}	1.015	1.015
Fe^{++}	3.02e-06	3.02e-06

* The aqueous concentration of CO_3^{2-} and Al^{+++} based on the values reported by Nghiem et al., 2004

Table 6-12: Mineral dissolution/precipitation reaction data (Zhang,2013; Xu et al., 2003; Johnson et al., 2004; Palandri and Kharaka, 2004)

Mineral	Chemical Composition	Log(rate constant) (mol/m2/s) @ 25^0C)	Reactive surface area (m^2/m^3)	E(J/mol)
Albite	$Al_2Si_2O_5(OH)_4$	-13.00	346.51	67,830
Calcite	$CaCO_3$	-8.80	385.385	41,870
Anorthite	$CaAl_2Si_2O_8$	-13.00	346.51	67,830
Chamosite	$CaMg(CO_3)_2$	-12.90	996.515	88,000
Quartz	SiO_2	-13.90	3775.07	87,500

6.1.1 **Geochemical response**

The dissolution of gaseous CO_2 in brine is caused by the geochemical interaction between brine and CO_2. The dissolution of CO_2 generates the aqueous chemical species of H^+, H_2CO_3, HCO_3^-, and CO_2^{3-}. The increase in the concentration of H^+ reduces the pH of the brine, giving rise to acidic conditions in the saline reservoir. Figure 6-14 shows the spatial distribution of pH during the 10,000 years of the CO_2 storage period. Figure 6-14 also shows the comparison between the computed changes in pH during different time periods from the current study and the reported changes in pH by Zhang (2013). Due to the high permeability assumed for the caprock, the CO_2–rich brine moves upwards. This causes a reduction in pH in the overburden layers. The pH value reduces to 5.50 after 30 years of CO_2 injection. The acidized area by CO_2 dissolution continues to spread during CO_2 injection period and the post-injection period as shown in Figure 6-14. The pH value reduces to 4.40 after 5,000 years of post-injection period. Modeling results show that the change in pH after 5,000 years was insignificant.

Mineral dissolution and precipitation takes place due to the interaction between the acidic brine and the rock. Mineral dissolution releases primary aqueous species such as Fe^{++} and SiO_2 (aq) ions into the brine. This is evident from the increase in molality (mg/l) of Fe^{++} and SiO_2 (aq) ions in the aqueous phase as shown in Figure 6-15 and Figure 6-16. A comparison between the computed changes in aqueous concentration during different time periods from the current study and the reported changes in aqueous concentrations by Zhang (2013) are shown in Figure 6-15 and Figure 6-16. Modeling results show that the dissolution of Anorthite and Quartz releases silicate ions (SiO_{2aq}) into the brine, which is used in the precipitation of minerals which include Albite and Chamosite. The dissolution of Anorthite also releases Ca^{++} and Al^{+++} ions which aide in the precipitation of Albite, Calcite, and Chamosite. Due to the availability of significant amount of Na^{++} in the brine, Albite precipitates in large quantities when compared to Calcite and Chamosite. The amount of mineral dissolved and precipitated during the CO_2 storage period (10,000 years) is shown in Figure 6-17.

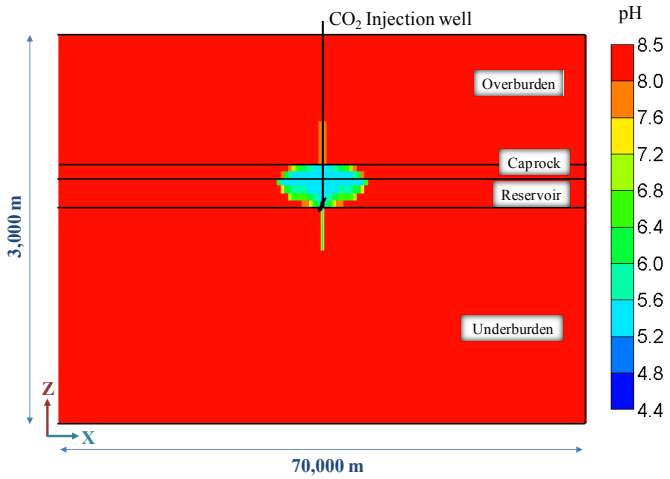

(a) 30 years of CO_2 injection (Current study)

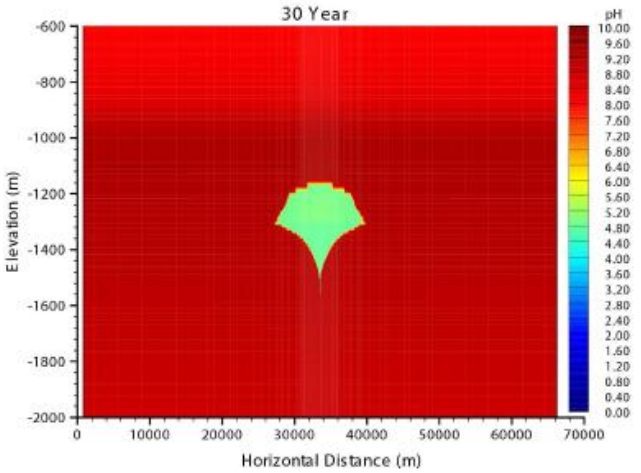

(b) 30 years of CO_2 injection (Zhang, 2013)

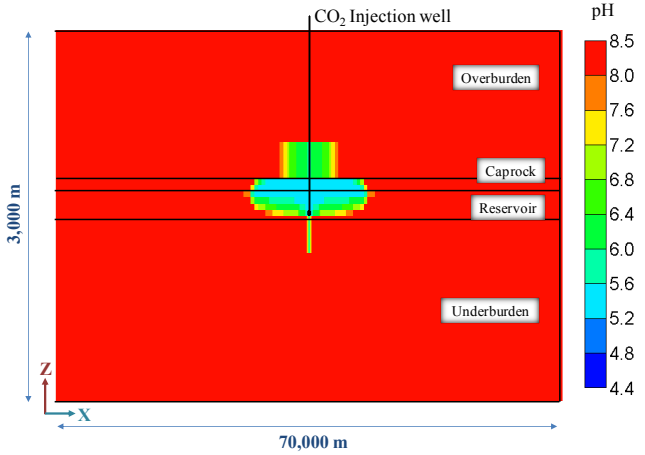

(c) 500 years of post-injection period (Current study)

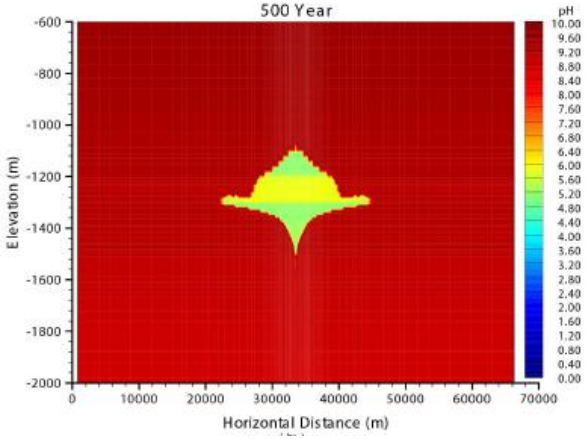

(d) 500 years of post-injection period (Zhang, 2013)

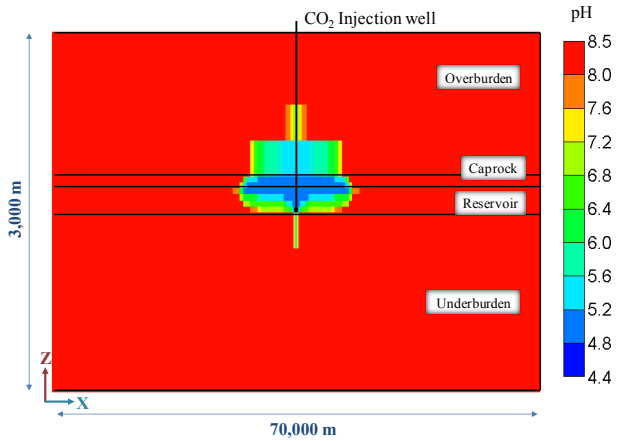

(e) 1,000 years of post-injection period (Current study)

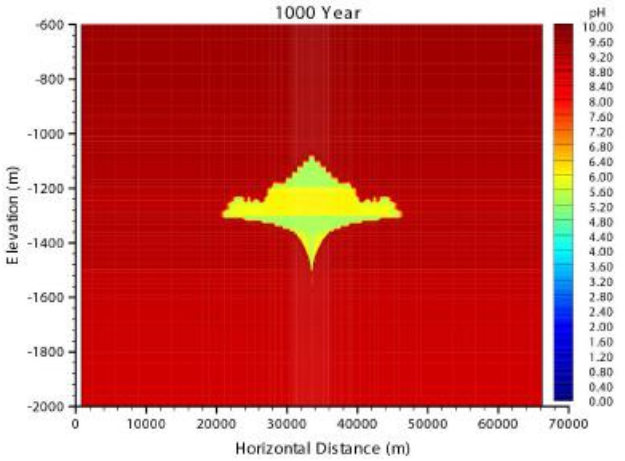

(f) 1,000 years of post-injection period (Zhang, 2013)

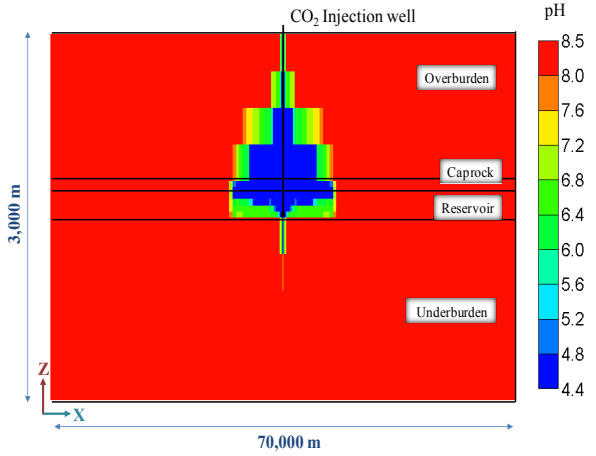

(g) 5,000 years of post-injection period (Current study)

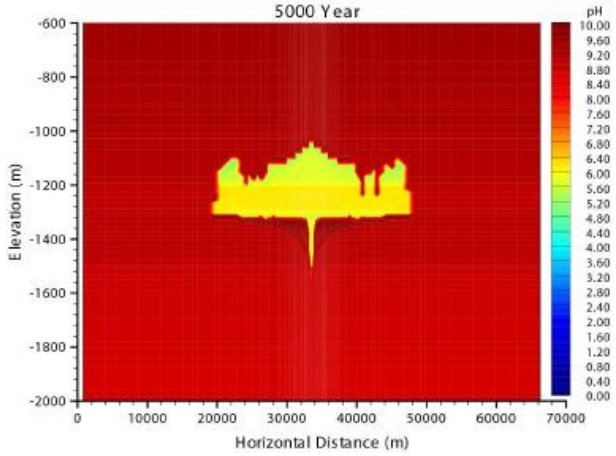

(h) 5,000 years of post-injection period (Zhang, 2013)

Figure 6-14: Computed pH during 5,000 years.

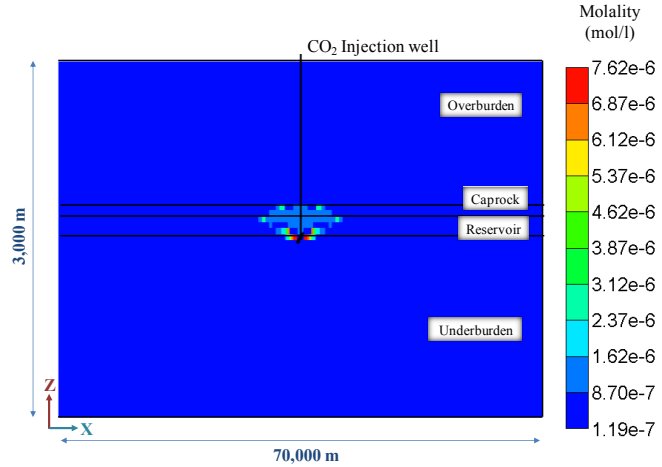

(a) 100 years of post-injection period (Current study)

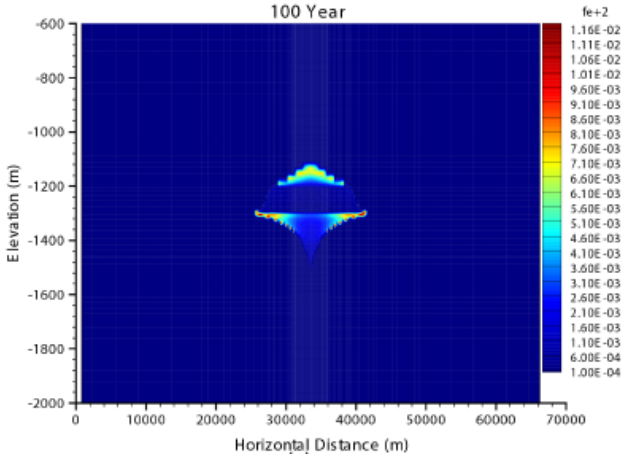

(b) 100 years of post-injection period (Zhang, 2013)

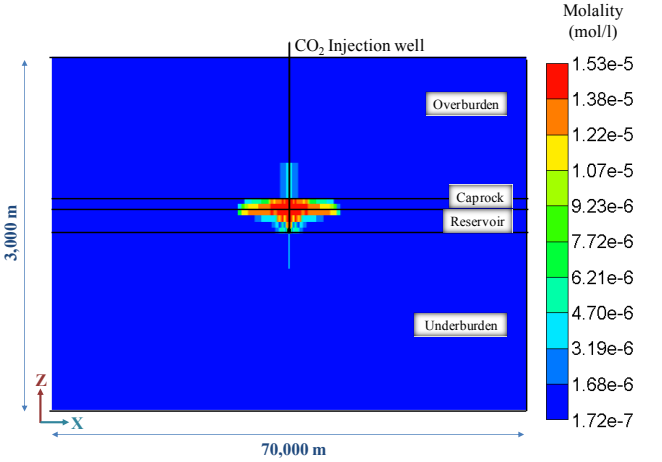

(c) 1,000 years of post-injection period (Current study)

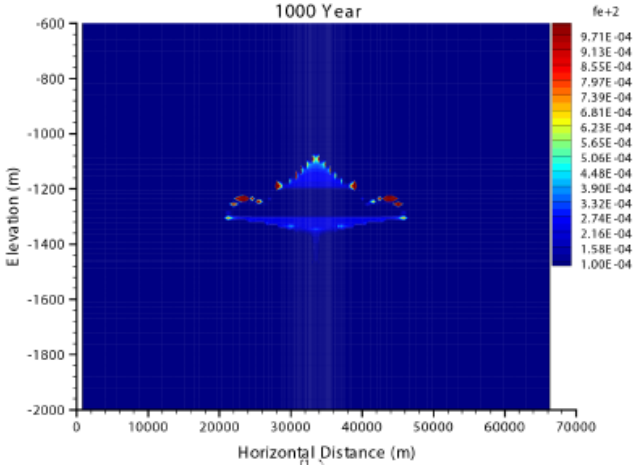

(d) 1,000 years of post-injection period (Zhang, 2013)

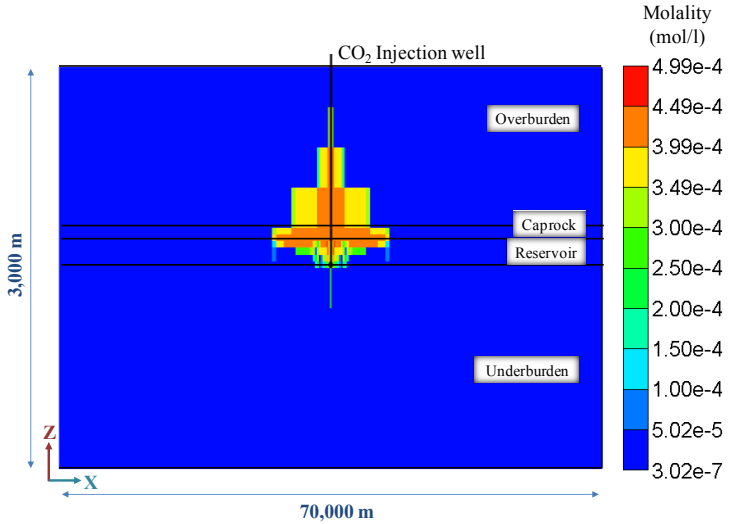

(e) 10,000 years (Current study)

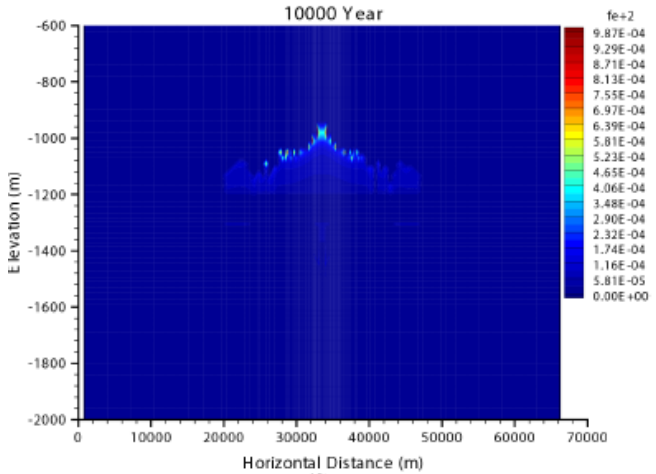

(f) 10,000 years (Zhang,2013)

Figure 6-15: Computed change in Fe^{++} concentration in the aqueous phase.

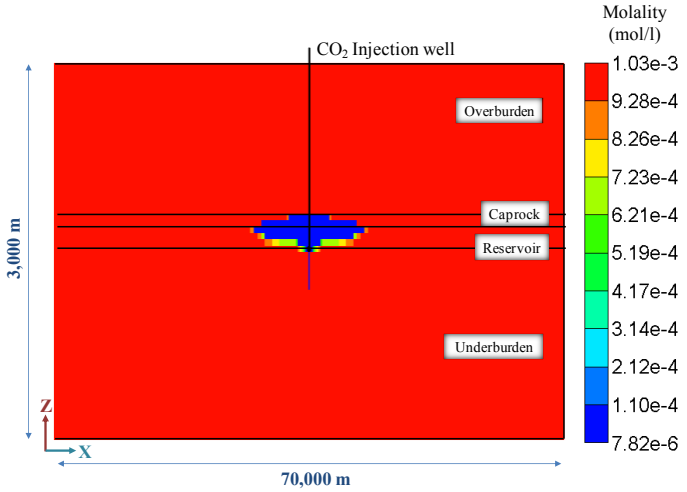

(a) 100 years of post-injection period (Current study)

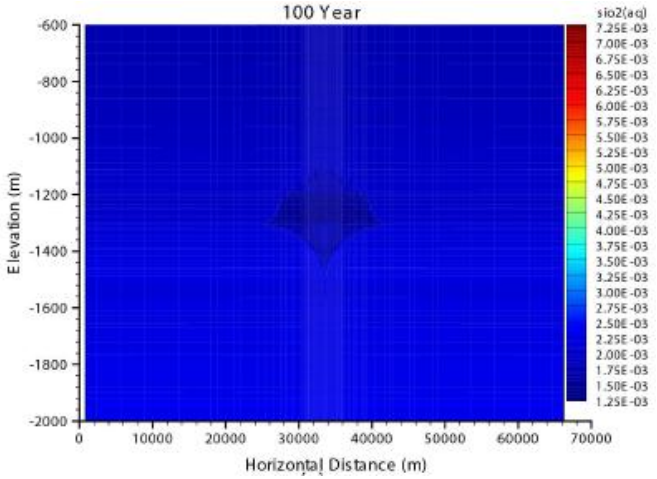

(b) 100 years of post-injection period (Zhang, 2013)

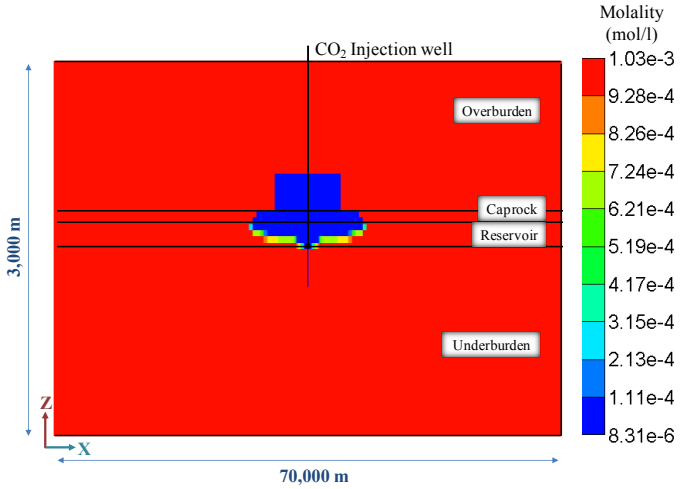

(c) 1,000 years of post-injection period (Current study)

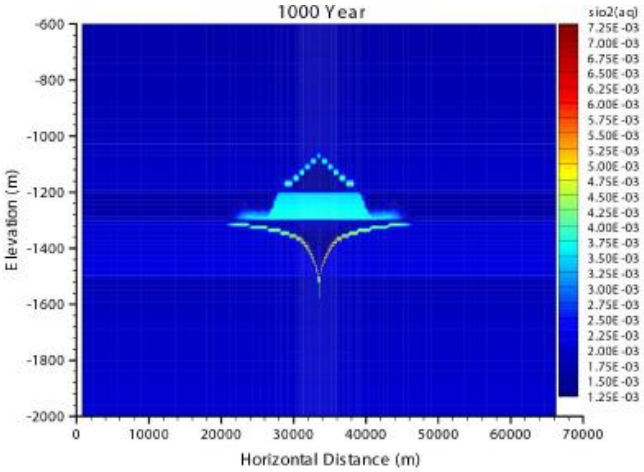

(d) 1,000 years of post-injection period (Zhang, 2013)

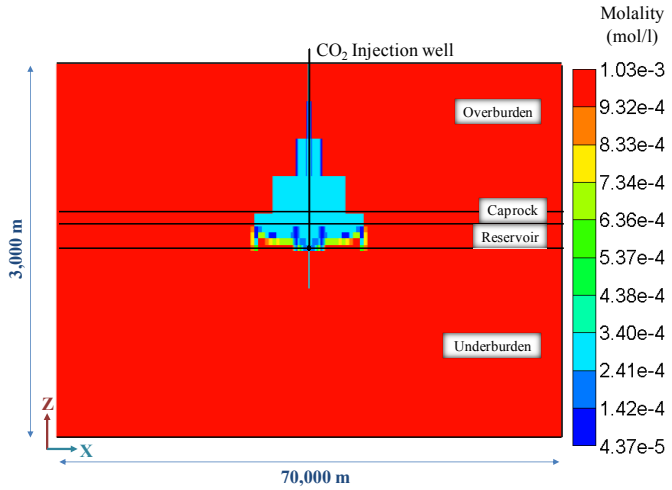

(e) 10,000 years (Current study)

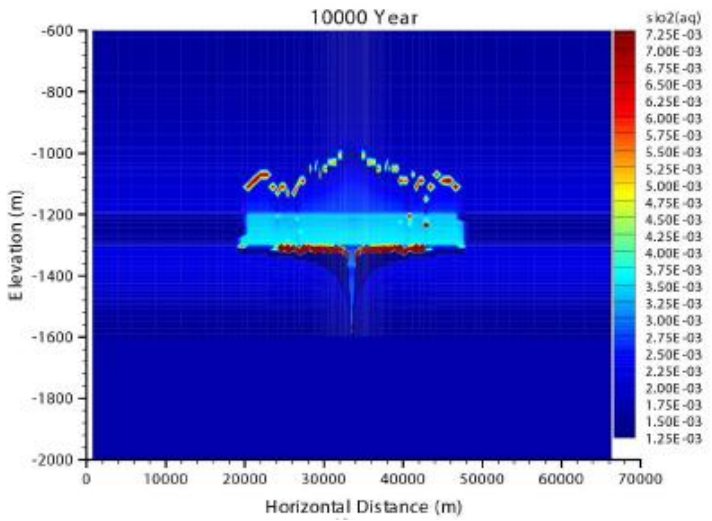

(f) 10,000 years (Zhang, 2013)

Figure 6-16: Computed change in $SiO_{2\,(aq)}$ concentration in the aqueous phase.

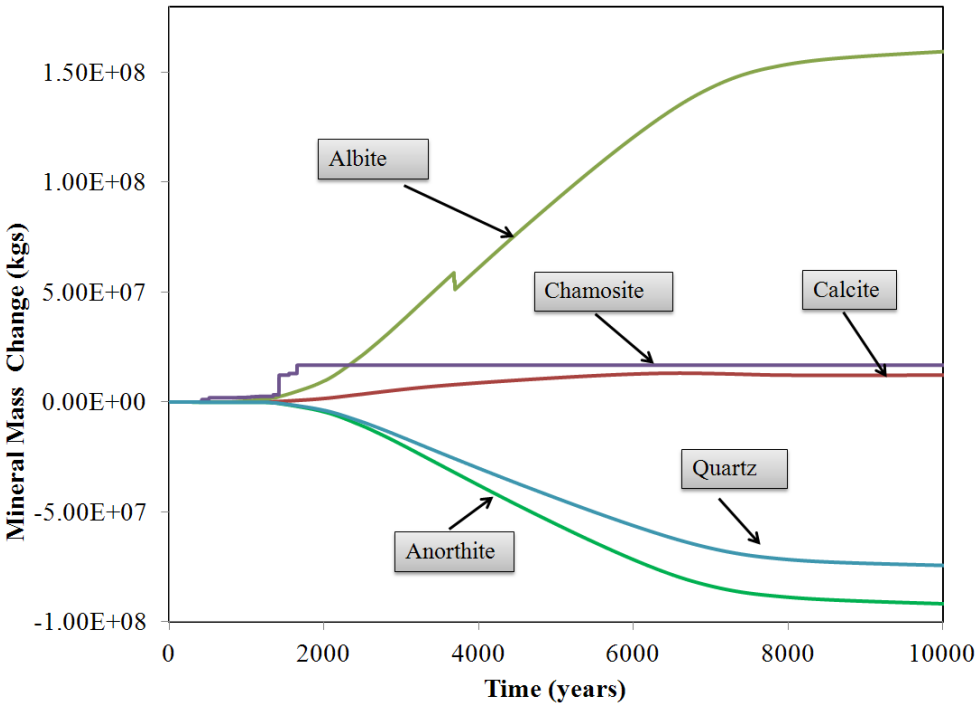

Figure 6-17: Computed changes in mineral mass due to mineralizaiton.

6.1.2 Geomechanical response

When CO_2 was injected at a rate of 4.32 metric tonnes per day, the maximum change in reservoir pressure at the end of 30-year CO_2 injection was about 10,375 kPa. This change in pressure translates to an increase of 76.32% above the average initial reservoir pressure. Figure 6-18 shows the increase in fluid pressure during 30 years of CO_2 injection. Figure 6-18 also shows the comparison between the computed pressure distribution from the current study and the computed pressure distribution reported by Zhang (2013). The computed pressures from the current study seem to be in the range of the computed pressure values reported by Zhang (2013). CO_2 injection causes poro-elastic expansion of the rock. The increase in pressure changes the volumetric strain with time. Figure 6-19 shows the changes in volumetric strain due to CO_2 injection. Modeling results show that the maximum volumetric strain at the end of 30-year CO_2 injection was about 0.0019 as shown in Figure 6-19 (g). The maximum volumetric strain reported by

Zhang (2013) at the end of 30-year CO_2 injection was about 0.0021 as shown in Figure 6-19 (h). The difference in the computed volumetric strain can be considered insignificant.

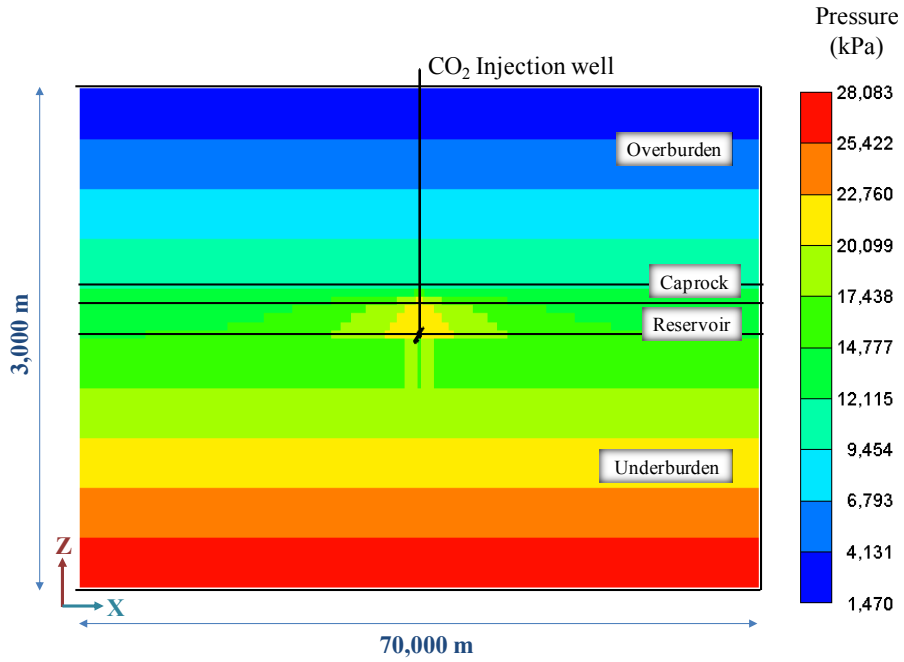

(a) 5 years of CO_2 injection (Current study)

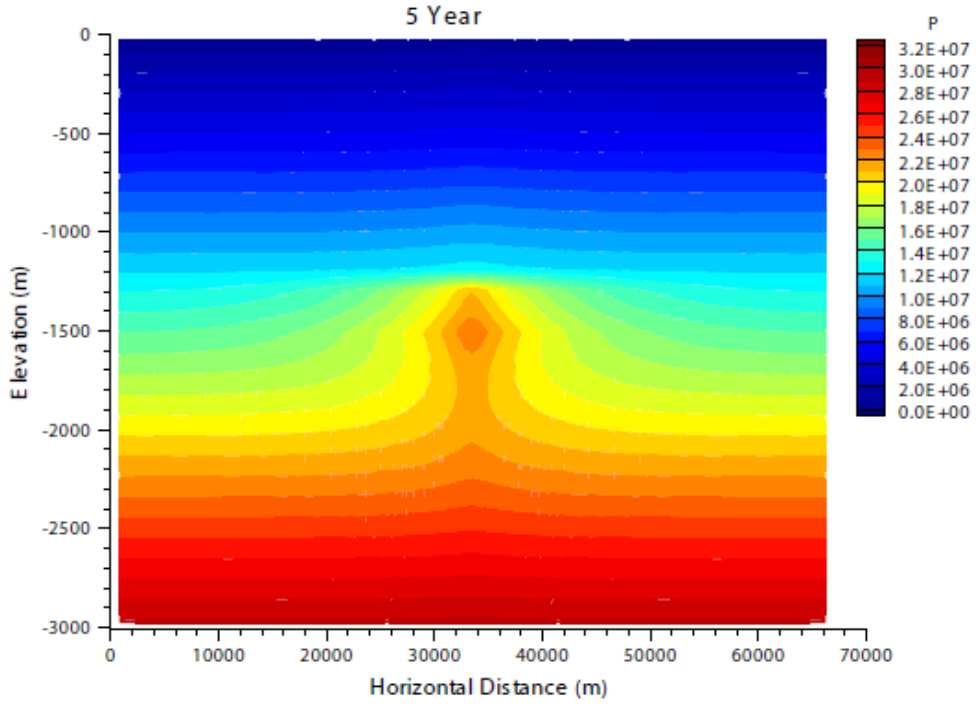

(b) 5 years of CO_2 injection (Zhang, 2013)

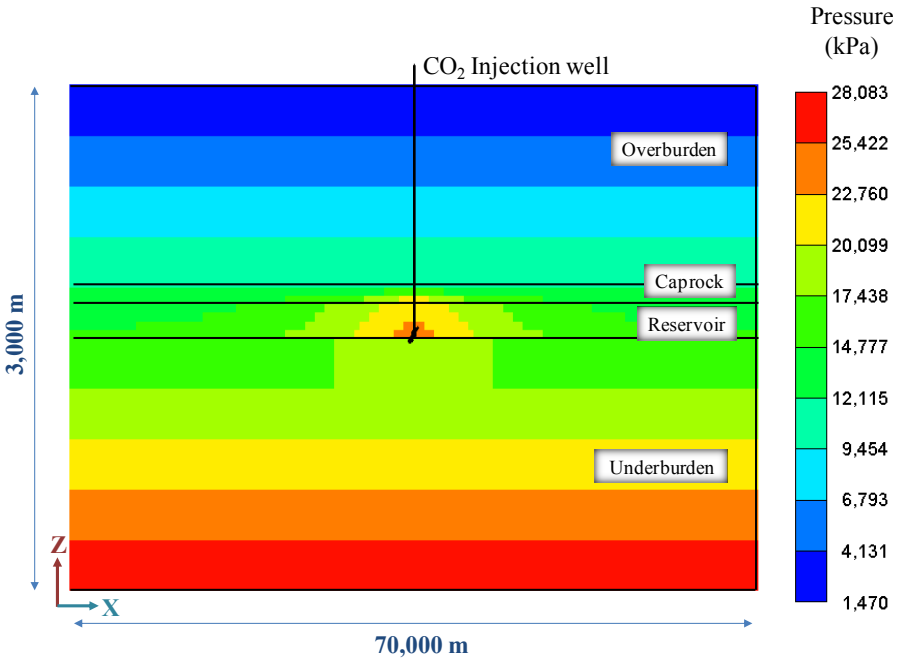

(c) 10 years of CO_2 injection (Current study)

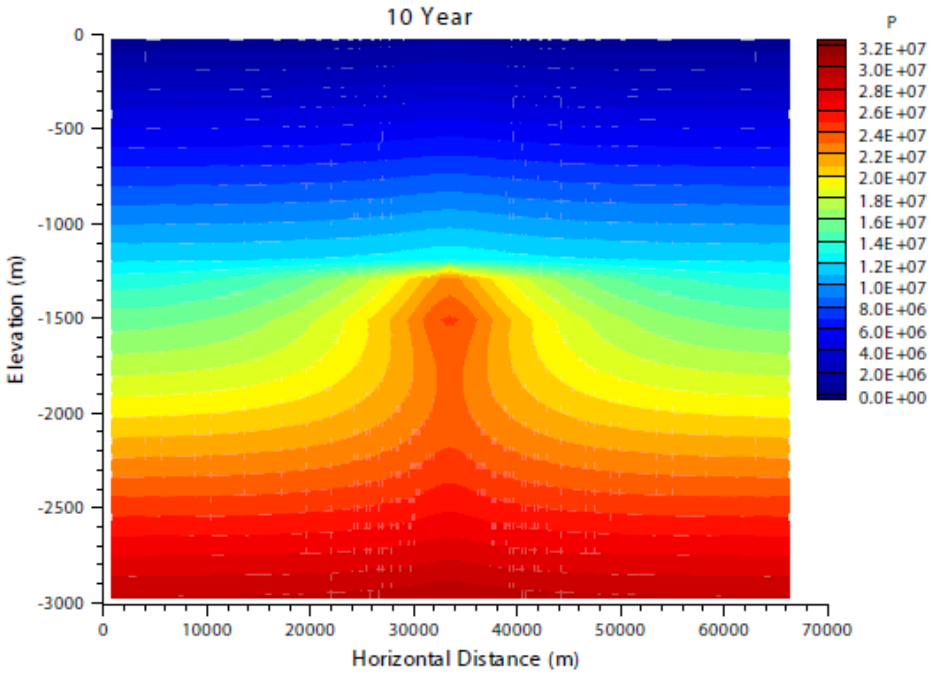

(d) 10 years of CO_2 injection (Zhang, 2013)

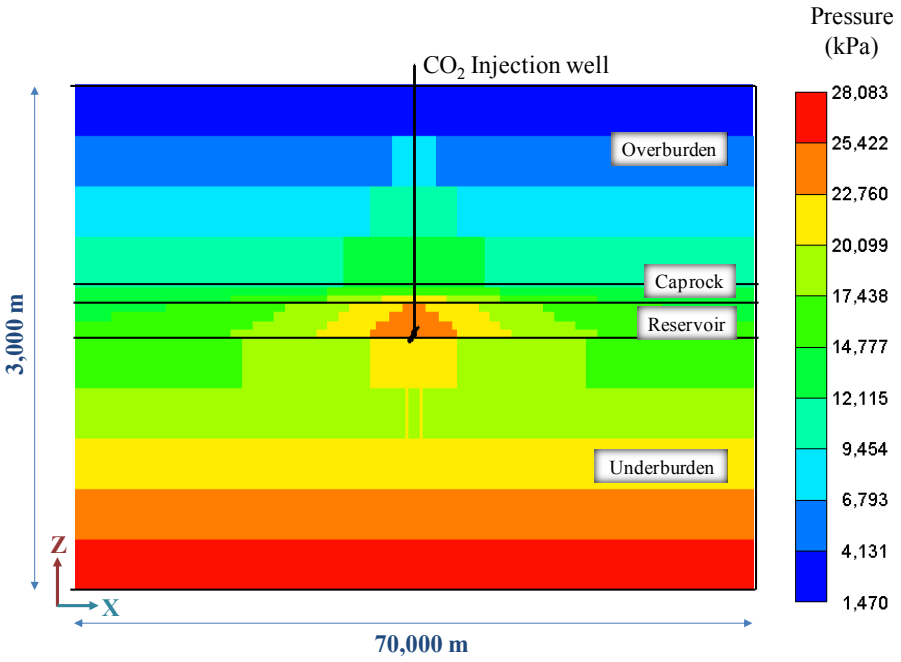

(e) 20 years of CO_2 injection (Current study)

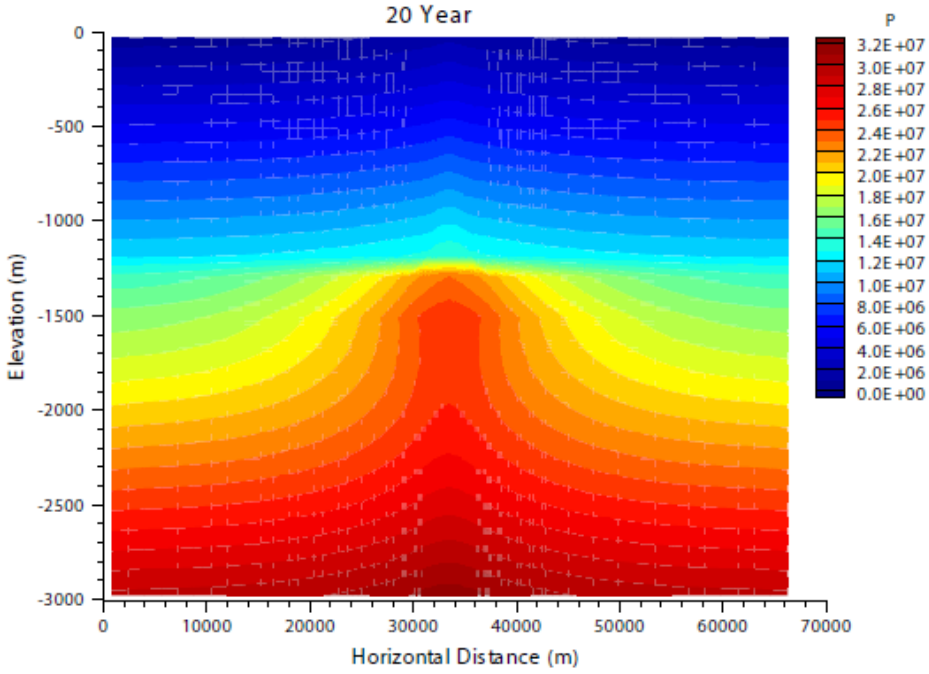

(f) 20 years of CO_2 injection (Zhang, 2013)

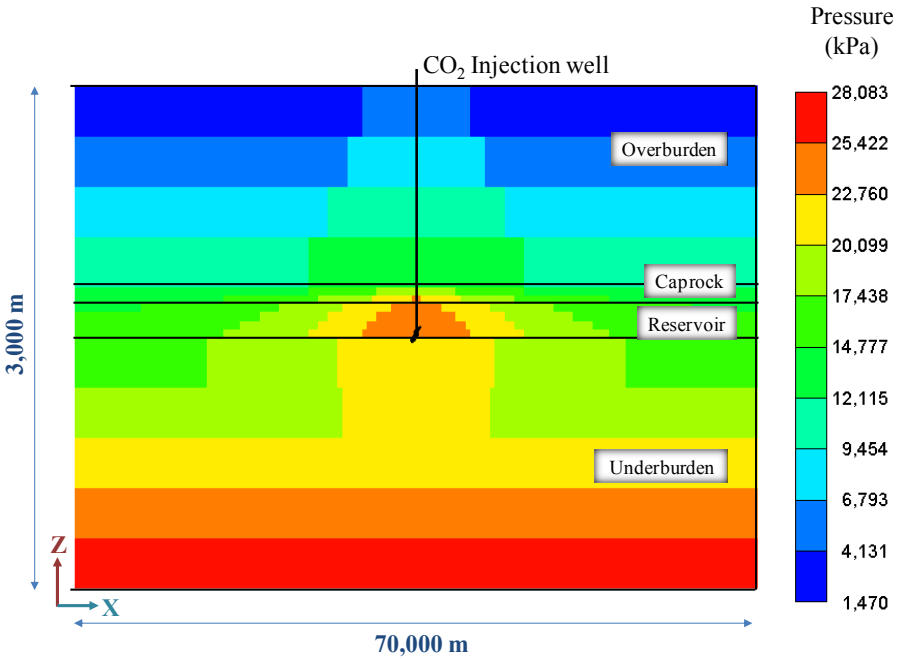

(g) 30 years of CO_2 injection

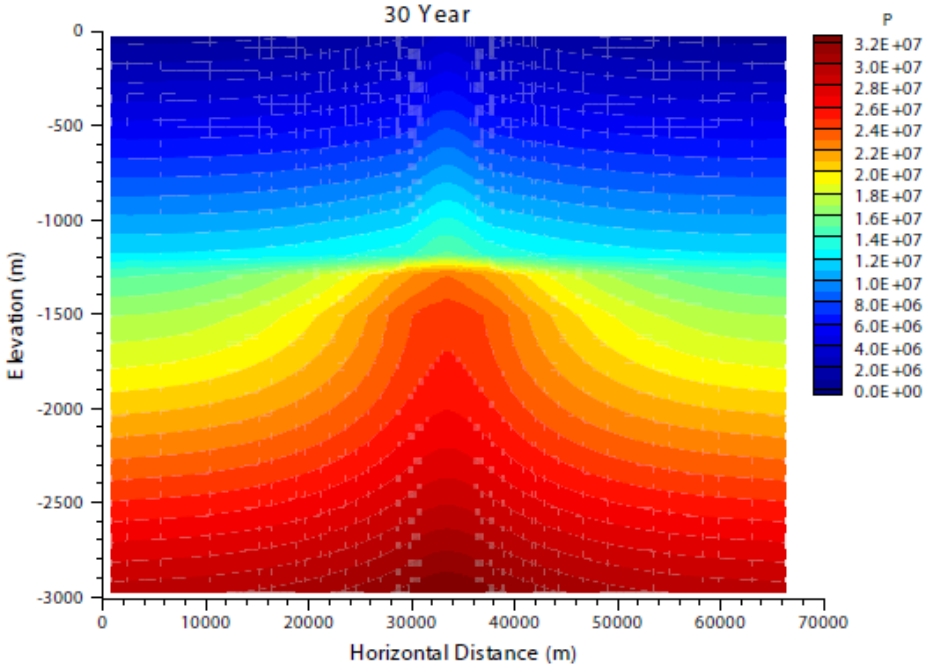

(h) 30 years of CO_2 injection

Figure 6-18: Pressure distribution during CO_2 injection.

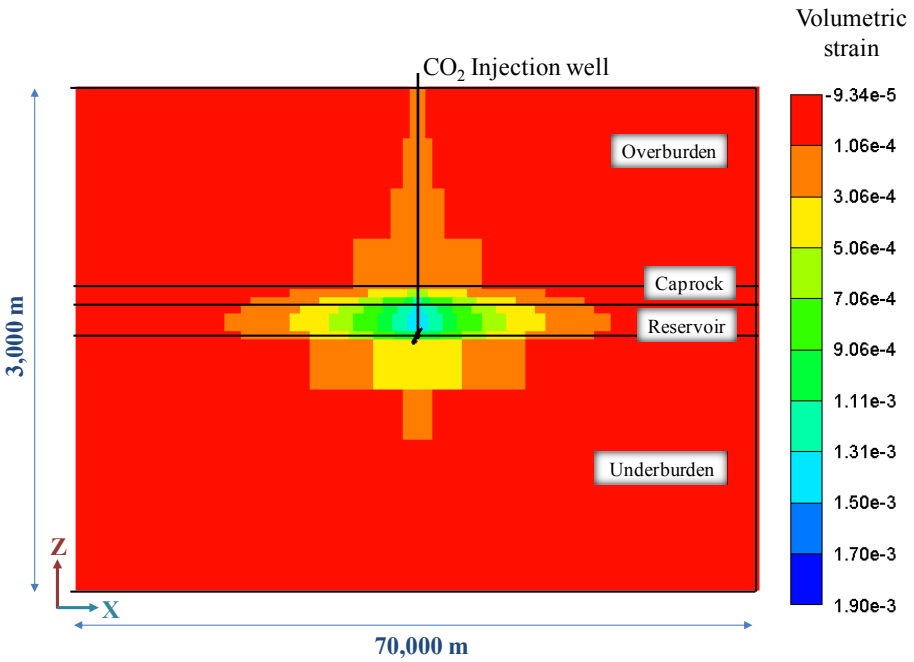

(a) 5years of CO_2 injection (Current study)

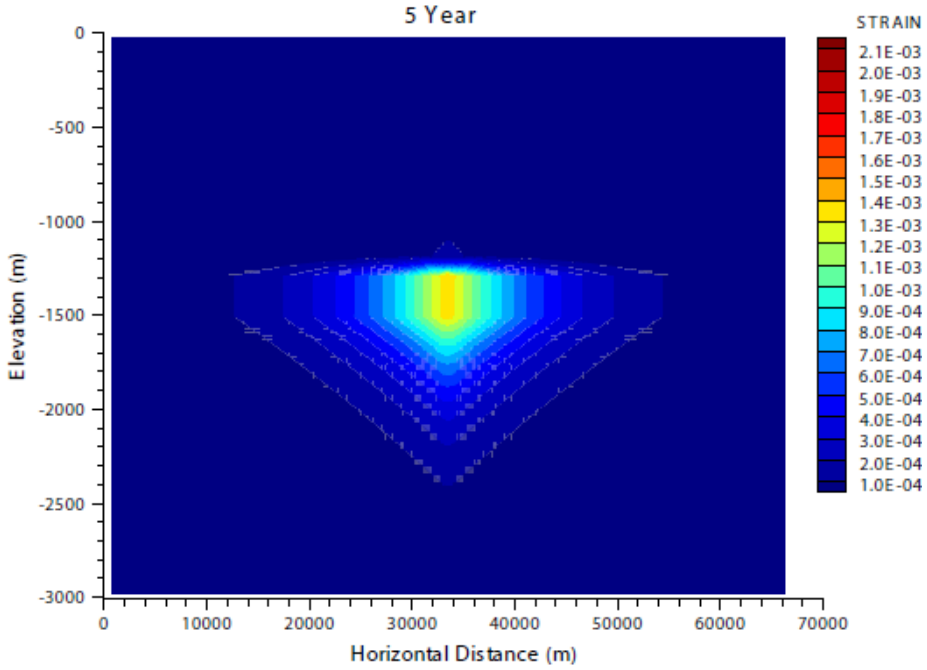

(b) 5years of CO_2 injection (Zhang, 2013)

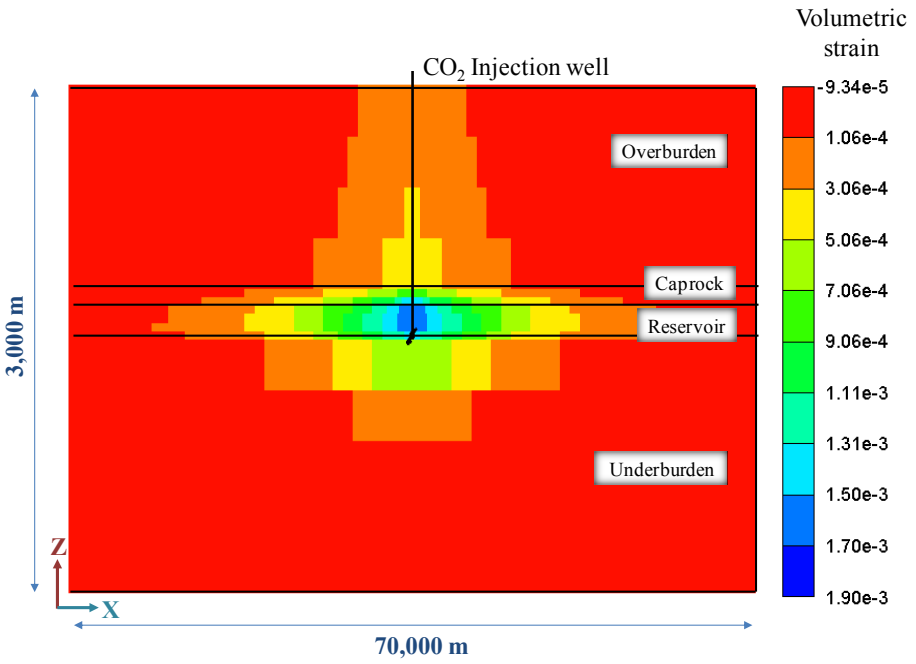

(c) 10 years of CO_2 injection (Current study)

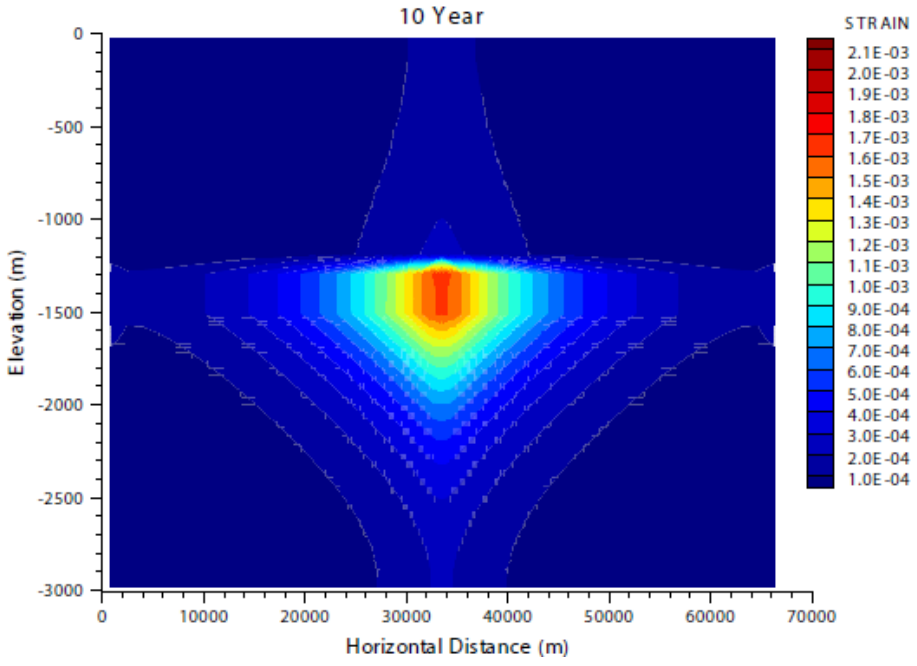

(d) 10 years of CO_2 injection (Zhang,2013)

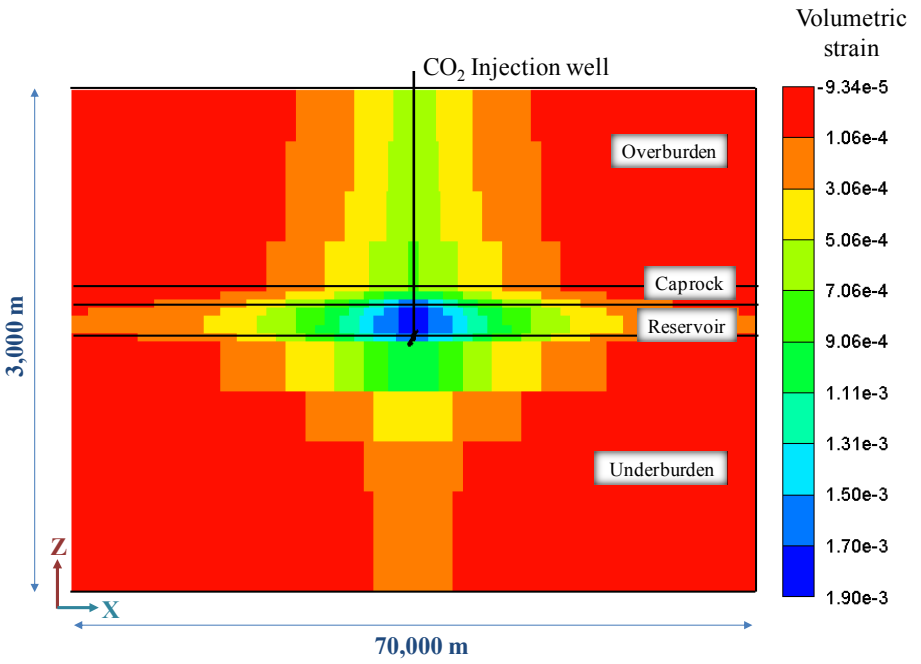

(e) 20 years of CO_2 injection (Current study)

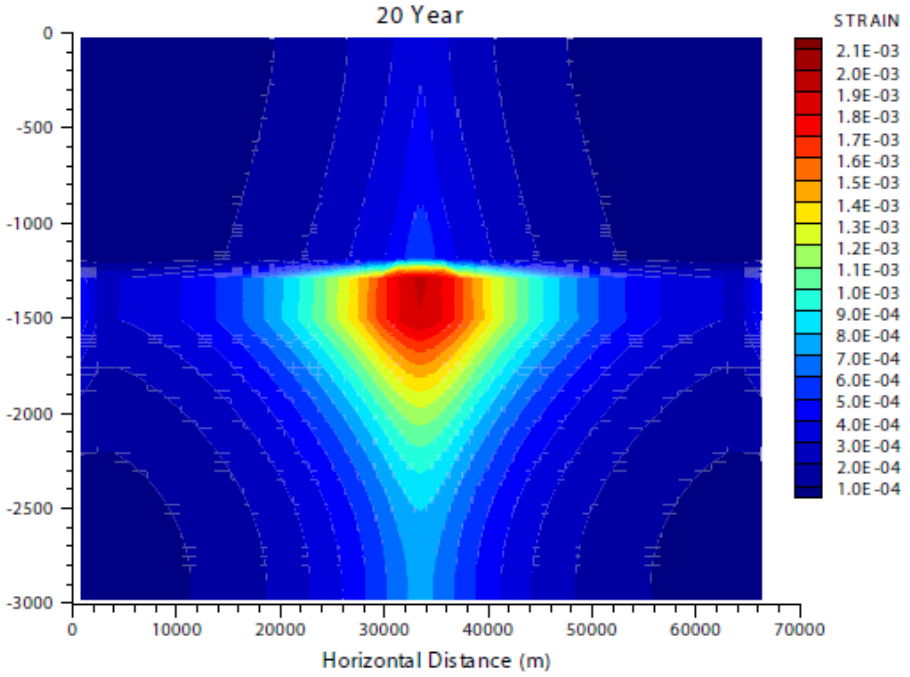

(f) 20 years of CO_2 injection (Zhang,2013)

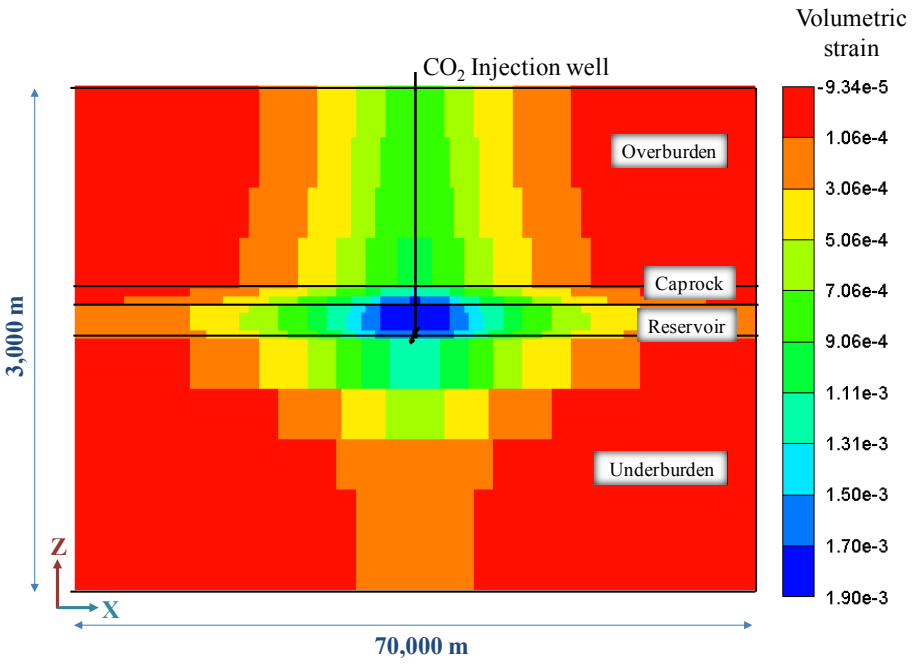

(g) 30 years of CO_2 injection (Current study)

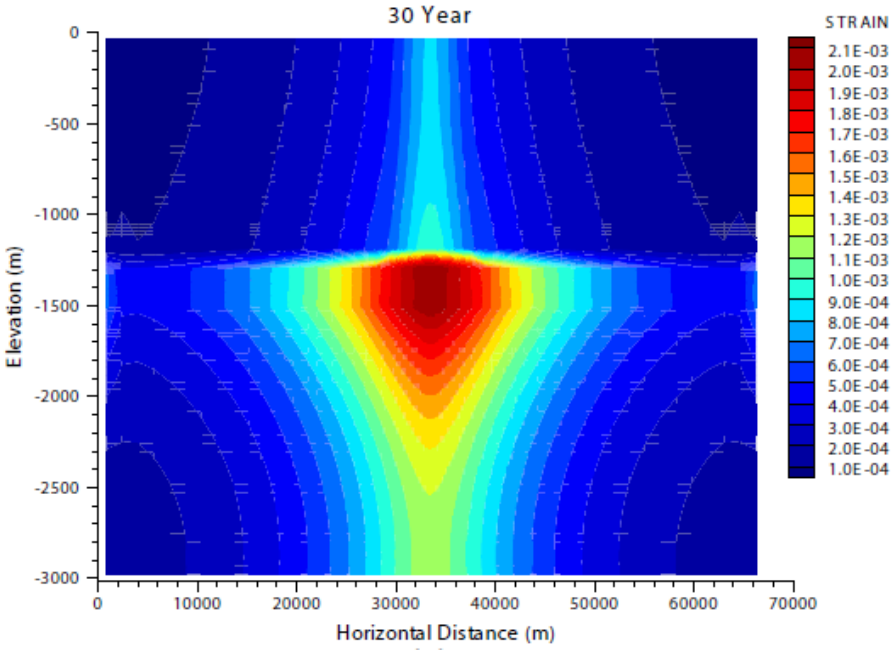

(h) 30 years of CO_2 injection (Zhang, 2013)

Figure 6-19: Volumetric strain distribution during CO_2 injection.

Figure 6-20 shows the computed ground displacements at various time periods during CO_2 injection.The maximum computed vertical displacement is about 1.44 m after 30 years of injection. Figure 6-21 shows a comparison between the computed ground displacements at various time periods from this study with the computed ground displacements that were reported by Zhang (2013). The maximum computed ground displacement reported by Zhang (2013) after 30 years of CO_2 injection was about 1.30 m.The difference in the magnitude of the computed ground displacements and the reported values after 30 years of CO_2 injection is about 11%. When the reservoir permeability was increased to 140 mD, the computed ground displacements matched well with the values reported by Zhang (2013) as shown in Figure 6-22.

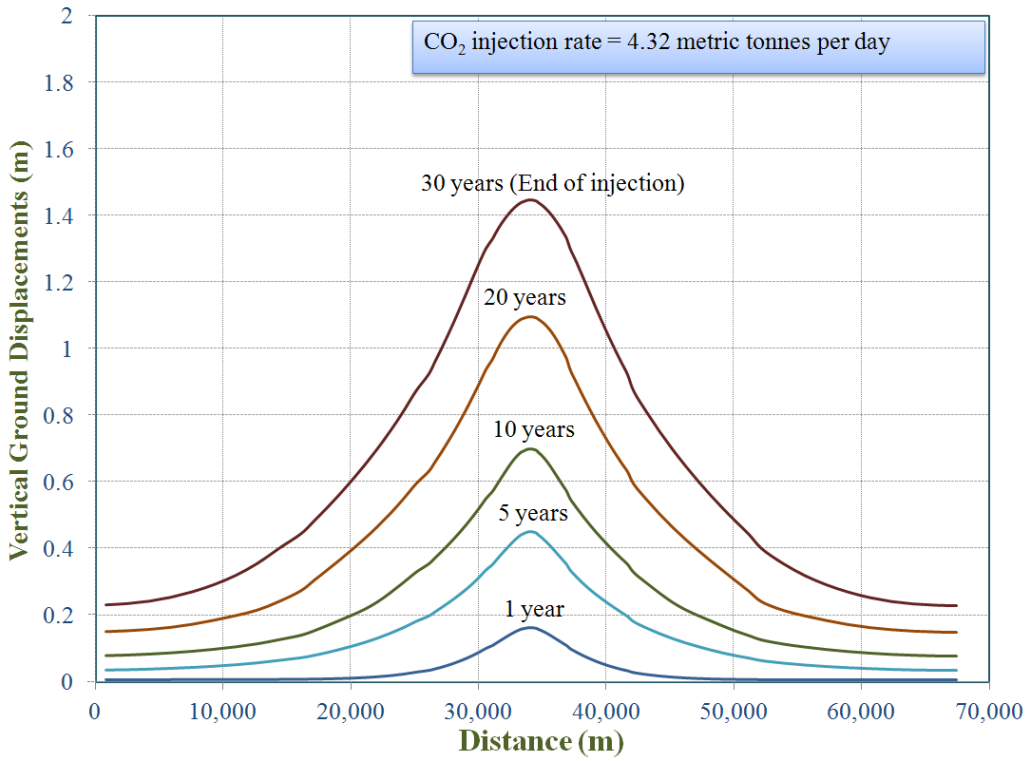

Figure 6-20: Ground displacements during 30 years of CO_2 injection.

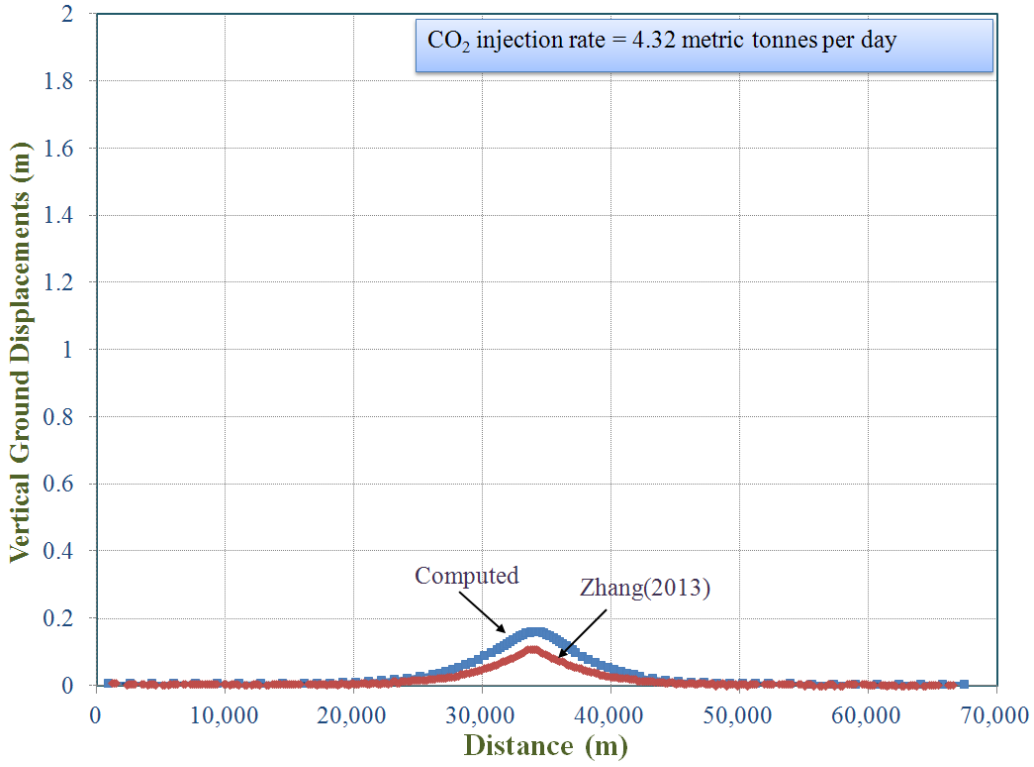

(a) 1 year of CO_2 injection

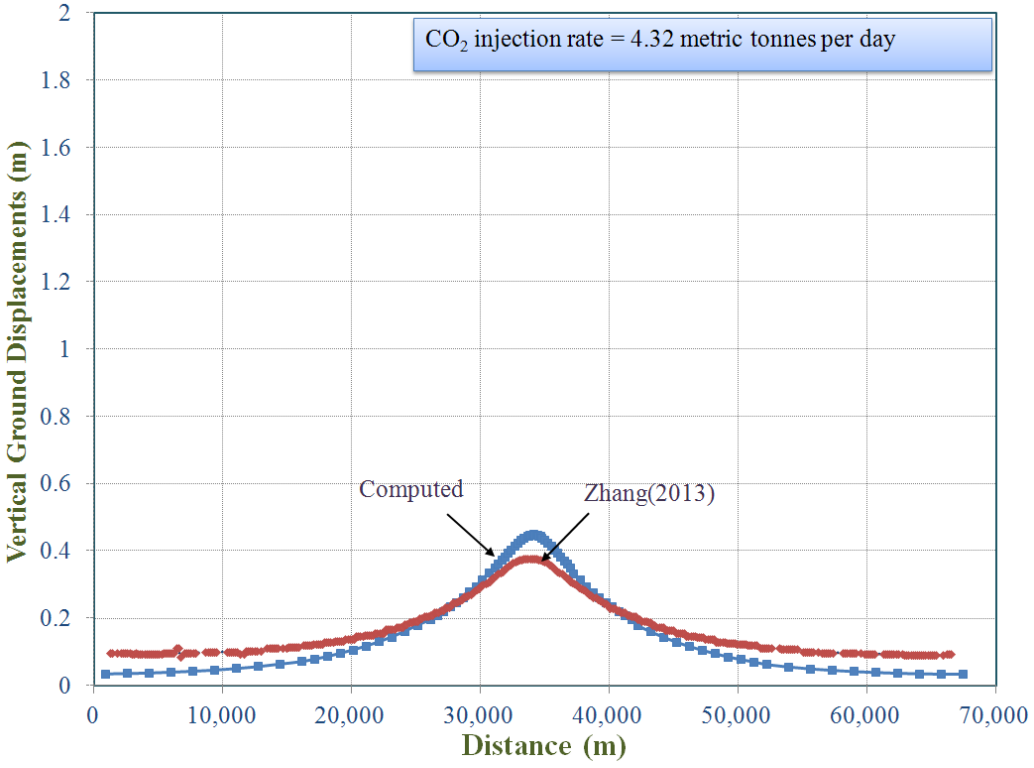

(b) 5 years of CO_2 injection

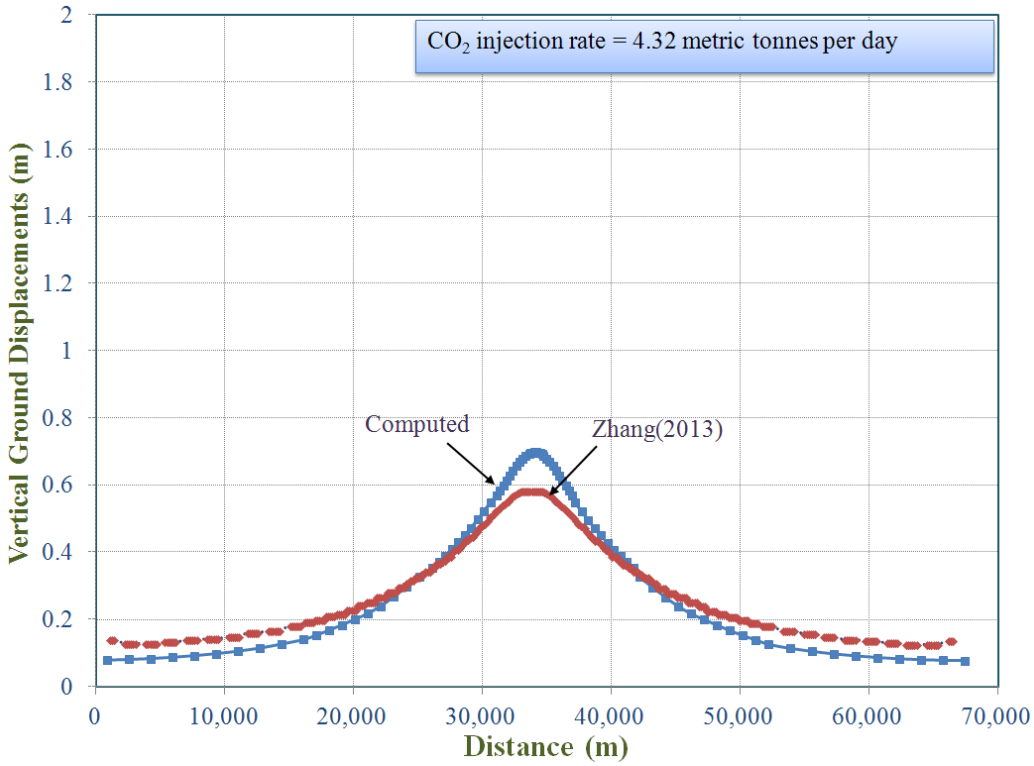

(c) 10 years of CO_2 injection

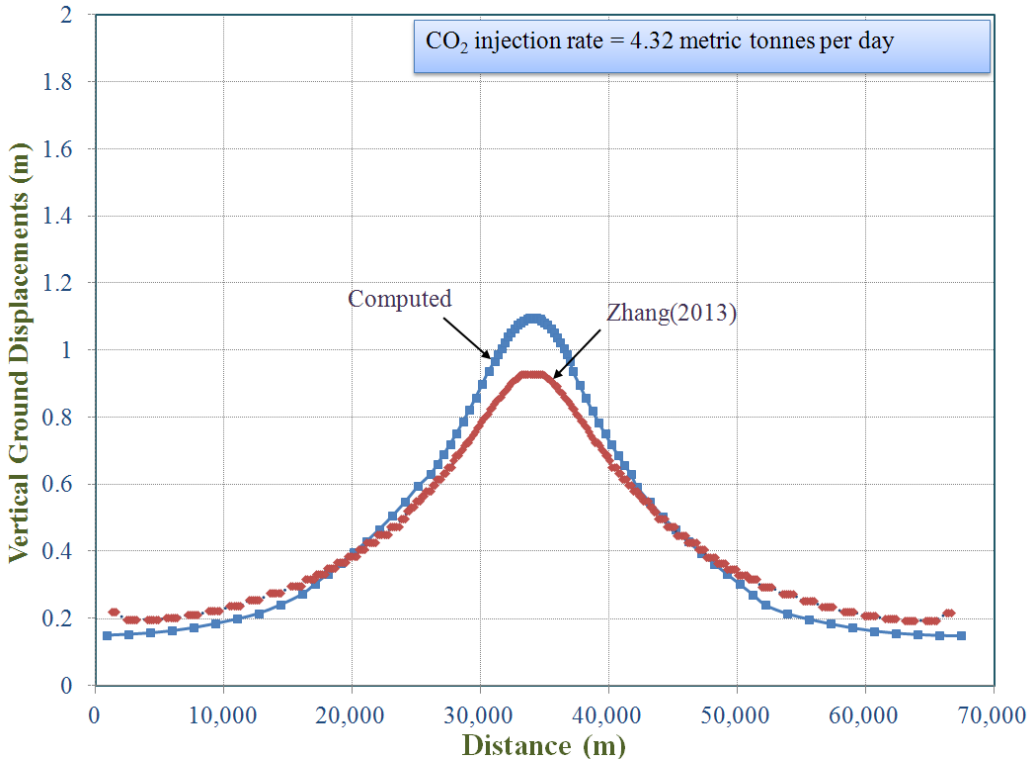

(d) 20 years of CO_2 injection

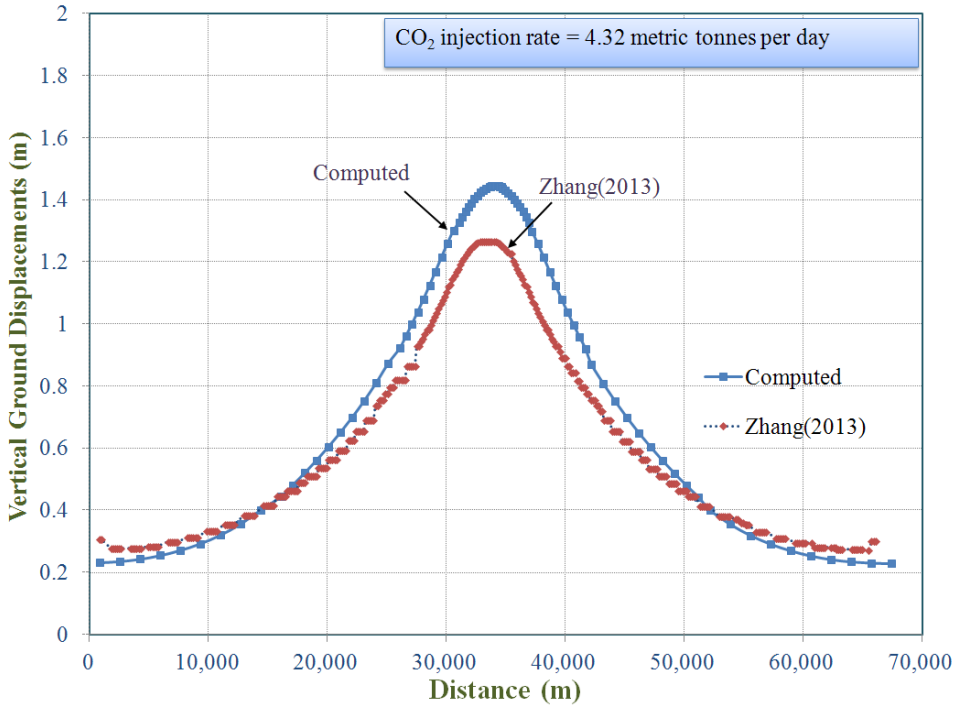

(e) 30 years of CO_2 injection

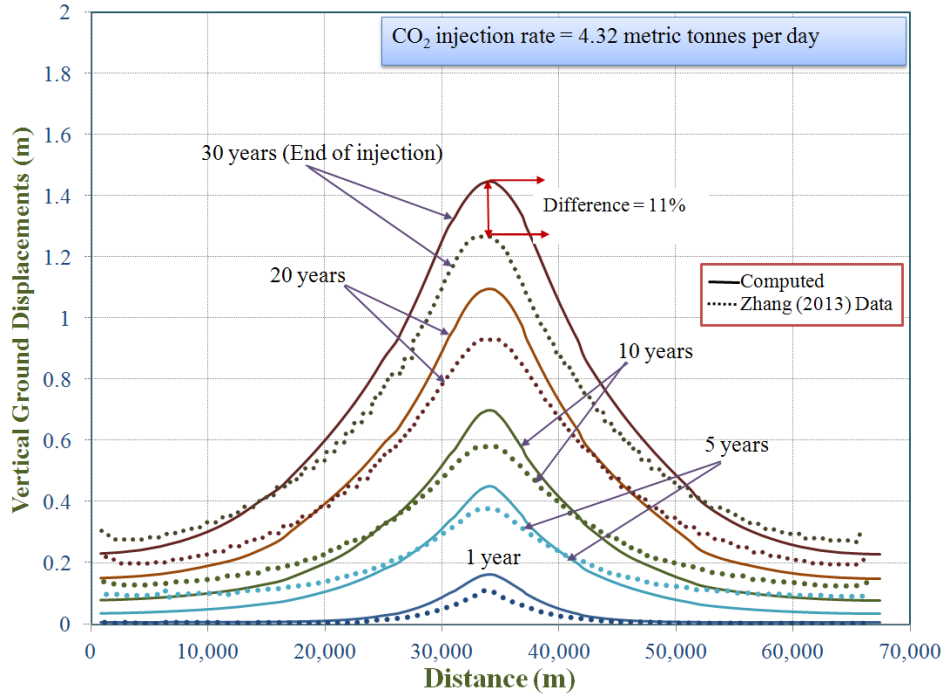

e) 1 year to 30 years of CO_2 injection

Figure 6-21: Comparison of computed ground displacements with the values reported by Zhang(2013).

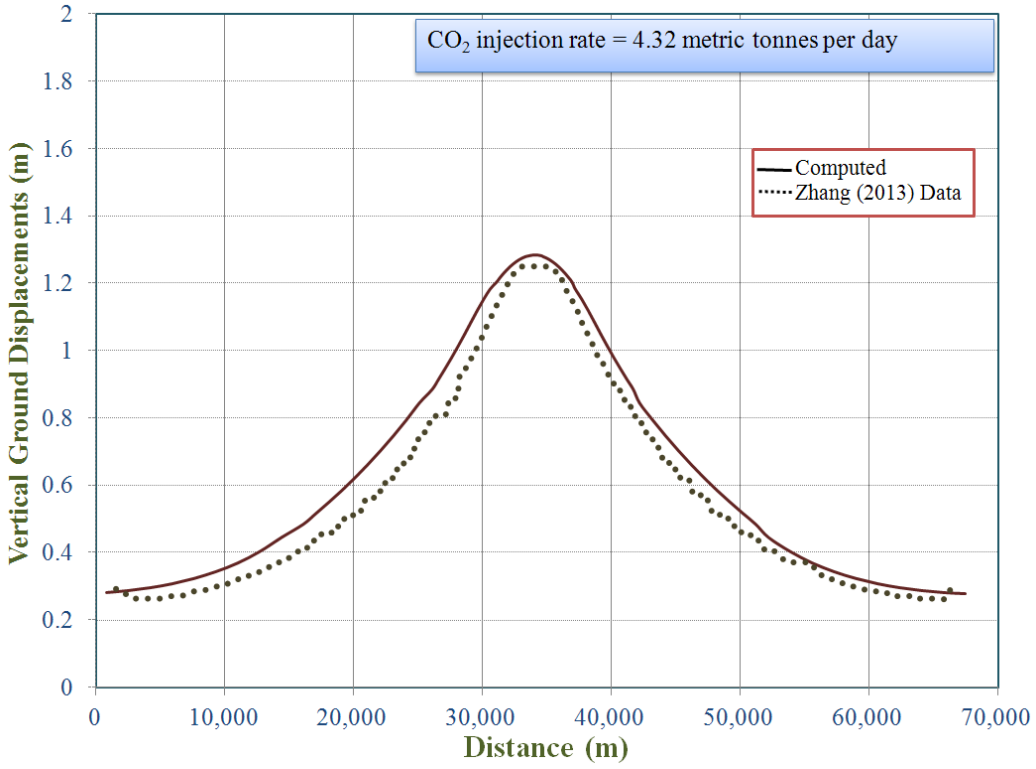

Figure 6-22: Comparison of computed ground displacements after 30 years of CO_2 injection with modified reservoir permeability.

Since the boundaries of the model are not fixed, the computed ground displacements will continue to increase at the far end of the model during CO_2 injection as shown in Figure 6-22. In order to obtain more accurate results, the boundaries of the model must be constrained. Thus, a model was constructed using the same geometrical details and material properties as described previously, with the boundaries fixed. Figure 6-23 shows the computed ground displacements during CO_2 injection. The maximum computed ground displacements after 30 years of CO_2 injection was 1.68 m. This translates to a 17% increase in computed ground displacements as compared to the model without fixed boundaries (1.44 m).

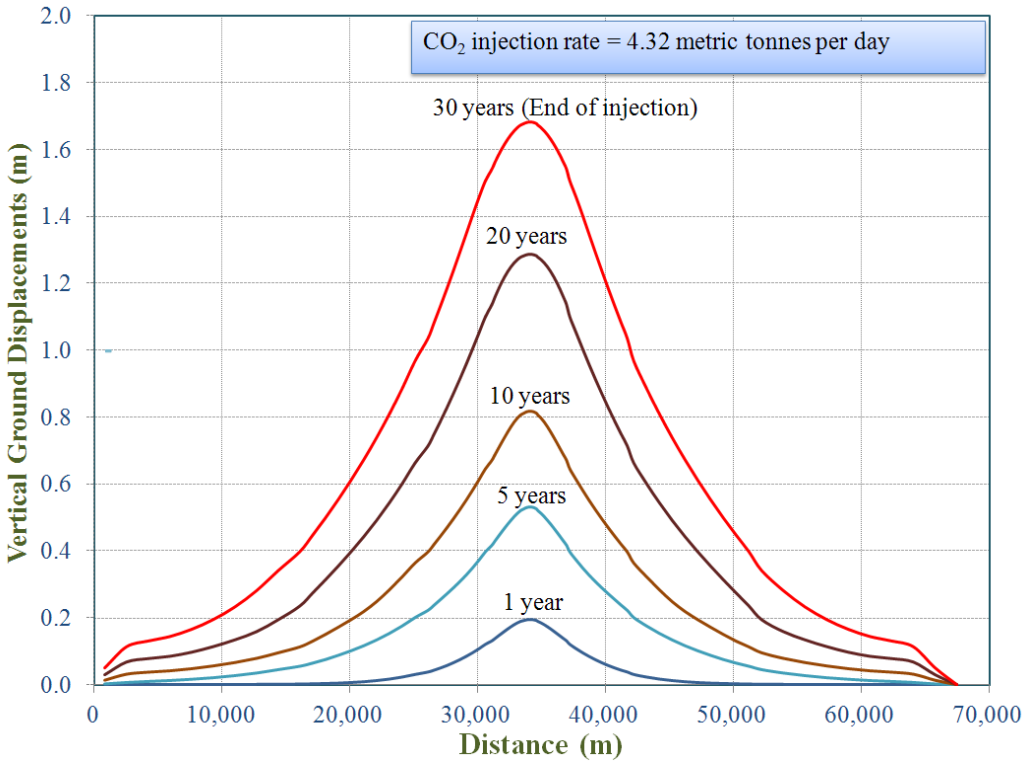

Figure 6-23: Ground displacements during 30 years of CO_2 injection with fixed model boundaries.

Chapter 7: MODELING OF LARGE-SCALE CO_2 INJECTION IN SALINE AQUIFERS

7.1 Introduction

In this study, large-scale CO_2 injection in the range of 5 to 10 million metric tonnes per year was carried out to examine the extent of CO_2 migration, pressure response, and vertical ground displacements over a long-term period (1,000 years). For the purpose of this study, multiphase fluid flow models coupled with geomechanics with the inclusion of salinity were constructed similar to the models used in Chapter 5.Since geochemical reactions do not have any significant influence on the computed ground displacements, the geochemical reactions have been suppressed in this study. The axisymmetric models consisted of 230 grid-blocks in the radial-direction and 13 layers in the z-direction. A radial length of 150,000 m was considered in these models. Such a large lateral extent was chosen to ensure that the boundary conditions have minimal effect on the geomechanical modeling results. A reservoir thickness of 500 m was used. The porosity and permeability of the reservoir in these models were assumed to be 20% and 100 millidarcies (mD), respectively. The base of these models was constrained in the vertical direction and lateral boundaries were set on rollers.

The CO_2 injection was simulated for 50 years with the primary injection rate constraint being 5 million metric tonnes per year and 10 million metric tonnes per year. As a secondary constraint, the maximum bottomhole pressure of 31,457 kPa was assumed. The initial average reservoir pressure was assumed to be 21,184 kPa. The geomechanical properties were similar to those used Chapter 5 .A brief discussion of results for the long-term, large-scale CO_2 injection is given in the following sections.

7.1.1 **Case 1: CO_2 injection rate of 5 million metric tonnes per year**

In this modeling scenario, CO_2 was injected with a primary injection rate constraint of 5 million metric tonnes per year and a secondary maximum bottomhole pressure of 31,457 kPa. The change in reservoir pressure at the end of 50-year CO_2 injection is shown in Figures 7-1. The maximum change in reservoir pressure was about 2,309 kPa, which corresponds to an increase of 11% above initial reservoir pressure. The change in reservoir pressure during the post-injection period of 50 years is shown in Figures 7-1. Post-injection results show that the reservoir pressure drops by 1916.5 kPa (approximately 83% drop) at the end of 20 years. The drop in reservoir pressure after 50 years of post-injection is about 2,077 kPa (approximately 90 % drop). These modeling results indicate that the increase in the reservoir pressure due to CO_2 injection decays with time during post-injection period (in this case, nearly 50 years of post-injection period). CO_2 injection causes poro-elastic expansion of the rock. The increase in pressure changes the volumetric strain with time. Figure 7-2 shows the changes in volumetric strain due to CO_2 injection. The maximum value of volumetric strain after 50 years of CO_2 injection is about 4.41e-05.

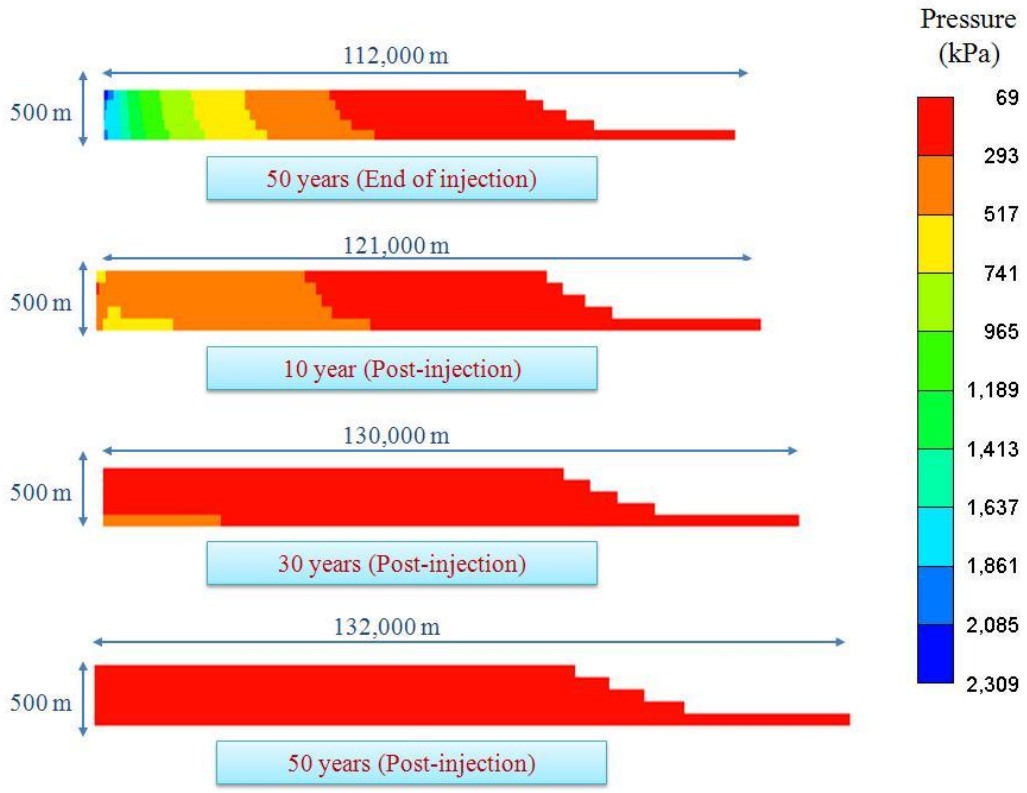

Figure 7-1: Change in reservoir pressure due to CO_2 injection.

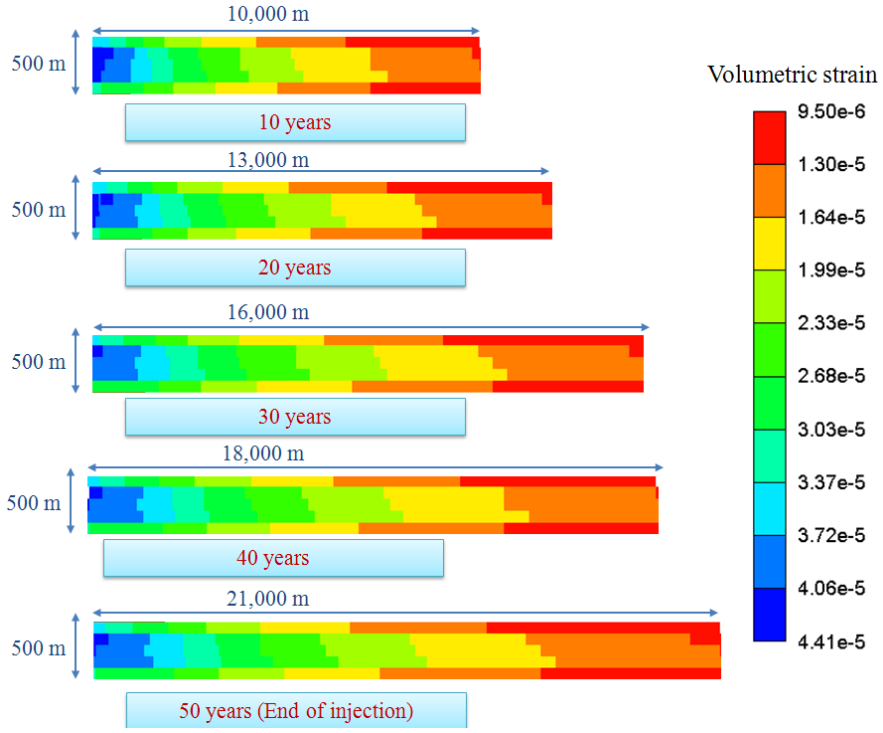

Figure 7-2: Change in volumetric strain in the reservoir during CO_2 injection.

Figures 7-3 show the vertical ground displacements at various time periods during CO_2 injection and the post-injection period. The maximum computed vertical ground displacement (uplift) was about 2.28 cm after 50 years of CO_2 injection. The change in ground displacements during the post-injection period of 200 years is shown in Figures 7-3. Modeling results show that the ground displacements drop by 1.83 cm (approximately 80% drop) at the end of 20 years. The drop in ground displacements after 50 years of post-injection is about 2.04 cm (approximately 90 % drop). The modeling results indicate that the ground displacements after 200 years of post-injection period are insignificant. Figure 7-4 shows a comparison between ground displacements at the end of 50 years of CO_2 injection for a couple fluid flow and geomechanics model without salinity and a coupled fluid flow and geomechanics model with salinity. The maximum computed ground displacement in the couple fluid flow and geomechanics model without salinity was about 1.64 cm after 50 years of injection. The difference in the magnitude of ground displacement is about 0.64 cm, which translates to a 39% increase in ground displacements when salinity was included in the coupled fluid flow and geomechanics model. This difference in the ground displacements can be related to the significant difference in the the magnitude of fluid pressure buildup due to CO_2 injection in the couple fluid flow and geomechanics model without salinity and the coupled fluid flow and geomechanics model with salinity as shown in Figure 7-5.

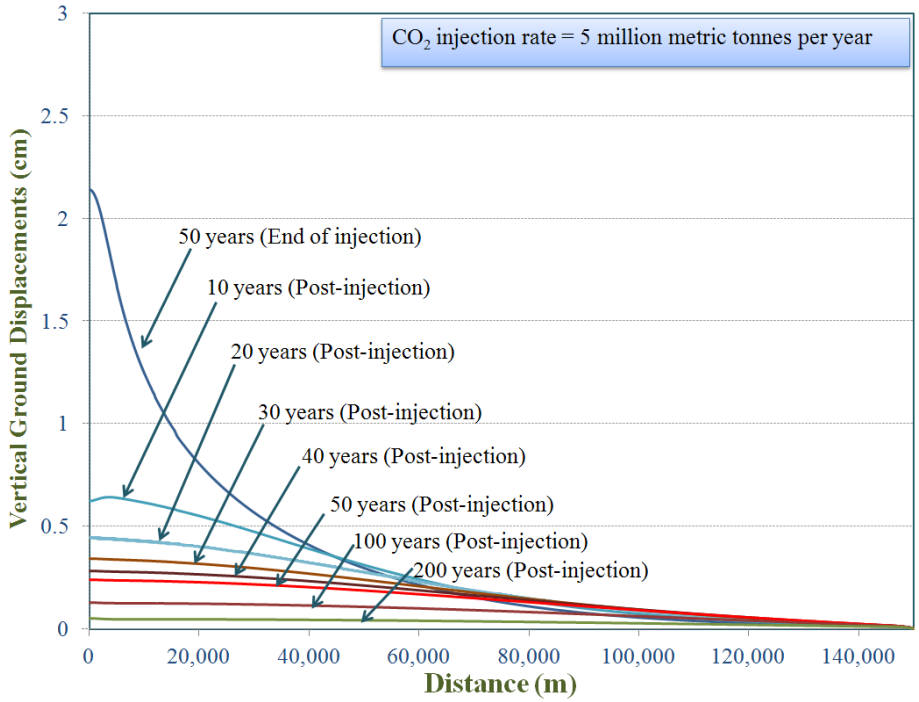

Figure 7-3: Computed vertical ground displacement at various time.

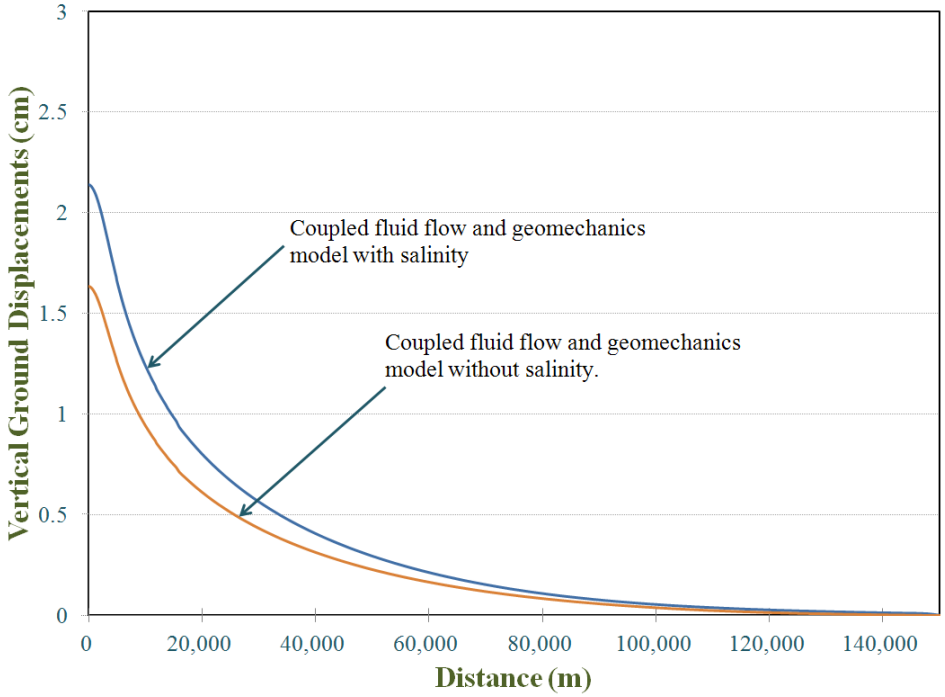

Figure 7-4: Comparison of computed ground displacement after 50 years of CO_2 injection.

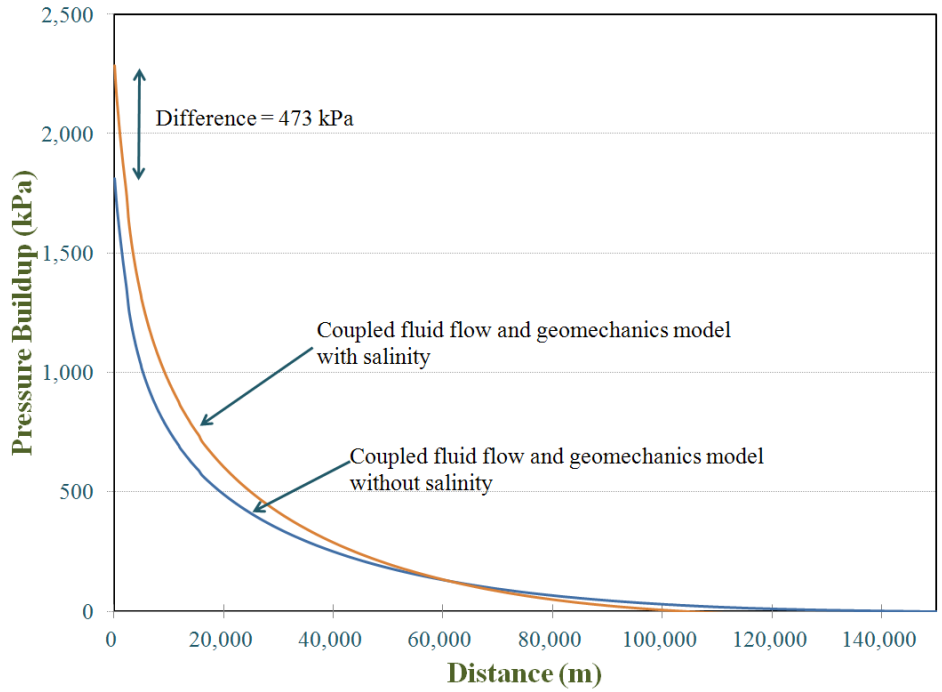

Figure 7-5: Comparision between the increase in pressure after 50 years of CO_2 injection.

7.1.2 Case 2: CO_2 injection rate of 10 million metric tonnes per year

In this modeling scenario, CO_2 was injected with a primary injection rate constraint of 10 million metric tonnes per year and a secondary maximum bottomhole pressure of 31,457 kPa. The change in reservoir pressure due to 50 years of CO_2 injection is shown in Figures 7-6. The maximum change in reservoir pressure was about 4,067 kPa, which corresponds to an increase of 19.20% above initial reservoir pressure. The post-injection results show that the reservoir pressure drops by 3,267 kPa (approximately 80% pressure drop) at the end of 20 years. The drop in reservoir pressure after 50 years of post-injection is about 3,641 kPa (approximately 90% pressure drop). CO_2 injection causes poro-elastic expansion of the rock. The increase in pressure changes the volumetric strain with time. Figure 7-7 shows the changes in volumetric strain due to CO_2 injection. The maximum value of volumetric strain after 50 years of CO_2 injection is about 8.49e-05.

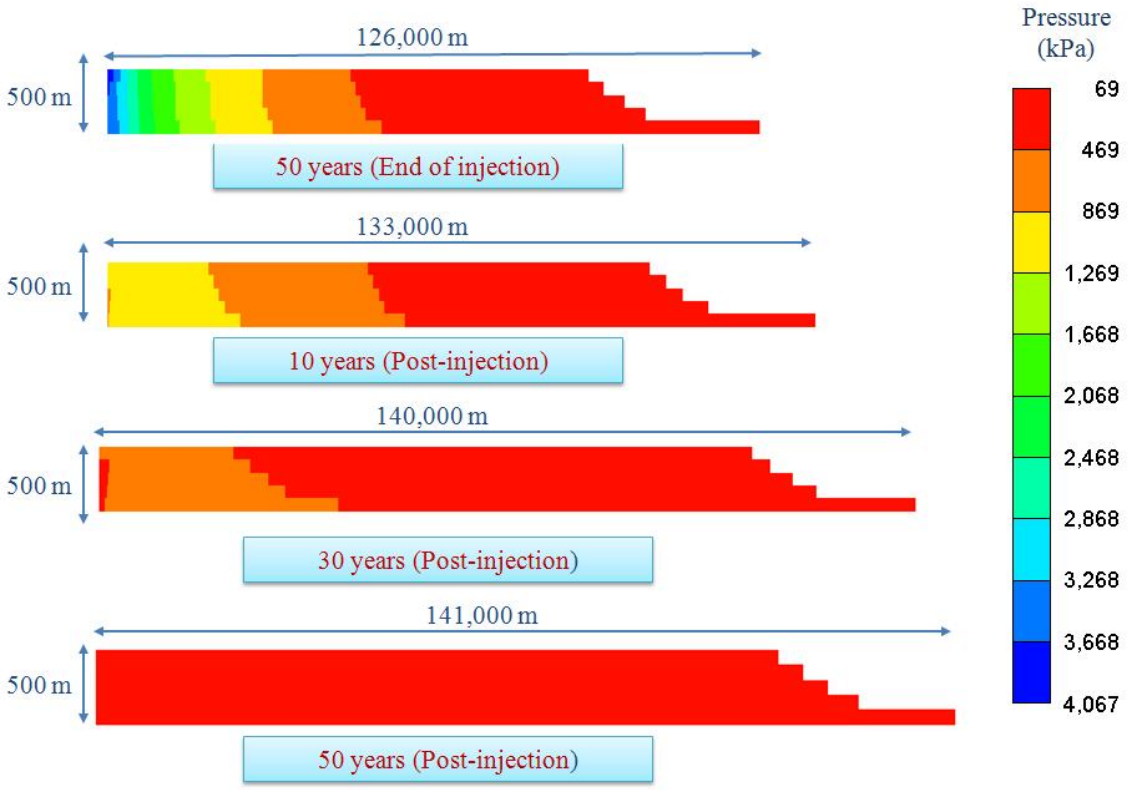

Figure 7-6: Change in reservoir pressure with time due to CO_2 injection.

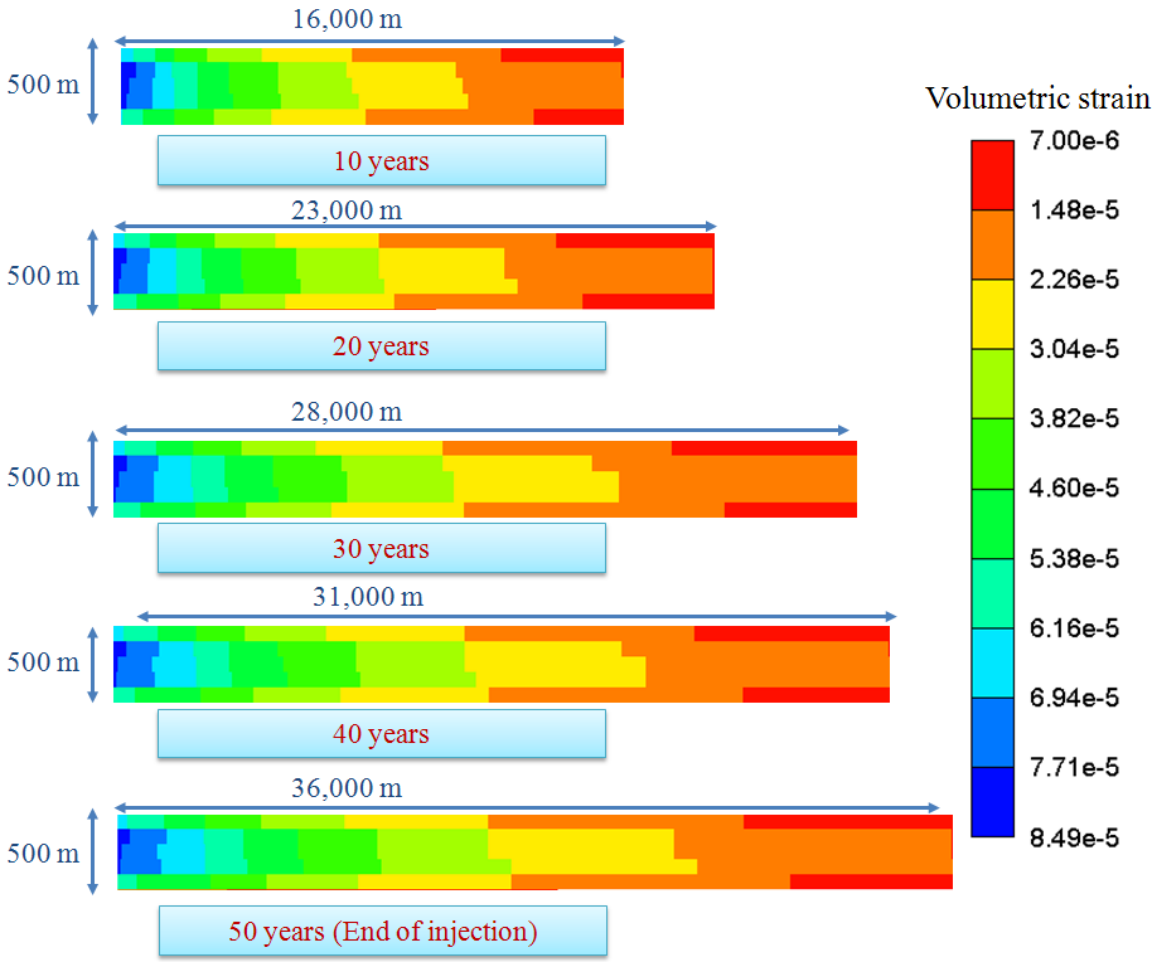

Figure 7-7: Change in volumetric strain in the reservoir during CO_2 injection.

Figures 7-8 show the vertical ground displacements at various times during CO_2 injection and the post-injection period. The maximum computed vertical ground displacement (uplift) was about 4.04 cm after 50 years of CO_2 injection. Post-injection results show that the ground displacements drop by 3.39 cm (approximately 84% drop) at the end of 20 years. The drop in ground displacements after 50 years of post-injection is about 3.81 cm (approximately 94.3% drop). The modeling results indicate that the ground displacements after 200 years of post-injection period are insignificant. Figure 7-9 shows a comparison between ground displacements at the end of 50 years of CO_2 injection for a couple fluid flow and geomechanics model without salinity and a coupled fluid flow and geomechanics model with salinity. The maximum computed ground displacement in the

couple fluid flow and geomechanics model without salinity was about 3.10 cm after 50 years of injection. The difference in the magnitude of ground displacement is about 0.94 cm, which translate to a 30% increase in ground displacements when salinity was included in the coupled fluid flow and geomechanics model. This difference in the ground displacements can be related to the signifcant difference in the the magnitude of fluid pressure buildup due to CO_2 injection in the couple fluid flow and geomechanics model without salinity and the coupled fluid flow and geomechanics model with salinity as shown in Figure 7-10.

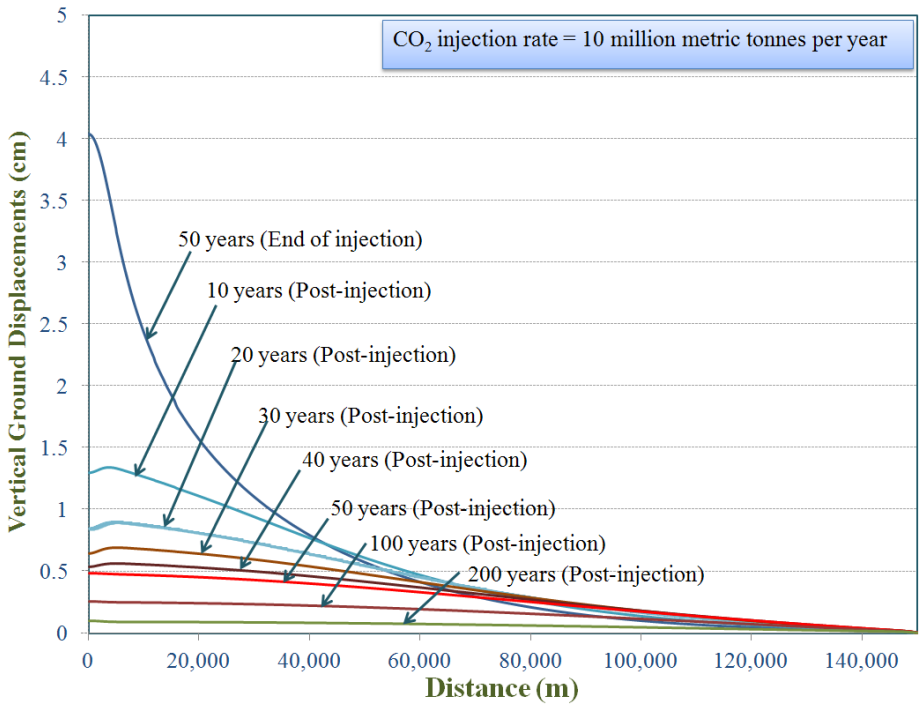

Figure 7-8: Computed vertical ground displacement at various time periods.

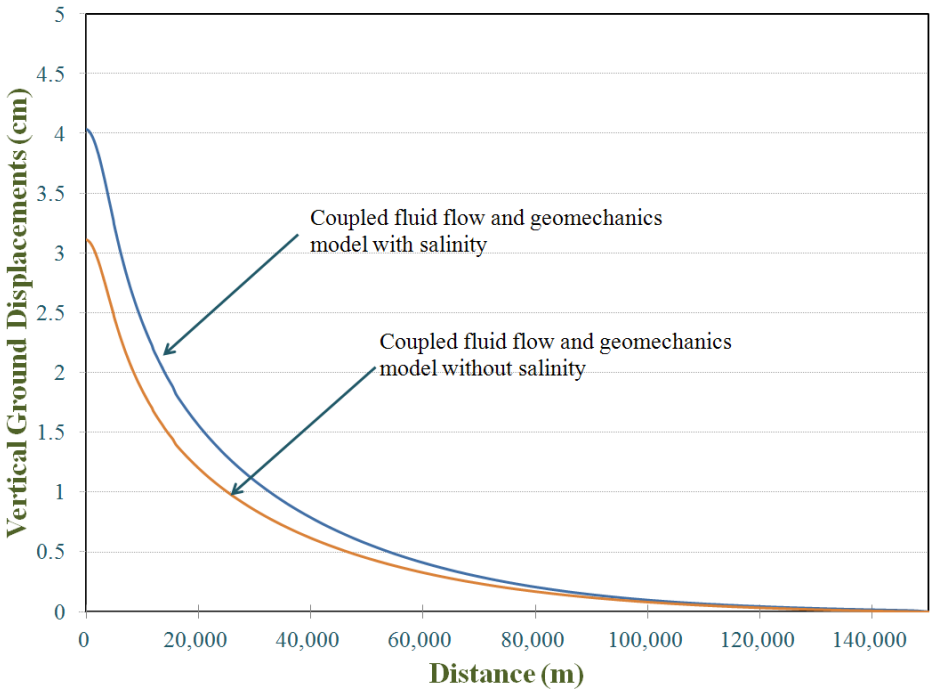

Figure 7-9: Comparision of computed ground displacement after 50 years of CO_2 injection.

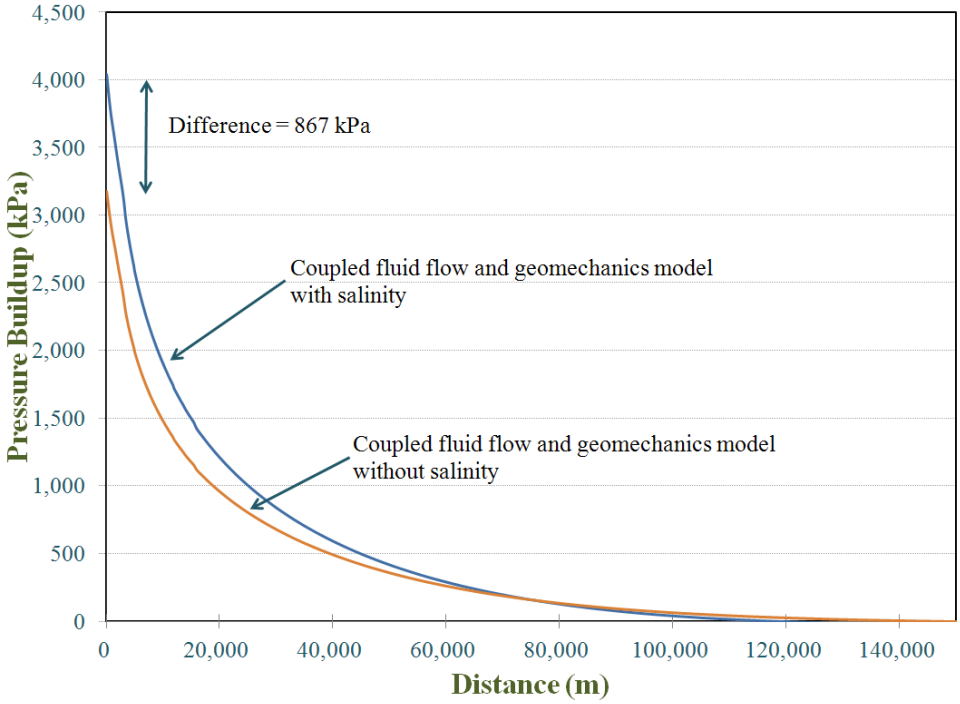

Figure 7-10: Comparision of the increase in pressure after 50 years of CO_2 injection.

7.2 CO_2 leakage due to wellbore damage

Geological storage of CO_2 involves pumping of large quantities (upto 10 million tonnes/year) of CO_2 into deep, permeable rock formations. The density of the injected CO_2 is significantly higher (~800 kg/ m^3) than gaseous CO_2 at a reservoir depth of 1,940 m. Although CO_2 has higher density in supercritical state, it is less dense and viscous than the formation brine (Gasda et al., 2008). As reported in the previous sections, injected CO_2 will rise to the top, bypassing large portion of formation brine due to gravity overrides and viscous instability. The relatively low-permeability caprock will act as a barrier to stop further vertical migration of CO_2.However, if favorable pathways exist through the caprock, the injected CO_2 may escape into the overburden geological layers. In spite of favorable geology, wellbore integrity can also be a significant risk factor with respect to the long-term storage of CO_2 (Choi et al., 2013). There are several ways in which a damage zones maybe created around the well bore which alters the wellbore integrity. They are as follows:

1. The mechanical action of drilling may create a fractured zone adjacent to the borehole. Leakage pathways may be created in the form of fractures in the wellbore cement and along wellbore-cement-rock interfaces influencing CO_2 injectivity, storage capacity, and seal integrity (Carroll et al., 2013; Jun et al.,2013; Mason et al., 2013; Walsh et al., 2012).
2. Improper mixing or placement of cement in between the casing and formation rock may create small micro-annuli through which fluids can flow (Gasda et al., 2008).
3. During the lifetime of a well, the casing is subjected to large pressure variations which may cause the cement to fracture (Gasda et al., 2008).
4. Interaction of cement with aggressive fluids such as carbonic acid (H_2CO_3) and sulphuric acid (H_2SO_4) (Gasda et al., 2008).
5. Interaction between the steel casing and H_2CO_3 in the absence of a cement sheath may lead to corrosion (Loizzo et al., 2010).

Since leakage through the wellbore is considered a major source of concern for the large-scale deployment of CO_2 storage, several studies have been performed to address the issues related to wellbore integrity and CO_2 leakage risk (Azaroual et al., 2012; Benge, 2009; Choi et al., 2013; Gasda et al., 2008; Gasda et al., 2013;Houdu et al.,2008; Loizzo et al.,2010; Pawar et al.,2009; Watson and Bachu,2008). Reliable data about safe storage of CO_2 is almost non-existent and analysis of existing data that has been reported in the literature have shown that majority of CO_2 leaks are small with limited or negligible consequences (Loizzo et al., 2010). Although CO_2 leakage to the overburden layers or the atmosphere causes no significant damage, it will still defeat the purpose of storing it beneath the ground. Given the frequent occurrences of CO_2 leakages, reliable estimates of both the quantity of CO_2 leaking out of the reservoir and the consequences of CO_2 leakage are required to be addressed. These estimates can be used to deploy practices and preventive measures for the long-term storage of CO_2 in deep geological formations (Loizzo et al., 2010).

7.2.1 **Modeling details of CO_2 leakage**

The objective of this study was to investigate the influence of a hypothetical vertical permeable zone (damage zone) around the wellbore on the CO_2 leakage rate during long-term CO_2 injection. The influence of the damage zone permeability on the amount of CO_2 leakage into the overburden layers was also investigated. For the purpose of this study, axisymmetric, coupled multiphase fluid flow and geomechanical models were constructed. For the purpose of comparison between the ground displacements due to CO_2 injection, two separate models were constructed:

1) With a damage zone around the wellbore
2) No damage zone around the wellbore

The model geometry consists of an overburden layer, a tight caprock layer, a reservoir layer and an underburden layer as shown in Figure 7-11. The damage zone was

assumed to extend from the bottom of the reservoir to about 100 m above the caprock layer as shown in Figure 7-11. The axisymmetric models consist of 172 grid-blocks in the radial-direction and 25 layers in the z-direction. A radial length of 150,000 m was considered in these models. The size of the permeable grid block was 1 m. Since no reliable data on the properties of the damage zone surrounding the well casing exists in the literature, the permeability of the damage zone around the wellbore was assumed to be ranging between 1000 mD to 100,000 mD. This permeability is approximately equivalent to having a fracture width of 1 mm and a fracture permeability of 1,000 D to 100,000 D. Geomechanical and rock properties were similar to those used in the previous sections.

A hypothetical large-scale CO_2 injection scenario was considered to determine the extent of CO_2 migration, CO_2 leakage rate, and the vertical ground displacements over a period of 1,000 years. The CO_2 injection was simulated for 50 years with the primary injection rate constraint being 5 million metric tonnes per year. As a secondary constraint, the maximum bottomhole pressure of 31,457 kPa was assumed. The initial average reservoir pressure was assumed to be 19,031 kPa in the model.

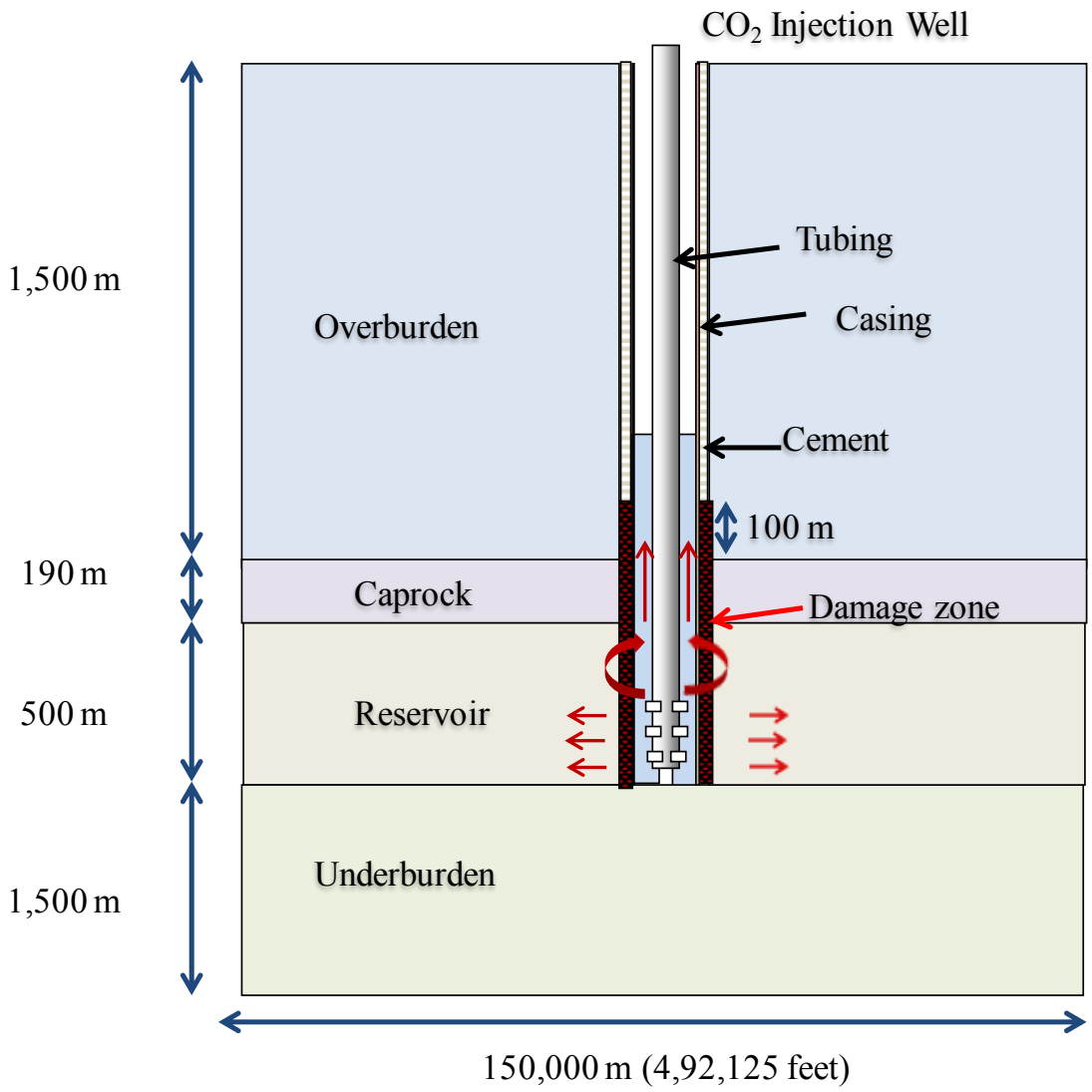

Figure 7-11: Schematic diagram of the hypothetical wellbore damage considered in this study.

7.2.2 **Modeling results of CO_2 leakage**

After 50 years of CO_2 injection, 250 million metric tonnes of CO_2 was injected into the reservoir. Figure 7-12 shows the amount of CO_2 that has leaked into the overburden for different damage zone permeability. Results show that after 50 years of the post-injection period, the computed amount of CO_2 leaking in the overburden was very small. This may be due to the gradual drop in fluid pressure to hydrostatic

conditions, along the damage zone in the reservoir during the post-injection period as shown in Figure 7-13. Table 7.1 shows the CO_2 leakage (%) into the overburden for different damage zone permeability. Modeling results show that the damage zone permeability has significant influence on the amount of CO_2 leaking into the overburden.

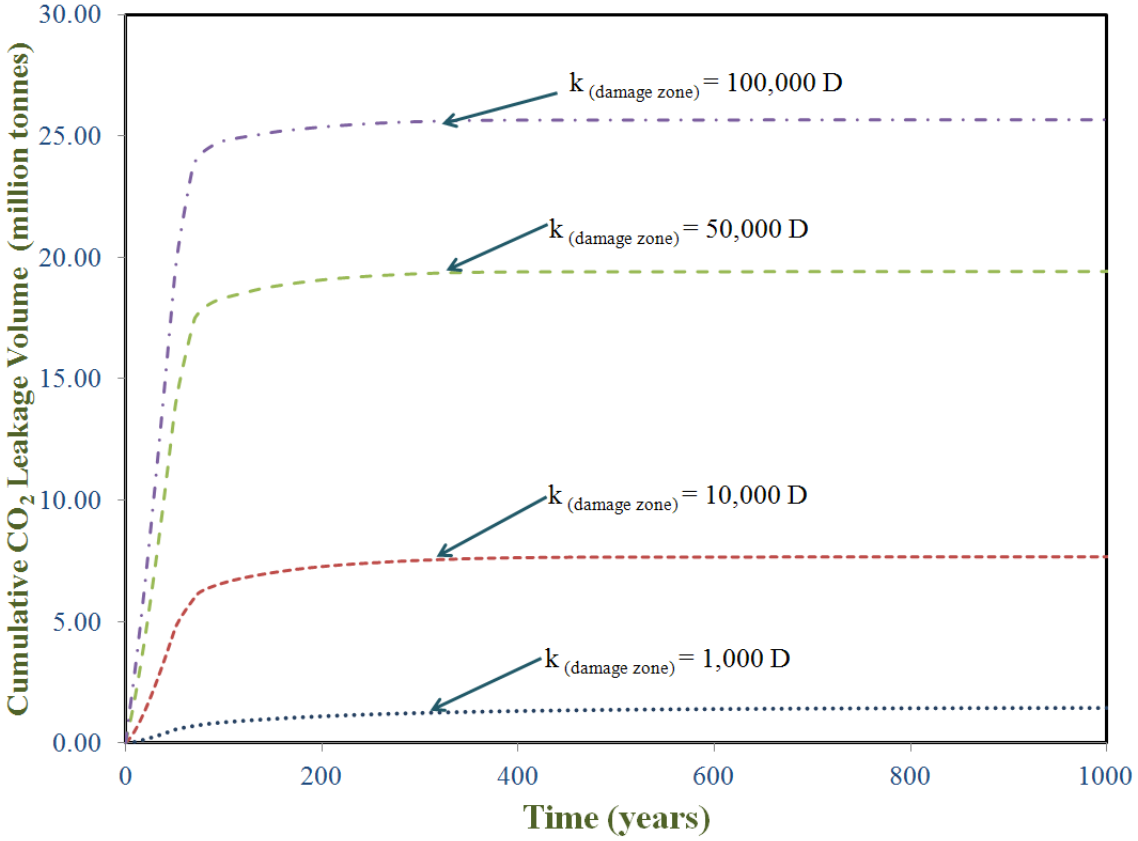

Figure 7-12: Computed cumulative CO_2 volume that has leaked into the overburden.

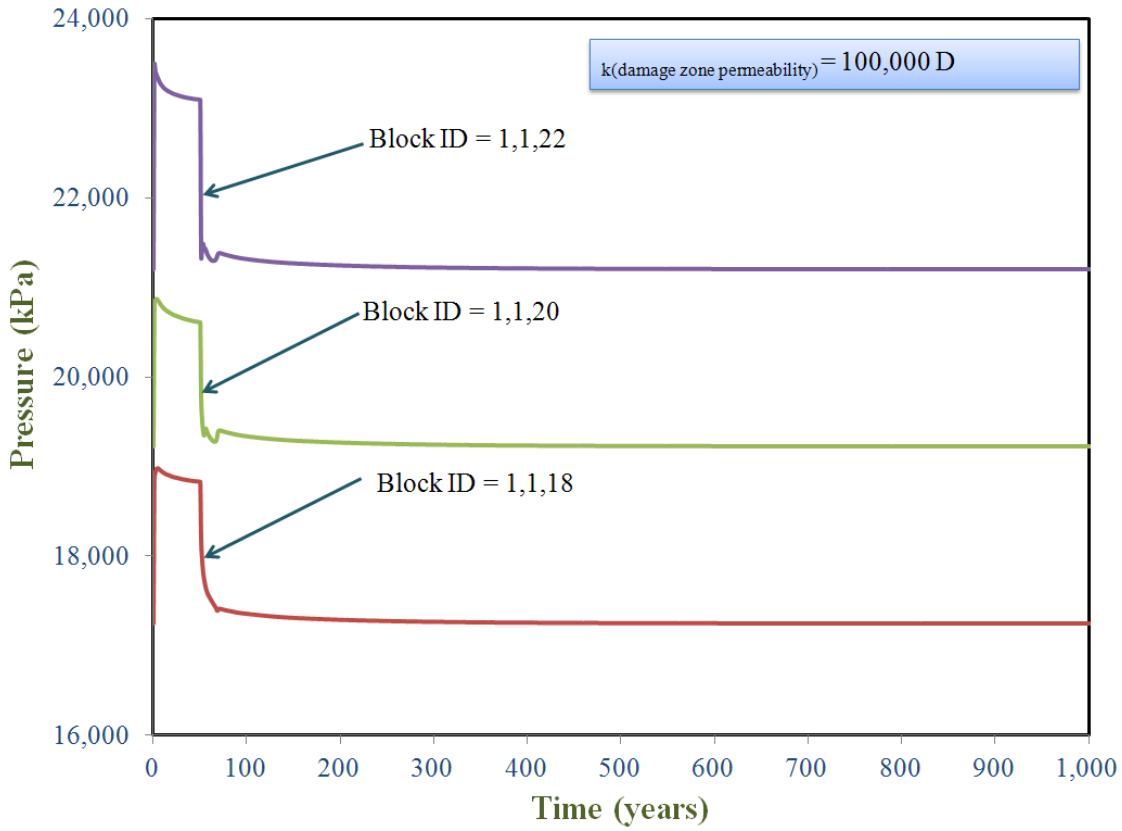

Figure 7-13: Change in pressure in the damage zone with time.

Table 7-1: CO2 leakage (%) for different damage zone permeability

Damage zone permeability	CO_2 Leakage (%)
1,000 D	0.58
10,000 D	3.07
50,000 D	7.76
100,000 D	10.25

7.2.3 **Ground response**

Figures 7-14 shows the vertical ground displacements at the end of CO_2 injection for the coupled multiphase fluid flow and geomechanical model with and without a permeable zone around the wellbore. The maximum computed vertical ground displacement (uplift) after 50 years of CO_2 injection was about 1.58 cm in the model without damage around the wellbore.Figure 7-14 shows that the damage zone permeability has a significant influence on the computed ground displacements. The maximum computed ground displacements after 50 years of CO_2 injection was about 2.42 cm when the damage zone permeability was about 100,000 D.

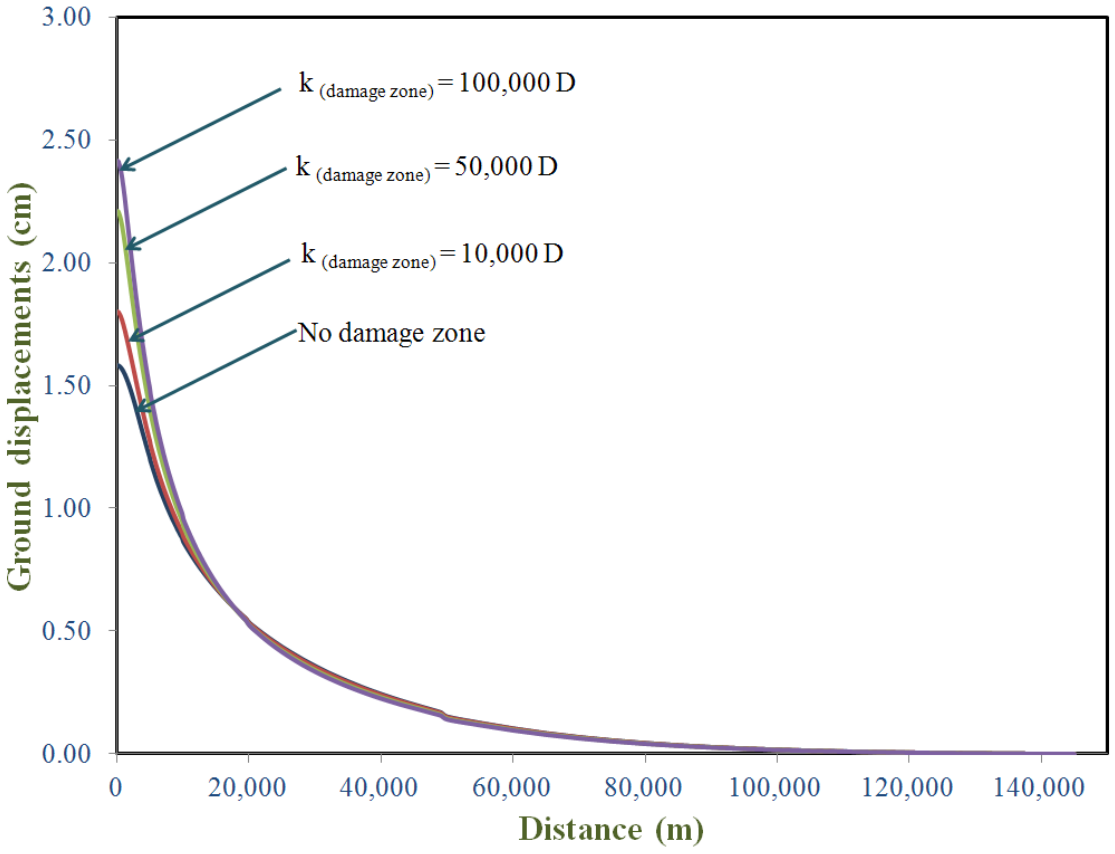

Figure 7-14: Computed vertical ground displacement at the end of CO_2 injection.

7.2.4 **Influence of the vertical extent of the damage zone on the amount of CO_2 leakage**

In this study, a coupled multiphase fluid flow and geomechanical model was constructed to investigate the influence of the vertical extent of the damage zone on the amount of CO_2 leaking into the overburden and the ground displacements. The damage zone was assumed to extend from the bottom of the reservoir to the ground surface as shown in Figure 7-15. The permeability of the damage zone around the wellbore was assumed to be 1000 D, 10,000 D, 50,000 D, and 100,000 D. Figures 7-16 shows the cumulative CO_2 volume which has leaked into the overburden for different damage zone permeability. The maximum computed CO_2 volume that has leaked into the overburden when the damage zone permeability was 100,000 D was about 37 million metric tonnes. This CO_2 volume leaking into the overburden is significantly higher when compared to the case where the hypothetical damage zone extended 790 m from the base of the reservoir into the overburden (CO_2 volume = 25 million metric tonnes). Table 7.2 shows a comparison between the computed CO_2 leakage (%) for different vertical extents of the hypothetical damage zone considered in this study. Results shown in Table 7.2 indicate that both, the vertical extent of the damage zone and the damage zone permeability have a significant influence on the CO_2 leakage (%).

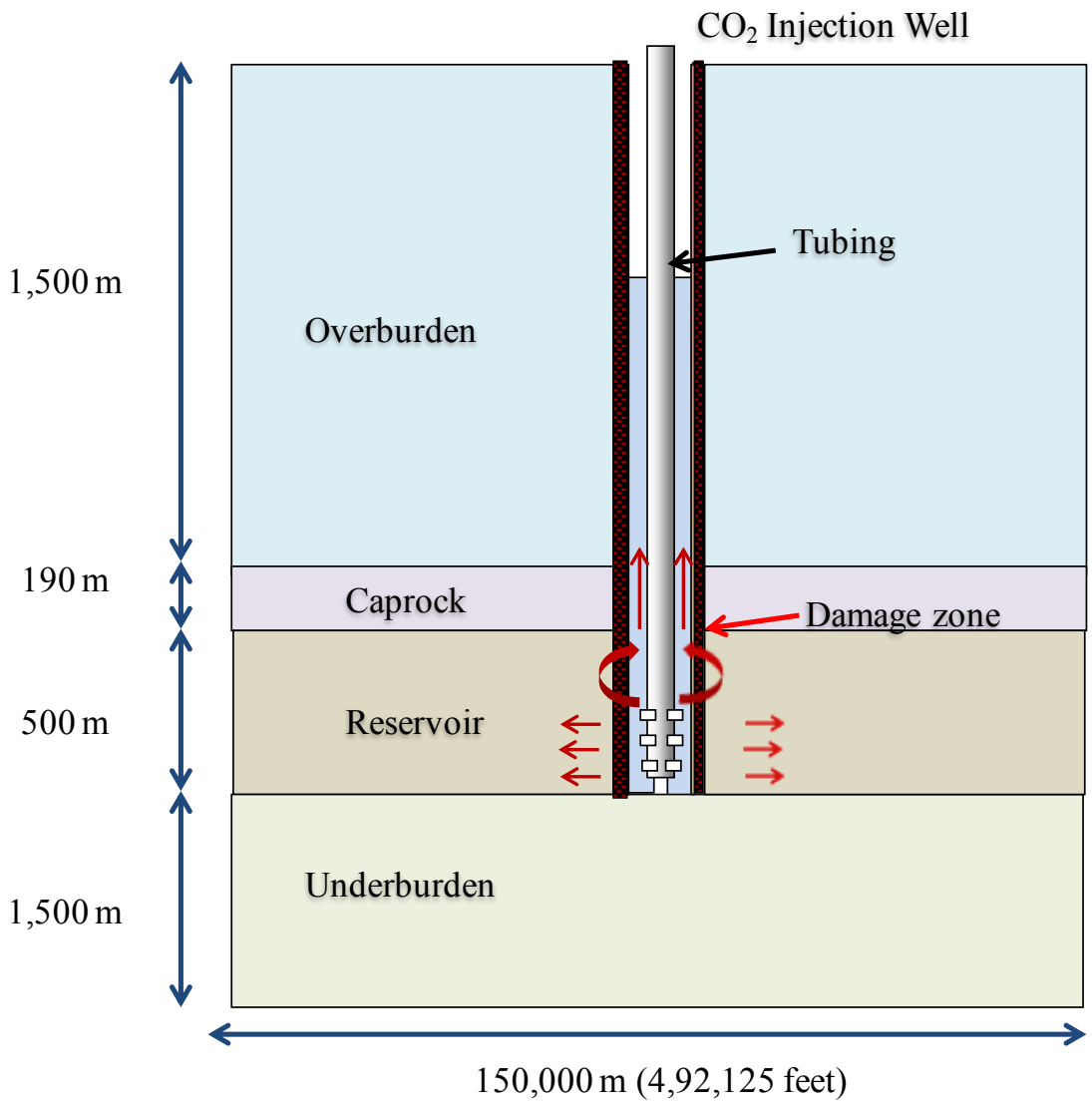

Figure 7-15: Schematic diagram of the hypothetical wellbore damage considered in this study.

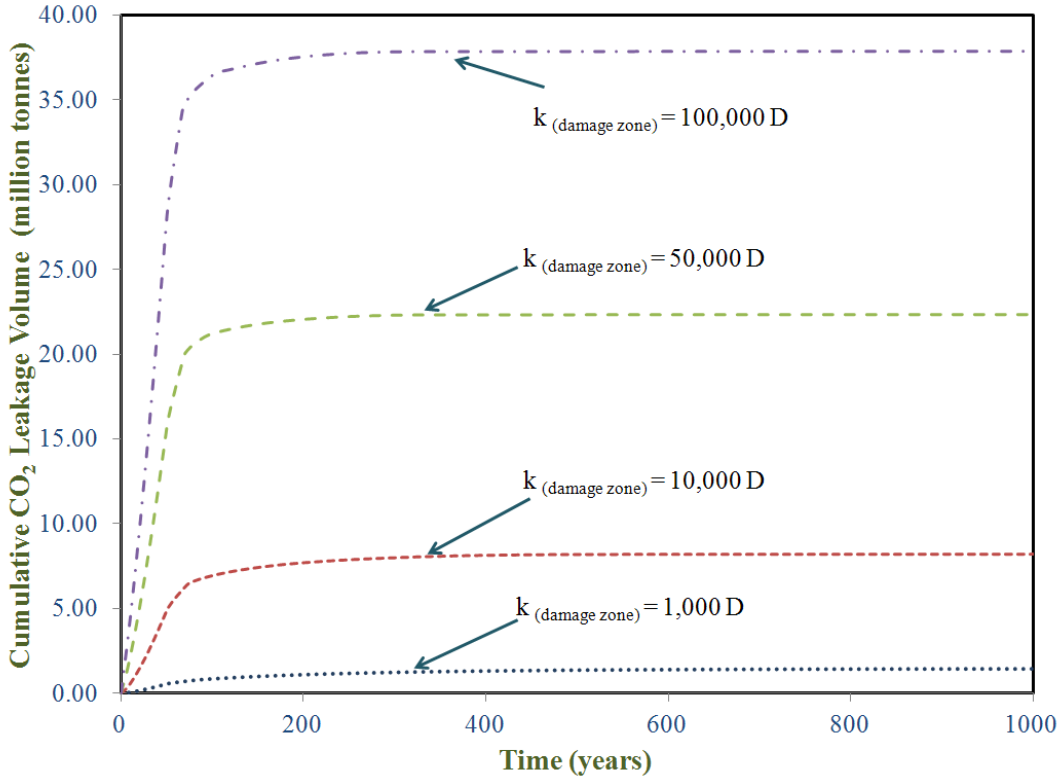

Figure 7-16: Computed cumulative CO_2 volume that has leaked into the overburden.

Table 7-2:CO_2 leakage (%) for different damage zone permeability

Damage zone permeability (D)	CO_2 Leakage (%)	
	Damage zone extending 100 m above caprock layer	Damage zone extending to the surface
1,000	0.58	0.58
10,000	3.07	3.27
50,000	7.76	8.92
100,000	10.25	15.13

Figures 7-17 shows the vertical ground displacements at the end of CO_2 injection for the coupled multiphase fluid flow and geomechanical model with and without a permeable zone around the wellbore. The maximum computed vertical ground displacement (uplift) after 50 years of CO_2 injection was about 1.58 cm in the model with no damage around the wellbore. The maximum computed ground displacement after 50 years of CO_2 injection was about 2.60 cm when the damage zone permeability was about 100,000 D. The computed ground displacements obtained in this study were higher than the ground displacements that were computed when the damage zone extended upto 100 m above the caprock layers from the base of the reservoir as shown in Table 7-3.However, this difference in the magnitude of ground displacements can be considered insignificant. Thus, surface displacements may not be a good indicator of the extent of damage zone around the wellbore.

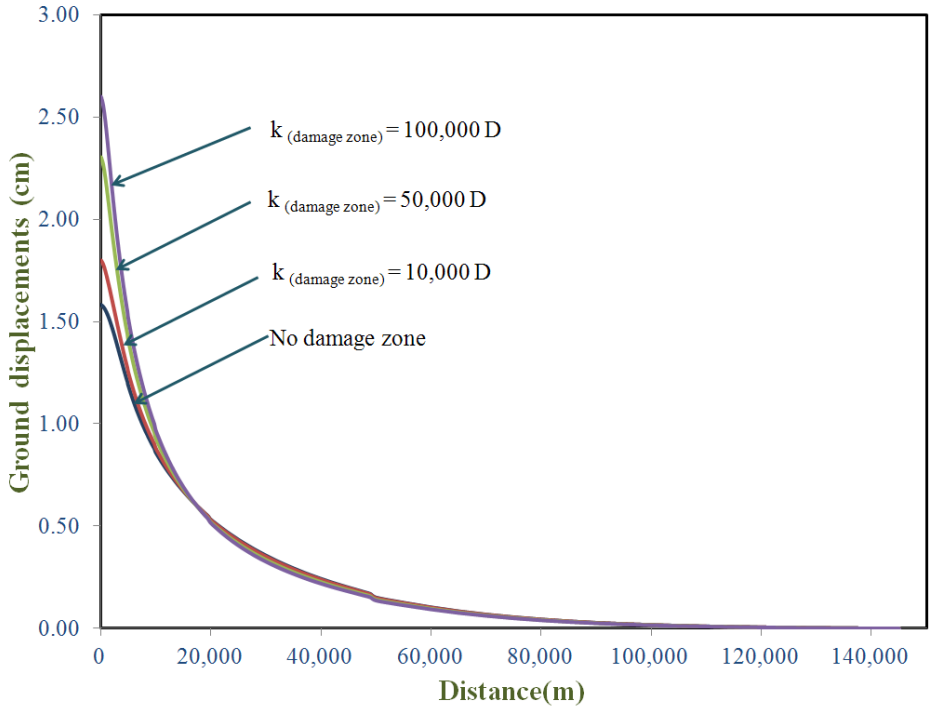

Figure 7-17: Computed vertical ground displacement at the end of CO_2 injection.

Table 7-3: Ground displacements for different damage zone permeability

Damage zone permeability (D)	**Ground displacements (cm)**	
	Damage zone extending 100 m above caprock layer	**Damage zone extending to the surface**
No damage zone	1.58	1.58
10,000	1.80	1.80
50,000	2.21	2.30
100,000	2.41	2.60

Chapter 8: SUMMARY AND CONCLUSIONS

8.1 Summary

The primary objective of this study is to investigate the influence of different geochemical process on the geomechanical response of the overburden during long-term CO_2 injection. In this study, radially symmetric, multiphase, and single porosity models were constructed to study the influence of geochemical changes on the geomechanical response of the overburden over a long term (1,000 years). The model geometry consists of an overburden layer, a tight caprock, a sandstone reservoir formation and an underburden to represent a hypothetical CO_2 storage site. Three models were constructed to investigate the influence of geochemical reactions, brine salinity, and CO_2 solubility on rock properties (porosity and permeability), and the geomechanical response of the rock system. These three models consist of: 1) A geochemical model to determine the influence of geochemical reactions on rock properties such as porosity and permeability, 2) Coupled fluid flow, geomechanics models, and geochemical models with and without geochemical reactions to determine the influence of geochemical reactions on the geomechanical response of the system, 3) Coupled fluid flow and geomechanical models with and without salinity to determine the influence of salinity on CO_2 solubility and the geomechanical response of the system.

A hypothetical injection scenario was assumed for the models where CO_2 was injected at a rate of 0.365 million metric tonnes per year or 1,000 metric tonnes per day for 25 years with a maximum bottom-hole pressure of 31,457 kPa. The model simulations were carried out for 1,000 years to examine the extent of CO_2 migration, geochemical reactions such as mineral dissolution/ precipitation, the change in rock properties, and pressure response. Modeling results show that the change is porosity due to geochemical reactions was insignificant (2%). The reaction rate constants were then artificially increased to investigate the influence of the geochemical reaction rates on the rate of mineral dissolution/precipitation. The maximum change in the computed porosity

was 0.07 (fraction) after 1,000 years. This change in porosity translates to a 35% change of the original porosity.

In the coupled multiphase fluid flow and geomechanical model with geochemical reactions, a constant elastic modulus of 40 GPa and a Poisson' ratio of 0.25 was used for all rock formations. The computed fluid pressure gradient in the reservoir was 10.86 kPa/m. Due to the high salinity value assumed in this study (195,000 ppm), the computed fluid pressure gradient is higher than the fluid pressure gradient for freshwater (9.79 kPa/m). When CO_2 was injected at a primary injection rate of 0.365 million metric tonnes per year, and a secondary constraint of maximum bottomhole pressure of 31,457 kPa, the maximum change in reservoir pressure at the end of 25-year was about 243 kPa. This change in pressure translates to an increase of 1.15% above the average initial reservoir pressure. The increase in pressure during CO_2 injection is very small due to the assumed value of high reservoir permeability (100 mD) and the infinite extent of the reservoir. Modeling results show that the reservoir pressure drops significantly during the first 10 years of the post-injection period (~ 70%).The maximum computed vertical displacement due to 25 years of CO_2 injection was about 0.16 cm.The magnitudes of ground displacement are small due to small changes in fluid pressure during injection. The coupled fluid flow and geomechanical model with salinity and no geochemical reactions yielded similar results as above. This shows the geochemical reactions do not have any influence on the pressure response and computed ground displacements.

In the coupled fluid flow and geomechanical model without salinity, the aqueous mass density is calculated as a linear function of pressure. The computed aqueous mass density for the coupled fluid flow and geomechanics model with salinity and the coupled fluid flow and geomechanics model without salinity are significantly different. When CO_2 was injected at a primary injection rate of 0.365 million metric tonnes per year, and a secondary constraint of maximum bottomhole pressure of 31,457 kPa, the maximum change in reservoir pressure at the end of 25-year CO_2 injection was about 216 kPa. This change in pressure translates to an increase of 1.02% above the average initial reservoir pressure. The maximum computed ground displacement in the coupled fluid flow and

geomechanics model without salinity was about 0.115 cm after 25 years of injection.The difference in ground displacements betweeen the coupled fluid flow model with and without salinity was about 0.045 cm. This difference in the ground displacements can be related to the difference in the the magnitude of fluid pressure buildup due to CO_2 injection in the couple fluid flow and geomechanics model without salinity and the coupled fluid flow and geomechanics model with salinity. CO_2 dissolution or solubility in brine decreases with salinity. Under such circumatances the displacement of the highly viscous brine during CO_2 injection by the less viscous CO_2 requires more effort thus leading to an increase in fluid pressure. The increase in fluid pressure results in an increase of the ground dispalcements. In order to investigate the influence of CO_2 solubility on the ground displacements, a coupled fluid flow and geomechanics models with different values of brine salinity were constructed. Modeling results show that the maximum reduction in CO_2 dissolution was about 44% when compared to the coupled fluid flow and geomechanics model without salinity. Modeling results show that brine salinity and CO_2 solubility in brine has an influence on the computed ground displacements.

In this study, multiphase, single porosity, and axisymmetric models were also constructed to investigate the influence of large-scale CO_2 injection (5 million metric tons per year - 10million metric tons per year) on the geomechanical response of the overburden. Since geochemical reactions do not have any significant influence on the computed pressure and ground displacements, the geochemical reactions were suppressed in this study. Two hypothetical large-scale CO_2 injection scenarios were considered to examine the extent of CO_2 migration, pressure response, and vertical ground displacements over a long-term period (1,000 years). The CO_2 injection was simulated for 50 years in all the scenarios with the primary rate constraint being 5 million metric tonnes per year and 10 million metric tonnes per year. As a secondary constraint, the maximum bottomhole pressure of 31,457 kPa was assumed. The initial average reservoir pressure was assumed as 21,184 kPa in the model.

The maximum change in reservoir pressure when CO_2 was injected at a rate of 5 million metric tonnes per year was about 2,309 kPa which corresponds to an increase of 11% above initial reservoir pressure. Modeling results show that the reservoir pressure drops by 1916.5 kPa (approximately 83% drop) at the end of 20 years. The drop in reservoir pressure after 50 years of post-injection is about 2,077 kPa (approximately 90 % drop). These modeling results indicate that the increase in the reservoir pressure due to CO_2 injection decays with time during post-injection period (in this case, nearly 50 years of post-injection period). The maximum computed vertical ground displacement (uplift) was about 2.28 cm after 50 years of CO_2 injection. Post-injection results show that the ground displacements drop by 1.83 cm (approximately 80% drop) at the end of 20 years. The drop in ground displacements after 50 years of post-injection is about 2.04 cm (approximately 90 % drop). Modeling results show that the ground displacements after 200 years of post-injection period were insignificant. The maximum computed ground displacement in the couple fluid flow and geomechanics model without salinity was about 1.64 cm after 50 years of injection. The difference in the magnitude of ground displacement is about 0.64 cm,which translates to a 39% increase in ground displacements when salinity was included in the coupled fluid flow and geomechanics model. This difference in the ground displacements can be related to the signifcant difference in the the magnitude of fluid pressure buildup due to CO_2 injection in the couple fluid flow and geomechanics model without salinity and the coupled fluid flow and geomechanics model with salinity (~ 437 kPa).

In the case where CO_2 was injected at a rate of 10 million metric tonnes per year, similar pressure responses were observed. The maximum change in reservoir pressure after 50 years of CO_2 injection was about 4,067 kPa, which corresponds to an increase of 19.20% above initial reservoir pressure. The post-injection results show that the reservoir pressure drops by 3,267 kPa (approximately 80% pressure drop) at the end of 20 years. The drop in reservoir pressure after 50 years of post-injection is about 3,641 kPa (approximately 90% pressure drop). The maximum computed vertical ground displacement (uplift) was about 4.04 cm after 50 years of CO_2 injection. Post-injection results show that the ground displacements drop by 3.39 cm (approximately 84% drop) at

the end of 20 years. The drop in ground displacements after 200 years of post-injection is about 3.81 cm (approximately 94.3% drop). The modeling results indicate that the ground displacements after 200 years of post-injection period were insignificant. The maximum computed ground displacement in the couple fluid flow and geomechanics model without salinity was about 3.10 cm after 50 years of injection. The difference in the magnitude of ground displacement is about 0.94 cm, which translates to a 30% increase in the ground displacements when salintiy was included in the coupled fluid flow and geomechanics model. This difference in the ground displacements can be related to the signifcant difference in the the magnitude of fluid pressure buildup due to CO_2 injection in the couple fluid flow and geomechanics model without salinity and the coupled fluid flow and geomechanics model with salinity (~ 867 kPa).

In this study, the influence of a vertical permeable zone (damage zone) around the wellbore, on the CO_2 leakage rate and ground displacements, during long-term CO_2 injection was also investigated. The influence of the damage zone parameters such as permeability and the vertical extent of the damage zone on the leakage rate were also taken into consideration. A hypothetical large-scale CO_2 injection scenario was considered to determine the extent of CO_2 migration, CO_2 leakage rate, and the vertical ground displacements over a period of 1,000 years. This particular analysis is based on coupled fluid flow and geomechanics (i.e., no geochemical reactions were considered). The CO_2 injection was simulated for 50 years with the primary injection rate constraint being 5 million metric tonnes per year. The initial average reservoir pressure was assumed to be 19,031 kPa in the model. Since no reliable data on the properties of the damage zone surrounding the well casing exists in literature, the permeability of the damage zone around the wellbore was assumed to be in the range of 1 mD to 100,000 mD. This permeability is approximately equivalent to having a fracture width of 1 mm and a fracture permeability of 1,000 D to 100,000 Darcy. Geomechanical and rock properties were similar to those used in the coupled fluid flow and geomechanical model with geochemical reactions as discussed in Chapter 5.

After 50 years of CO_2 injection at a rate of 5 million tonnes per year, approximately 250 million metric tons of CO_2 was injected into the reservoir. Due to the presence of a hypothetical vertical permeable zone (k = 100, 000 D) around the wellbore extending from the base of the reservoir to 100 m above the caprock (i.e., 790 m of damage zone), about 25 million metric tonnes of CO_2 leaked into the overburden layers. This computed volume of CO_2 that has leaked into the overburden layers translates to 10.25% loss of injected CO_2. The maximum computed ground displacements after 50 years of CO_2 injection was about 2.42 cm when the damage zone permeability was 100,000 D. When the vertical extent of the damage zone was increased to 2,180 m (base of the reservoir to the ground surface), about 37 million metric tonnes of CO_2 leaked into the overburden layers when the permeability of the damage zone was 100,000 D. This computed volume of CO_2 that has leaked into the overburden layers translates to 15.13% loss of injected CO_2. The maximum computed ground displacements after 50 years of CO_2 injection was about 2.60 cm when the damage zone permeability was about 100,000 D. Modeling results from this study show that both, the permeability of the damage zone and the vertical extent of the damage zone have a significant influence on the volume of CO_2 leaking into the overburden and the ground displacements.

8.2 Conclusions

- The amount of mineral dissolution and precipitation depends upon the rate constant of mineral reactions.
- The mineral reaction data used in this study did not yield any significant mineral dissolution or precipitation (change in computed rock porosity was about 2%).
- When the reaction rate of minerals was artificially increased significantly, the maximum change in reservoir rock porosity was about 35%. This reduction in reservoir porosity was due to mineral precipitation.
- In the study involving short-term injection (i.e., 25 years of injection), pressure buildup is insignificant. This could be due to value of high reservoir permeability (100 mD) and the infinite extent of the reservoir. Also, the computed ground

displacements during CO_2 injection are considered insignificant. This could be due to the small injection volume (0.365 million tonnes per year) assumed in the study.

- Large-scale CO_2 injection (upto 10 million metric tonnes per year over 50 years of injection) causes significant increase in computed pressure and ground displacements during the injection period.
- In the study involving short-term injection (i.e., 25 years of injection) and long - term injection (i.e., 50 years of injection), the magnitude of the ground displacements obtained in the coupled fluid flow and geomechanics model with salinity are higher than the ground displacements in the coupled fluid flow and geomechanics model without salinity. This could be due to the difference in the magnitude of computed fluid pressure buildup in these models.
- The inclusion of geochemical reactions in the coupled fluid flow and geomechanical models did not have any significant influence on the computed pressure and ground displacements due to CO_2 injection. In other words, coupled fluid flow and geomechanical model would give similar results at a significantly lower computational effort. However, when the influence of salinity is incorporated in the coupled fluid flow-geochemical-geomechanical model, the computed displacements and fluid pressure distribution are significantly different. This indicates the need for the inclusion of salinity in the model, even though the computational effort is higher.
- The permeability and the vertical extent of the damage zone around the wellbore has significant influence on the computed amount of CO_2 leakage For a damage zone permeability of 100,000 D, the maximum computed CO_2 leakage (%) after 1,000 years was about 15.2 %, when the damage zone extended from the bottom of the reservoir to the surface. However, the maximum computed CO_2 leakage (%) after 1,000 years was about 10.2 %, when the damage zone extended from the bottom of the reservoir to about 100m above the caprock layer. (i.e., 790 m of damage zone).

- After 50 years of the post-injection period, the computed amount of CO_2 leaking into the overburden was very small. This may be due to the gradual drop in fluid pressure along the damage zone during the post-injection period.
- Both, the permeability and the vertical extent of the hypothetical damage zone have a significant influence on the computed ground displacements. The maximum computed ground displacement after 50 years of CO_2 injection, in the presence of a damage zone (k = 100,000 D) which extended from the base of the reservoir to the ground surface (2,180 m) was about 2.60 cm. In the case where the damage zone extended upto 100 m above the caprock layer from the base of the reservoir, the maximum computed displacement for the same damage zone permeability was about 2.42 cm. Since the difference in computed surface displacement is small, it appears that surface displacements may not be a good indicator of the extent of damage zone around the wellbore.

REFERENCES

1. ABAQUS. ABAQUS Manuals. ABAQUS version 6.12-1. Dassault Systems Simulia Corp (SIMULIA), 2012.

2. ADM, Inc., Archer Daniels Midland Company.Available: http://www.adm.com

3. Andreani, M.; Gouze, P.; Luquot, L.; Jouanna, P. Changes in seal capacity of fractured claystone caprocks induced by dissolved and gaseous CO_2 seepage. Geophys. Res. Lett. 2008, 35(14).

4. Arts, R.; Chadwick, A.; Eiken, O.; Thibeau, S.; Nooner, S. Ten years experience of monitoring CO_2 injection in the Utsira Sand at Sleipner, First Break 2009, 26, 65-72.

5. Audigane, P.; Gaus, I.; Czernichowski-Lauriol, I.; Pruess, K.; Xu, T. Two-dimensional reactive transport modeling of CO_2 injection in a saline aquifer at the Sleipner site. Am. J. Sci. 2007 , 307 (7), 974-1008.

6. Azaroual, M.; Andre, L.; Peysson,Y.; Prionon,J.; Broseta,D.; Dedecker, F.; Egermann,P., Desroches,J.; Hy-Billiot,J. Behavior of the CO2 injection well and the near wellbore during carbon dioxide injection in saline aquifers.In:Proceedings,TOUGHSymposium; Berkeley,California,USA,September 17-19, 2012.

7. Bachu, S.; Gunter, W. D.; Perkins, E.H. Aquifer disposal of CO_2: Hydrodynamic and mineral trapping. Energy Conversion and Management 1994, 35 (4), 269-279.

8. Bachu, S. Sequestration of CO_2 in geological media: Criteria and approach for site selection in response to climate change. Energy Conversion and Management 2000, 41 (9), 953-970.

9. Bachu, S.; Bonijoly, D.; Bradshaw, J.; Burruss, R.; Holloway, S.; Christensen, N. P. CO_2 storage capacity estimation: Methodology and gaps. Int. J. Greenhouse Gas Control 2007, 1(4) , 430-443.

10. Bachu, S.; Bennion, D. Interfacial tension between CO_2, freshwater, and brine in the range of pressure from (2 to 27) MPa, temperature from (20 to 125) C, and water salinity from (0 to 33400) mg/L. J. Chem. Eng. Data 2009, 54(1), 765-775.

11. Balashov, V.N.; Guthrie,G.D.; Hakala, J.A.; Lopano, C.L.; Rimstidt J.D.; Brantley, S.L. Predictive modeling of CO_2 sequestration in deep saline sandstone reservoirs: Impacts of geochemical kinetics. Appl. Geochem 2013, 30(1), 41-56.

12. Basbug, B.; Gumrah, F.; Oz, B. Simulating the effects of deep saline aquifer. 6th Canadian International Petroleum Conference; Calgary, Alberta, Canada, June 7 - 9, 2005.

13. Benge, G. Improving wellbore seal integrity in CO2 injections wells. Energy Procedia 2009, 1, 3523-3529.

14. Bergman, M.; Winter,E.M. Disposal of carbon dioxide in aquifers in the U.S.Energy Conversion and Management 1995, 36,523-526.

15. Bethke, C.M. Geochemical Reaction Modelling, Oxford University Press, New York. 1996.

16. Birkholzer, J.; Zhou, Q.; Tsang, C.-F. Large-scale impact of CO_2 storage in deep saline aquifer: A sensitivity study on pressure response in stratified systems. Int. J. Greenhouse Gas Control 2009, 3(1), 181-194.

17. Busch, A.; Gensterblum, Y. CBM and CO_2-ECBM related sorption processes in coal: a review. Int.J. Coal Geology 2011, 87, 49–71.

18. Bissell, R.C.; Vasco,D.W.; Atbi,M.; Okwelegbe,M.;Goldwater,M.H. A full field simulation of the In Salah gas production and CO2 storage project using a coupled geo-mechanical and thermal fluid flow simulator. Energy Procedia 2011, 4, 3290-3297.

19. Cantucci, B.; Montegrossi,.G.; Vaselli, O.; Tassi,F.; Quattrocchi,F.; Perkins,E.H. Geochemical modeling of CO2 storage in deep reservoirs: The Weyburn project (Canada) case study. Chemical Geology 2009, 265, 181-197.

20. Carroll, S.A.; McNab, W.W.; Dai,Z., Torres, S.C. Reactivity of Mount Simon sandstone and the Eau Claire shale under CO_2 storage conditions. Environ. Sci. Technol. 2012, 47(1), 252-261.

21. Chadwick, R. A.; Williams, G.A.; Williams, J.D.O.; Noy,D.J. Measuring pressure performance of a large saline aquifer during industrial-scale CO2 injection: The Utsira Sand, Norwegian North Sea. Int.J.Greenhouse Gas Control 2012, 10, 374-388.

22. Chadwick, R. A.; Zweigel, P.; Gregersen, U.; Kirby, G. A.;Holloway, S.; Johannessen, P. N. Geological reservoir characterization of a CO_2 storage site: The Utsira Sand, Sleipner, northern North Sea. Energy 2004, 29 (9−10), 1371−1381.

23. Chadwick, A.; Arts, R.; Bernstone, C.; May, F.; Thibeau, S.; Zweigel, P. Best practice for the storage of CO_2 in saline aquifers: observations and guidelines from the SACS and CO_2 STORE projects. British Geological Survey Occasional Publication, Nottingham, UK.2008

24. Chen, Z.; Huan, G.; Ma, Y. Computational Methods for Multiphase Flows in Porous Media; Society for Industrial and Applied Mathematics (SIAM): Philadelphia, PA, 2006.

25. Choi, Y-S.; Young, D.; Nesic, S.; Gray, L.G.S. Wellbore integrity and corrosion of carbon steel in CO_2 geologic storage environments: A literature review. Int. J. Greenhouse Gas Control 2013,16S, S70-S77.

26. Computer Modeling Group (CMG). CMG-GEM Manuals, GEM Version 10; CMG; Calgary, Alberta, Canada, 2012.

27. Cooper, S.C.; Bartel, L.C.; Lorenz, J.C.; Aldridge,D.F.; Engler,B.P.; Symons, N.P.; Byrer,C.; McNemar,A.; Elbring, G.J. West Pearl Queen CO2 sequestration pilot test and modeling project 2006-2008. Sandia National Laboratories, SAND2008-4992, 2008.

28. CO2CRC: Storage Capacity Estimation, Site Selection and Characterisation for CO_2 Storage Projects; Cooperative Research Center for Greenhouse Gas Technologies; Kaldi, J., Gibson-Poole, C., Eds.; CO2CRC Report RPTO8-1001; Canberra, Australia, 2008.

29. Czernichowski-Lauriol, I.; Rochelle, C.; Gaus, I.; Azaroual, M.; Pearce. J.; Durst, P. Geochemical interactions between CO_2, pore-waters and reservoir rocks: Lessons learned from laboratory experiments, field studies and computer simulations. In Advances in the Geological Storage of Carbon Dioxide: International Approaches to Reduce Anthropogenic Greenhouse Gas Emissions; Lombardi, S., Altunina, S.E., Beaubien, S.E., Eds.; Springer: Dordrecht, Netherlands, 2006; pp 157-174.

30. Day, S.; Fry, R.; Sakurovs, R.Swelling of moist coal in carbon dioxide and methane. Int.J. Coal Geology 2011, 86, 197–203.

31. Desai, C.S; Siriwardane, H.J. Constitutive Laws for Engineering Materials with Emphasis on Geologic Materials; Prentice-Hall, Inc; Englewood Cliffs, NJ,1984.

32. Deflandre, J.-P.; Estublier,A.; Baroni,A.; Fornel,A.; Clochard,V.; Delepine,N. Assessing field pressure and plume migration in CO2 storages: application of case-specific workflows at In Salah and Sleipner. Energy Procedia 2013, 37, 3554-3564.

33. Dhakal, S. GHG emissions from urbanization and opportunities for urban carbon mitigation. Current Opinion in Environmental Sustainability 2010, 2(4), 277-283.

34. Dilmore, R.M.; Allen, D.E.; Jones, J.R.; Hedges, S.W.; Soong,Y. Sequestration of dissolved CO_2 in the Oriskany formation. Environ. Sci. Technol. 2008, 42(8), 2760-2766.

35. Doughty, C. Investigation of CO_2 plume behavior for a large-scale pilot test of geologic carbon storage in a saline formation. Transp. Porous Media 2010, 82 (1), 49−76.

36. Deng,H.; Ellis, B.R.; Peters,C.A.; Fitts, J.P.; Crandall, D.; Bromhal, G.S.Modifications of carbonate fracture hydrodynamic properties by CO2-Acidified brine flow. Energy Fuels 2013, 27(1), 4221-4231.

37. Durst, P.; Azaroual, M.; Czernichowski-Lauriol, I. Weyburn database validation problem for predictive geochemical modeling. Report BRGM/RP-52375-FR 2003, 46.

38. Dutta, P.; Bhowmik, S.; Das, S. Methane and carbon dioxide sorption on a set of coals from India. Int.J. Coal Geology 2011, 85, 289–299.

39. Eiken, O.; Ringrose, P.; Hermanrud, C. Lessons learned from 14 years of CCS operations: Sleipner, In Salah and Snøhvit. Energy Procedia 2011, 4(1), 5541−5548.

40. Eke, P. E.; Naylor, M.; Haszeldine, S.; Curtis, A. CO_2/brine surface dissolution and injection: CO_2 storage enhancement. SPE Projects, Facilities & Construction 2011 , 6 (1), 41-53.

41. Ellis, B.; Peters, C.; Fitts, J.; Bromhal, G.; McIntyre, D.; Warzinski,R.; Rosenbaum, E. Deterioration of a fractured carbonate caprock exposed to CO_2-acidified brine flow. Greenhouse Gases: Sci. Technol.2011, 1(1), 248−260.

42. Ennis-King, J.; Paterson, L. Reservoir engineering issues in the geological disposal of carbon dioxide. Proceedings of the Fifth International Conference on Greenhouse Gas Control Technologies; Cairns, Australia, August 13-16, 2000.

43. Ennis-King, J.; Paterson, L. Engineering aspects of geological sequestration of carbon dioxide. SPE Asia Pacific Oil and Gas Conference and Exhibition; Melbourne, Australia, October 8-10, 2002; SPE Paper 77809.

44. Fang, Y.; Baojun, B.; Dazhen, T., Dunn-Norman, S.; Wronkiewicz, D. Characteristics of CO2 sequestration in saline aquifers.Pet.Sci. 2010,7 ,83-92.

45. Flett, M.A.; Gurton, R.M.; Taggart, I.J. Heterogeneous saline formations: long-term benefits for geo-sequestration of greenhouse gases. GHGT7: Proceedings of the 7th International Conference on Greenhouse Gas Technologies, September 5-9, 2004.

46. Garnier, C.; Finqueneisel, G.; Zimny, T.; Pokryszka, Z.; Lafortune, S.; Défossez, P.D.C.;Gaucher, E.C. Selection of coals of different maturities for CO2 Storage by modelling of CH4 and CO2 adsorption isotherms. Int.J. Coal Geology 2011, 87, 80–86.

47. Gasda, S.E.; Celia,M.A.; Wang, J.Z.; Duguid,A. Wellbore permeability estimates from vertical interference testing of existing wells. Energy Procedia 2013, 37, 5673-5680.

48. Gasda, S.E.; Nordbotten, J.M.; Celia, M.A. Determining effective wellbore permeability from a field pressure test: a numerical analysis of detection limits. Environ Geol 2008, 54, 1207-1215.

49. Gaus,I., Azaroual,M.; Czernichowski-Lauriol,I. Reactive transport modeling of the impact of CO2 injection on the clayey cap rock at Sleipner(North Sea). Chemical Geology 2005, 217, 319-337.

50. Gaus, I.; Audigane, P.; Andre, L.; Lions, J.; Nicolas, J.; Durst, P. Geochemical and solute transport modeling for CO_2 storage, what to expect from it?. Int. J. Greenhouse Gas Control 2008,2(4), 605-625.

51. Gherardi, F.; Xu, T.; Pruess, K. Numerical modeling of self-limiting and self-enhancing caprock alteration induced by CO_2 storage in a depleted gas reservoir. Chem. Geol. 2007, 244(1), 103−129.

52. Goodarzi, S.; Settari, A.; Keith, D. Geomechanical modeling for CO_2 storage in Nisku aquifer in Wabamun lake area in Canada. Int. J. Greenhouse Gas Control 2012 ,10(1), 113-122.

53. Goodman, A.; Hakala, A.; Bromhal, G.; Deel, D.; Rodosta, T.;Frailey, S.; Small, M.; Allen, D.; Romanov, V.; Fazio, J.; Huerta, N.;McIntyre, D.; Kutchko, B.; Guthrie, G. U.S. DOE methodology for the development of geologic storage potential for carbon dioxide at the national and regional scale. Int. J. Greenhouse Gas Control 2011, 5 (4), 952−965.

54. Gunter, W. D.; Perkins, E. H.; McCann, T.J. Aquifer disposal of CO_2-rich gases: Reaction design for added capacity. Energy Convers. Manage. 1993, 34 (9-11), 941-948.

55. Gunter, W.D.; Perkins,E.H.; Hutcheon, I. Aquifer disposal of acid gases: Modelling of water-rock reactions for trapping of acid wastes. Appl. Geochem 2000, 15(8), 1085-1095.

56. Gu, F., (2009). Reservoir and Geomechanical Coupled Simulation of CO_2 Sequestration and Enhanced Coalbed Methane Recovery. Ph.D. Dissertation,

Department of Civil and Environmental Engineering, University of Alberta at Edmonton, Alberta.

57. Gunter, W. D.; Bachu, S.; Benson, S.M. The role of hydrogeological and geochemical trapping in sedimentary basins for secure geological storage for carbon dioxide. The Geological Society of London; Special Publication 2004, 129-145.

58. Harpalani, S.; Prusty, B.K.; Dutta, P. Methane/CO_2 sorption modeling for coalbed methane production and CO_2 sequestration. Energy and Fuels 2006,20, 1591-1599.

59. Harvey, A.H.Semiempirical Correlation for Henry's Constants over Large Temperature Ranges, AIChE Journal 1996, 42 (5), 1491-1494.

60. Heinemann, N.; Wilkinson, M.; Pickup, G.E.; Haszeldine,R.S..; Cutler, N.A. CO_2 storage in the offshore UK Bunter sandstone formation. Int. J. Greenhouse Gas Control 2012,6(1), 210-219.

61. Hill, B.; Hovorka,S.; Melzer,S.; Geologic carbon storage through enhanced oil recovery. Energy Procedia 2013, 37, 6808-6830.

62. Holtz, M. H. Residual gas saturation to aquifer influx: A calculation method for 3-d computer reservoir model construction.SPE Gas Technology Symposium; Calgary, Alberta, Canada. 30 April 30-May 2, 2002; SPE Paper 75502.

63. Hosa, A., Esentia, M., Stewart, J., Haszeldine, S., (2010). Benchmarking worldwide CO_2 saline aquifer injections. Scottish Centre for Carbon Capture and Storage.

64. Hosa, A.; Esentia, M.; Stewart, J.; Haszeldine, S. Injection of CO_2 into saline formations: Benchmarking worldwide projects. Chem.Eng. Res. Des. 2011, 89(1), 1855−1864.

65. Houdu, E.; Poupard.O.; Meyer,V; Oxand,S.A. Supercritical CO2 leakage modeling for well integrity in geological storage project. Proceedings of the COMSOL Conference; Hannover, Germany. November, 4-6, 2008.

66. Hu, Y.; Ray, J.R.; Jun,Y-S. Na^+, Ca^{2+}, and Mg^{2+} in brines affect supercritical CO_2-brine-Biotite interactions: Ion exchange, Biotite dissolution, and Illite. Environ. Sci. Technol. 2013, 47(1), 191-197.

67. Iding, M.; Ringrose, P. Evaluating the impact of fractures on the long-term performance of the In Salah CO_2 storage site. Energy Procedia 2009, 1 (1), 2021−2028.

68. IEA Greenhouse gas R&D programme (IEA-GHG). *Aquifer storage-Development Issues*, November 2008.

69. IPCC. *IPCC Special Report on Carbon Dioxide Capture and Storage.* Prepared by Working Group III of the Intergovernmental Panel on Climate Change [Metz, B, Davidson, O, de Coninck, H C, Loos, M and Meyer,L A (eds.)]. Cambridge University Press, New York, 2005.

70. Ji, X.; Zhu, C.Predicting possible effects of H2S impurity on CO_2 transportation and geological storage. Environ. Sci. Technol. 2013, 47(1), 55-62.

71. Johnson, J.W.; Nitao, J.J.; Morris, J.P.; Reactive transport modeling of cap rock integrity during natural and engineered CO_2 storage; Lawrence Livermore National Laboratory; Benson, S., Eds.; CO_2 Capture Project Summary, (2), Elsevier, 2004.

72. Juanes, R; Spiteri, E. J.; Orr, F. M.; Blunt, M.J. Impact of relative permeability hysteresis on geological CO_2 storage. Water Resour. Res 2006, 42 (12), 1-13.

73. Jun, Y.-S.; Giammar, D.; Werth, C. Impacts of geochemical reactions on geologic carbon sequestration. Environ. Sci. Technol. 2013, 47(1), 3-8.

74. Keating, E.H.; Newell, D.L.; Viswanathan, H.; Carey, J.W.; Zyvoloski, G.; Pawar, G. CO_2/Brine transport into shallow aquifers along fault zones. Environ. Sci. Technol. 2013, 47(1), 290-297.

75. Khakim, M.; Tsuji, T.;Matsuoka, T. Geomechanical modeling for InSAR-Derived deformation at steam-injection oil sand fields. J. Pet. Sci.Eng. 2012 ,96-97, 152-161.

76. Kvamme, B.; Liu, S. (2009). Reactive transport of CO_2 in saline aquifers with implicit geomechanical analysis. Energy Procedia 2009 , 1(1), 3267-3274.

77. Lasaga, A.C. Chemical kinetics of water-rock interactions. J.Geophy. Res. 1984 , 89 , 4009-4025.

78. Li, Y.-K.; Nghiem, L. Phase equilibrium of oil,gas and water/brine mixtures from a cubic equation of state and Henry's law. Can. J. Chem. Eng 1986, 64(3), 486-496.

79. Lee, Z.H.; Sethupathi,S.; Lee,K.T.; Bhatia,S.; Mohamed,A.R. An overview on global warming in Southeast Asia: CO2 emission status, efforts done, and barriers.Renewable and Sustainable Reviews 2013, 28,71-81.

80. Liu, F.; Lu, P.; Zhu, C.; Xiao, Y. Coupled reactive flow and transport modeling of CO_2 sequestration in the Mt.Simon sandstone formation,Midwest U.S.A. Int. J. Greenhouse Gas Control 2011 ,5(2), 294-307.

81. Liu, Q.; Maroto-Valer, M. M. Parameters affecting mineral trapping of CO_2 sequestration in brines. Greenhouse Gases: Science and Technology 2011 ,1(3), 211-222.

82. Loizzo, M.; Akemu, O.A.P.; Jammes,L., Desroches,J.; Lombardi,S.; Annunziatellis,A. Quantifying the risk of CO2 leakage through wellbores. SPE SPE International Conference on CO2 Capture, Storage, and Utilization; New Orleans, Louisiana, USA, November 10-12, 2010; SPE Paper 139635.

83. Luquot, L.; Gouze, P. Experimental determination of porosity and permeability changes induced by injection of CO_2 into carbonate rocks. Chem. Geol. 2009, 265(1-2), 148-159.

84. Martinez, M.J.; Newell, P.; Bishop, J. E.; Turner, D. Z. Coupled multi-phase flow and geomechanics model for analysis of joint reactivation during CO2 sequestration operations. Int.J. Greenhouse Gas Control 2013, 17, 148-160.

85. Mathieson, A.; Midgely, J.; Wright, I.; Saoula, N.; Ringrose, P. InSalah CO_2 Storage JIP: CO_2 sequestration monitoring and verification technologies applied at Krechba,Algeria. Energy Procedia 2011 ,4(1), 3596-3603.

86. Mason, H.E.; Du Frane, W.L. Walsh, S.D.C.; Dai, Z.; Charnvanichborikan, S.; Carroll, S. Chemical and mechanical properties of wellbore cement alerted by CO2-rich brine using a multianalytical approach. Environ. Sci. Technol. 2013, 47, 1745-1752.

87. McNab, W.W.; Carroll, S.A. Wellbore integrity at the Krechba carbon storage site, In Salah, Algeria: 2. Reactive transport modeling of geochemical interaction near the cement-formation interface. Energy Procedia 2011, 4, 5195-5202.

88. Medina, C.R.; Rupp, J.A.; Barnes, D.A. Effects of reduction in porosity and permeability with depth on storage capacity and injectivity in deep saline aquifers: A case study from the Mount Simon sandstone aquifer. Int.J. Greenhouse Gas Control 2011, 5, 146-156.

89. Micheal, K.; Golab, A.; Ennis-King, J.; Allinson, G.; Sharma, S.; Aiken, T. Geological storage of CO_2 in saline aquifers—A review of the experience from existing storage operations. Int. J. Greenhouse Gas Control 2010, 4(4), 659-667.

90. Ming, T.; de_Richter, R.; Liu, W.; Caillol, S.; Fighting global warming by climate engineering: Is the earth radiation management and the solar radiation management any option for fighting climate change. Renewable and Sustainable Energy Reviews 2014; 31, 792-834.

91. Morris, J.; Hao, Y.; Foxall, W.; McNab, W. A study of injection-induced mechanical deformation at the In Salah CO_2 storage project. Int.J.Greenhouse Gas Control 2011 , 5(2), 270-280.

92. National Research Council (NRC). America's climate choices.2011. Available at: http://www.nap.edu/catalog.php?record_id=12781.

93. National Petroleum Council (NPC). Conventional onshore oil including enhanced oil recovery.2011.Available at: http://www.gwpc.org/e-library/documents/co2/API%20CO2%20Report.pdf

94. Nghiem, L.; Sammon, P.; Grabenstetter, J.; Ohkuma, H. (2004). Modeling CO_2 storage in aquifer with a fully-coupled geochemical EOS compositional simulator. Fourtheenth Symposium on Improved Oil Recovery;Tulsa,OK,April17-21,2004;SPE 89474.

95. Olivier, J.G.J.; Janssens-Maenhout, G.; Peters, J.A.H.W. (2012). Trends in global global CO2 emmsions. Report, The Hague: PBL Netherlands Environmental Assessment Agency, Ispra: Joint Research Centre.

96. Ottiger, S.; Pini, R.; Storti,G.; Mazzotti,M. Measuring and modeling the competitive adsorption of CO_2, CH_4, and N_2 on a dry coal. Langmuir 2008, 24 (1), 9531-9540.

97. Oye,V.; Aker, E.; Daley,T.M.; Kuhn,D.; Bohloli,B.; Korneev,V. Microseismic monitoring and interpretation of injection data from the In Salah CO_2 storage site (Krechba), Algeria. Energy Procedia 2013, 37, 4191-4198.

98. Palandri, J., Kharaka, Y. K., 2004. A compilation of rate parameters of water-mineral interaction kinetics for application to geochemical modeling.Open File Report 2004-1068, U.S. Geological Survey.

99. Patzek, T.W.; Silin, D.B.; Fielding, E. Use of satellite radar images in surveillance and control to two giant oilfields in California. Proceedings of the SPE Annual Technical Conference and Exhibition; New Orleans, LA, Sept 30 – Oct 3, 2001; SPE 71610.

100. Pawar, R.; Warpinski, B.; Byrer, C.; Benson, R.; Grigg, R.; Stubbs, B.; Krumhansl, J.; Lorenz, J.; Svec, R.; Stauffer, P.; Zhang, D.; Westrich, H. Geologic Sequestration of CO2 in West Pearl Queen Field: Results of a Field Demonstration

Project. Proceedings of the 3rd Annual Conference on Carbon Capture and Sequestration, Alexandria, VA, May 3-5, 2004.

101. Pawar, R.J.; Watson, T.L.; Gable, C.W. Numerical simulation of CO_2 leakage through abandoned wells: Model for an abandoned site with observed gas migration in Alberta, Canada. Energy Procedia 2009, 3625-3632.

102. Perera, M.S.A.; Ranjith, P.G.; Choi, S.K.; Airey, D.; Weniger, P. Estimation of gas adsorption capacity in coal: a review and an analytical study. Int.J. Coal Preparation and Utilization 2012, 32, 25–55.

103. Perkins, E.H.; Gunter, W.D. Aquifer disposal of CO_2-rich greenhouse gases: Modelling of water-rock reaction paths in a siliciclastic aquifer. Proceedings of the 8th International Symposium on Water-Rock Interaction; Vladivostok, Russia, Aug 15-19, 1995.

104. Peng, D.Y.; Robinson, D.B. A new two-constant equation of state. Ind. Eng. Chem. Fundam 1976, 15(1), 59-64.

105. Ranganathan, P.; van Hemert, P.; Susanne, E.; Rudolph, J.; Zitha, .P.Z.J. Numerical Modeling of CO2 Mineralization during Storage in Deep Saline Aquifers 2011, 4, 4538-4545.

106. Riddiford, F.A.; Tourqui, A.; Bishop, C.D.; Taylor, B.; Smith,M. A cleaner development: The In Salah Gas Project, Algeria. Proceedings of the 6th International Conference on Greenhouse Gas Control Technologies; Kyoto, Japan, Oct 1-4, 2003.

107. Rowe, A.M.; Chou,J.C.S. Pressure-volume-temperature-concentration relation of aqueous NaCl solutions. Journal of Chemical and Engineering Data 1970, 15(1), 61-66.

108. Ringrose, P.; Atbi, M.; Mason, D.; Espinassous, M.; Myhrer, Ø.; Iding, M.; Mathieson, A.; Wright, I. (2009). Plume development around well KB-502 at the In Salah CO_2 storage site. European Association of Geoscientists and Engineers, First break 2009, 27, 85-89.

109. Rutqvist, J.; Tsang. C-F. A study of caprock hydromechanical changes associated with CO2-injection into a brine formation. Environmental Geology 2002, 42, 296-305.

110. Rutqvist, J. Status of the TOUGH-FLAC simulator and recent applications related to coupled fluid flow and crustal deformations. Comput. Geosci. 2011, 37 (6), 739-750.

111. Rutqvist,J.; Vasco,D.W.; Myer,L. Coupled reservoir-geomechanical analysis of CO2 injection and ground deformations at In Salah, Algeria. Int.J. Greenhouse Gas Control 2010, 4, 225-230.

112. Rutqvist, J.; Birkholzer, J.; Tsang, C. Coupled reservoir-geomechanical analysis of the potential for tensile and shear failure associated with CO_2 injection in multilayered reservoir-caprock system. Int. J. Rock Mech. Min. Sci 2008 ,45 (2), 132-143.

113. Rutqvist, J.; Vasco, D. W.; Myer, L. Coupled reservoir−geomechanical analysis of CO_2 injection at In Salah, Algeria. Energy Procedia 2009, 1 (1), 1847−1854.

114. Szulczewski, M.L.; MacMinn, C.W.L Herzog, H.J.; Juanes, R. Lifetime of carbon capture and storage as a climate-change mitigation technology. Proc.Natl.Acad.Sci 2012, 109(14), 5185-5189.

115. Sharma, S.; Cook,P. Australia's first geosequestration demonstration – The CO2CRC Otway basin pilot project. 6th Annual Conference on Carbon Capture and Sequestration, Pittsburgh, U.S.A, May 10, 2007.

116. Singh,V; Cavanagh,A; Hansen,H; Nazarian,B; Idling,M; Ringrose,P. Reservoir modeling of CO2 plume behavior calibrated against monitoring data from Sleipner,Norway. SPE Annual Technical Conference and Exhibition; Florence, Italy, September 19-22, 2010; SPE 134891.

117. Siriwardane, H.; Gondle, R. Numerical modeling and monitoring of fluid flow and ground response during fluid injection. Proceedings of the 13th International Association for Computer Methods and Advances in Geomechanics (IACMAG); Melbourne, Victoria, Australia, May 9−11, 2011.

118. Siriwardane,H.J.;Gondle,R.K.;Bromhal,G.S.Coupled flow and deformation modeling of carbon dioxide migration in the presence of a caprock fracture during injection. Energy Fuels 2013, 27(8), 4232-4243.

119. Shi, J. Q.; Sinayuc, C.; Durucan, S.; Korre, A. Assessment of carbon dioxide plume behavior within the storage reservoir and the lower caprock around the KB-502 injection well at In Salah. Int. J.Greenhouse Gas Control 2012, 7(1), 115−126.

120. Torp, T. A.; Gale, J. Demonstrating storage of CO_2 in geological reservoirs: The Sleipner and SACS projects. Energy 2004, 29 (9−10), 1361−1369.

121. Stevens, S.H., Spector, D., and Riemer, P. Enhanced Coalbed Methane Recovery Using CO2 Injection: Worldwide Resource and CO2 Sequestration Potential. SPE 48881, Annual Technical Conference and Exhibition, Beijing, China, November 2-6,1998.

122. Tran, D.; Nghiem, L.; Buchanan, L.. An overview of iterative coupling between geomechanical deformation and reservoir flow. SPE International Thermal Operations and Heavy Oil Symposium; Alberta,Canada, November 1-2,2005; SPE 97879.

123. Tran, D.; Shrivastava, V.; Nghiem, L.; Kohse, B. Geomechanical risk mitigation for CO_2 sequestration in saline aquifers. Proceedings of the SPE Annual Technical Conference and Exhibition; New Orleans, LA,Oct 4−7, 2009; SPE 125167.

124. Uddin, M.; Jafari, A.; Perkins, E. Effects of mechanical dispersion on CO2 storage in Weyburm CO2-EOR field – Numerical history match and prediction. Int.J.Greenhouse Gas Control 2013, 16S, S35-S49.

125. U.S.EPA.2012.Retrievedfrom www.epa.gov: http://www.epa.gov/r5water/uic/carbon-sequestration.htm

126. U.S.D.O.E. Carbon Utilization and Storage Atlas 2012. www.netl.doe.gov

127. Vandeweijer,V.; van der Meer, B.; Hofstee,C.; Mulder,F.; Hoore, D.D.; Graven, H. Monitoring the CO2 injection site : K12-B.Energy Procedia 2011, 4, 5471-5478.

128. van der Meer, B. Carbon dioxide storage in natural gas reservoirs. Oil Gas Sci. Technol. 2005, 60(3), 527-536.

129. Verdon, J.P.; Kendall, J.M.; Stork,A.L. Chadwick, R.A.; White, D.J.; Bissell,R.C. Comparison of geomechanical deformation induced by megatonne-scale CO_2 storage at Sleipner, Weyburn, and In Salah. Proceedings of National Academy of Science 2013.

130. Vilarrasa, V.; Olivella, S.; Carrera, J. (2011). Geomechanical stability of the caprock during CO_2 sequestration in deep saline aquifers. Energy Procedia 2011, 4(1), 5306-5313.

131. Wageningen, van W.F.C.; Wentinck, H.M.; Otto, C. Report and modeling of the MOVECBM field tests in Poland and Slovenia. Energy Procedia 2009, 2071–2078.

132. Walsh, S. D. C.; Du Frane, W. L.; Mason, H. E.; Carroll, S. A. Permeability of wellbore-cement fractures following degradation by carbonated brines. Rock Mech. Rock Eng. 2012, 46 (3), 455-464.

133. Watson, T.L.; Bachu, S. Identification of wells with high CO_2-leakage potential in mature oil fields developed for CO2-enhanced oil recovery. SPE/DOE Improved

Oil Recovery Symposium; Tulsa, Oklahoma, USA, April 19-23, 2008; SPE Paper 112924.

134. Westrich, H.; Lorenz, J.; Cooper, S.; Colon, C.J.; Warpinski, N.;Zhang, D.; Bradley, C.; Lichtner, P.; Pawar, R.; Stubbs, B.; et al. Sequestration of CO_2 in a depleted oil reservoir: An overview; National Energy Technology Laboratory: Pittsburgh,PA,2001,1-11.

135. White, C.M.; Smith, D.H.; Jones, K.L.; Goodman, A.L.; Jikich, S.A.; LaCount, R.B.; DuBose,S.B.; Ozdemir, E.; Morsi, B.I.; Schroeder, K.T. Sequestration of carbon dioxide in coal with enhanced coalbed methane recovery — a review. Energy & Fuels 2005, 19 (3), 659–724.

136. Winschel, R.A.; Locke, J.E.; Srivastava, R.S.; Bajura, R.A.; Wilson, T.H.; Siriwardane, H.J.; Rauch, H.W.; Patchen, D.G.; Hega, B.D.; Gondle, R. CO2 sequestration in unmineable coal with enhanced coalbed methane recovery: the Marshall county project. Proceedings of the International Pittsburgh Coal Conference, Istanbul, Turkey, October 11–14, 2010

137. Xiong, Y.; Hu, L., Wu, Y.-S. Coupled geomechanical and reactive geochemical simulations for fluid and heat flow in enhanced geothermal reservoirs. Proceedings of the Thirty- Eighth Workshop on Geothermal Reservoir Engineering; Stanford, California, USA, February 11-13, 2013.

138. Xu, T.; Apps, J.; Pruess, K. Analysis of mineral trapping for CO_2 disposal in deep aquifers. Ernest Orlando Lawrence Berkeley National Laboratory; Report LBNL-46992, 2001.

139. Xu, T.; Apps, J.A.; Pruess,K. Reactive geochemical transport simulation to study mineral trapping for CO2 disposal in deep arenaceous formations. J. Geophys. Res 2003, 108(B2), 3(1)-3(13).

140. Yang, Y.; Ronzio, C.; Jun, Y.-S. The effects of initial acetate on CO_2-brine-anorthite interactions under geologic CO_2 sequestration conditions. Environ. Sci. Tech. 2011, 4(1), 4596-4606.

141. Yoo,S.Y.; Mito,Y.; Ueda.A.; Matsuoka,T. Geochemical clogging in fracture and porous rock for CO_2 mineral trapping. Energy Procedia 2013, 37 (1), 5612-5619.

142. Zhou, Q.; Birkholzer, J.; Mehnert, E.; Lin, Y.-F.; Zhang, K. Modeling basin- and plume-scale processes of CO_2 storage for full-scale deployment. Ground Water 2010 , 48(4) , 494-514.

143. Zhang,R. Numerical simulation of thermal hydrological mechanical chemical processes during CO2 geological sequestration. Ph.D Dissertation, Colorado School of Mines, 2013.

144. www.CO_2NOW.org